

**ADAPTIVE GRAPH-BASED ALGORITHMS FOR
CONDITIONAL ANOMALY DETECTION AND
SEMI-SUPERVISED LEARNING**

by

Michal Valko

MSc. Comenius University, Bratislava, 2005

Submitted to the Graduate Faculty of
the Arts and Sciences in partial fulfillment
of the requirements for the degree of
Doctor of Philosophy in Machine Learning

University of Pittsburgh

2011

UNIVERSITY OF PITTSBURGH
COMPUTER SCIENCE DEPARTMENT

This dissertation was presented

by

Michal Valko

It was defended on

August 1st 2011

and approved by

Milos Hauskrecht, PhD, Associate Professor, Computer Science

G. Elisabeta Marai, PhD, Assistant Professor, Computer Science

Diane Litman, PhD, Professor, Computer Science

John Lafferty, PhD, Professor, Machine Learning (Carnegie Mellon University)

Dissertation Director: **Milos Hauskrecht, PhD**, Associate Professor, Computer Science

Copyright © by **Michal Valko**

2011

ADAPTIVE GRAPH-BASED ALGORITHMS FOR CONDITIONAL ANOMALY DETECTION AND SEMI-SUPERVISED LEARNING

Michal Valko, PhD

University of Pittsburgh, 2011

We develop graph-based methods for semi-supervised learning based on label propagation on a data similarity graph. When data is abundant or arrive in a stream, the problems of computation and data storage arise for any graph-based method. We propose a fast approximate online algorithm that solves for the harmonic solution on an approximate graph. We show, both empirically and theoretically, that good behavior can be achieved by collapsing nearby points into a set of local representative points that minimize distortion. Moreover, we regularize the harmonic solution to achieve better stability properties.

We also present graph-based methods for detecting conditional anomalies and apply them to the identification of unusual clinical actions in hospitals. Our hypothesis is that patient-management actions that are unusual with respect to the past patients may be due to errors and that it is worthwhile to raise an alert if such a condition is encountered. Conditional anomaly detection extends standard unconditional anomaly framework but also faces new problems known as fringe and isolated points. We devise novel nonparametric graph-based methods to tackle these problems. Our methods rely on graph connectivity analysis and soft harmonic solution. Finally, we conduct an extensive human evaluation study of our conditional anomaly methods by 15 experts in critical care.

TABLE OF CONTENTS

PREFACE	xv
1.0 INTRODUCTION	1
1.1 Motivation	1
1.2 Thesis Statement and Main Contributions	4
1.3 Organization of the Dissertation	5
2.0 RELATED WORK	6
2.1 Related work in Graph Quantization	6
2.2 Related Work in Semi-Supervised Learning (SSL)	8
2.2.1 Semi-Supervised Max-Margin Learning	8
2.2.1.1 Semi-supervised SVMs	9
2.2.1.2 Manifold regularization of SVMs	9
2.2.2 Online Semi-Supervised Learning	10
2.3 Related Work in Anomaly Detection (AD)	11
2.3.1 Unconditional Anomaly Detection	11
2.3.1.1 Approaches with prelabeled anomalies	13
2.3.1.2 Rare category detection	13
2.3.2 Conditional Anomaly Detection (CAD)	14
3.0 SEMI-SUPERVISED LEARNING	16
3.1 Graphs as Data Models	17
3.1.1 Stationary Distribution of a Random Walk	18
3.2 Regularized Harmonic Function	19
3.2.1 Soft Harmonic Solution	21

3.3	Max-Margin Graph Cuts	22
3.4	Joint Quantization and Label Propagation	24
3.4.1	Label Propagation	25
3.4.2	Quantization	25
3.4.3	Final Inference Scheme for Unlabeled Examples	27
3.4.4	Time Complexity	28
3.5	Online Semi-Supervised Learning With Quantized Graphs	29
3.5.1	Incremental k-centers	31
3.6	Parallel Multi-Manifold Learning	32
4.0	CONDITONAL ANOMALY DETECTION	33
4.1	Introduction to Conditonal Anomaly Detection	33
4.2	Definition of Conditional Anomaly	34
4.3	Relationship to Mislabeling Detection	35
4.4	Class-outlier Approach	36
4.5	Discriminative Approach	37
4.5.1	CAD with Random Walks	38
4.6	Regularized Discriminative Approach	39
4.6.1	Regularized Random Walk CAD	40
4.6.2	Conditional Anomaly Detection with Soft Harmonic Functions	41
5.0	THEORETICAL ANALYSIS	45
5.1	Soft Harmonic Solution	45
5.2	Analysis of Max-margin Graph Cuts	46
5.2.1	When Manifold Regularization Fails	46
5.2.2	Generalization Error	48
5.2.3	Threshold epsilon	51
5.3	Analysis of Joint Quantization and Label Propagation	53
5.4	Analysis of Online SSL on Quantized graphs	54
5.4.1	Bounding Transduction Error (5.7)	56
5.4.2	Bounding Online Error (5.8)	56
5.4.3	Bounding Quantization Error (5.9)	57

5.4.4	Discussion	61
5.5	Parallel Multi-Manifold Learning	61
5.6	Analysis of Conditional Anomaly Detection	62
6.0	EXPERIMENTS	64
6.1	Evaluations of Semi-Supervised Learning Models	64
6.1.1	UCI ML Datasets	64
6.1.1.1	Digit recognition	65
6.1.1.2	Letter recognition	65
6.1.1.3	Image segmentation	65
6.1.1.4	COIL	65
6.1.1.5	Car	65
6.1.1.6	SecStr	66
6.1.2	Vision Datasets	66
6.1.3	Max-margin Graph Cuts Experiments	67
6.1.3.1	Synthetic problem	67
6.1.3.2	UCI ML repository datasets	68
6.1.4	Joint Quantization and Label Propagation Experiments	69
6.1.4.1	Experimental setup	70
6.1.4.2	Results	70
6.1.5	Online Quantized SSL Experiments	71
6.1.5.1	UCI ML Repository Experiments	71
6.1.5.2	Face recognition	73
6.1.6	Parallel SSL	76
6.1.7	Conclusions	77
6.2	Evaluations of Conditional Anomaly Detection Methods	77
6.2.1	Synthetic Datasets	78
6.2.1.1	Core dataset	78
6.2.1.2	Mixtures of gaussians	78
6.2.2	Post-surgical cardiac patients (PCP)	79
6.2.2.1	Visit/Demographic Features	81

6.2.2.2	Lab features	81
6.2.2.3	Medication features	82
6.2.2.4	Procedure features	82
6.2.2.5	Heart support device features	82
6.2.2.6	Orders/labels	83
6.2.3	Algorithms for Comparison	83
6.2.3.1	Discriminative SVM anomaly detection	83
6.2.3.2	One-class SVM	84
6.2.3.3	Quadratic discriminant analysis	84
6.2.3.4	Weighted NN	84
6.2.3.5	Parameters for the graph-based algorithms	85
6.2.4	Evaluation of CAD with Known Ground Truth	86
6.2.4.1	CAD on synthetic datasets with known distribution	86
6.2.4.2	CAD on UCI ML datasets with ordinal response variable	87
6.2.4.3	CAD on Core dataset with fringe points	89
6.2.4.4	Conclusions	90
6.2.5	Evaluation of Expert Assessed Clinically Useful Anomalies	90
6.2.5.1	Pilot study in 2009	90
6.2.5.2	Soft harmonic anomaly detection	92
6.2.5.3	Conclusions	94
7.0	DISCUSSION	96
	BIBLIOGRAPHY	100

LIST OF TABLES

1	Mean anomaly AUROC and variance on three synthetic datasets	87
2	Mean anomaly agreement score and variance on 3 UCI ML datasets	88

LIST OF FIGURES

1	Conditional vs. unconditional anomalies	2
2	Disadvantages of nearest neighbor approach for conditional anomaly detection	3
3	a. Similarity graph b. Three regularized harmonic solutions	22
4	Running time for different methods on the SecStr dataset	28
5	Challenges for CAD: 1) fringe and 2) isolated points	37
6	Estimating class-conditional probabilities from two similarity graphs	39
7	Linear, cubic, and RBF decision boundaries for different methods	49
8	The thresholded empirical risk	53
9	Estimating the likelihood ratio from a single graph	63
10	Snapshots from the environment adaptation and office space datasets	67
11	Face-based authentication dataset (left) and examples of labeled faces (right) .	68
12	Comparison of SVMs, GC and MR on 3 datasets from the UCI ML repository .	68
13	Coil and Car datasets from UCI ML Repository	72
14	UCI ML: Quality of approximation as a function of time	73
15	UCI ML: Quality of approximation as a function of number of centroids	74
16	Comparison of 3 face recognizers on 2 face recognition datasets	75
17	Speedups in the total, inference, and similarity computation times	76
18	The three synthetic datasets with known underlying distributions	79
19	Processing of data in the electronic health record	80
20	Examples of temporal features for continuous lab values	82
21	The weight matrix for 100 negative and 100 positive cases of HPF4 order . . .	85
22	Computation time comparison for the three graph-based methods	88

23	Conditional anomaly detection on a synthetic <i>Core</i> dataset	89
24	Histogram of alert examples in the study according to their alert score	91
25	The relationship between the alert score and the true alert rate	93
26	Histogram of anomaly scores for 2 different tasks	94
27	Medical Dataset: Varying graph size	95
28	Medical Dataset: Varying regularization	95

LIST OF ALGORITHMS

1	Quantized semi-supervised learning with principal manifolds	27
2	Online quantized harmonic solution	30
3	RWCAD that calculates the anomaly score	41

LIST OF EQUATIONS

3.1	Closed form solution for a stationary distribution of the random walk	19
3.5	Soft harmonic solution	21
3.6	Closed form for the soft harmonic solution	21
3.8	Quantized unconstrained regularization	24
3.9	Joint quantization and soft harmonic solution	25
3.10	Quantization step	26
3.11	Approximate quantization step	26
3.12	Solution for the quantization step	26
4.1	Expected value of the n-th order statistic for the standard normal	35
4.2	Posterior probability estimation from a random walk	38
4.3	Regularization of the discriminative approach for CAD	40
4.4	Confidence from the soft label	42
4.5	Anomaly score for soft harmonic anomaly detection	42
4.6	Soft harmonic solution using matrix inversion	43
4.7	Soft harmonic solution using system of linear equations	43
4.8	Compact computation of harmonic solution for the backbone graph	44
5.1	Linear manifold regularization	47
5.3	Linear support vector machine	47
5.4	Risk of our solutions	48
5.5	Empirical risk on graph induced labels	48
5.6	Elastic net	54
5.10	Upper bound on the online regret	57

5.11 Upper bound on stability of quantized harmonic solution	58
5.12 Upper bound on the quality of quantization	58
5.13 Approximating Laplacian by block-diagonal structure	62
5.14 Approximation bound of block-diagonal structure	62
5.15 Class-conditional probability of a different label	62
5.16 Approximation of the likelihood ratio	63
5.17 Estimation expressed with similarity weights	63
5.18 Equivalent form of RWCAD algorithm	63

PREFACE

I spent 6 splendid years in Pittsburgh. I want to thank the people who made my journey to PhD possible and enjoyable. First of all, I would like to sincerely thank my advisor Milos Hauskrecht, who made me excited about Machine Learning. With Milos, all my work had a purpose and I was happy to work on important problems that people care about. Therefore, the thought of quitting my PhD (so common among my peers) never crossed my mind. Milos stood by me literally from day one, when he came to pick me up at the airport.

This thesis would not be about graph-based algorithms if not for Brano Kveton, who made me interested in them. He was my mentor during my internships at Intel Research. I am grateful for his friendship and encouragement that made me surpass the expectations I had for myself. Brano is an amazing researcher and he collaborated on many of the semi-supervised learning methods presented here. I would also like to thank my thesis committee, Liz Marai, Diane Litman and in particular John Lafferty, whose research with Jerry Zhu on harmonic functions has laid the foundation for this dissertation.

I was privileged to work with Greg Cooper, who should be a role model for any scientist. He has always impressed me with his professionalism by constantly having a big picture in mind. Greg was a part of a larger interdisciplinary group that I had a great opportunity to work in, ranging from biomedical informaticians to clinicians and pharmacists: Roger Day, who recruited me to the Bayesian club while he played tuba in 7 different bands; Shyam Visweswaran; Amy Seybert; Gilles Clermont; Wendy Chapman; and many others. I would like to thank our post-doc Hamed Valizadegan and Saeed Amizadeh, with whom I worked during my last year, and also other members of Milos' machine learning lab: Rich Pelikan, Iyad Batal, Shuguang Wang, Quang Nguyen, and Dave Krebs.

During my studies, I had the chance to do two internships with Intel Research, which

taught me a lot about research in the industry. Besides Brano, I would like to thank my research collaborators Ling Huang, Ali Rahimi, Daniel Ting from Berkeley, my colleges Georgios Theocharous, Kent Lyons, Jennifer Healey, John Mark Agosta, Nick Carter, and many other researches and interns.

I also want to thank my teachers from the Machine Learning Department at Carnegie Mellon University, where I learned so much about the field, namely John Lafferty, Larry Wasserman, Carlos Guestrin, Geoff Gordon, Eric Xing, and Gary Miller. I am also grateful to my teachers from Pitt and from Comenius University in Bratislava. But my love for math started with my high school teacher, Martin Macko, who taught me mathematics for 8 years in the best way I can imagine. It is because of him that I decided to do science and research. My mom had a role in that decision, too, and it is probably not a coincidence that she went to grad school for cybernetics.

I am grateful to our administrative staff, who helped to smooth my life at Pitt: Kathy O'Connor, Kathleen Allport, Wendy Bergstein, Loretta Shabatura, Nancy Kreuzer, and Keena Walker. These ladies are running this place and create a feeling like home. Also, I want to thank Phillipa Carter from the Graduate Studies who will remember me as somebody that would stalk her everywhere and would always want to skip the chain of command.

Besides my studies, my life in Pittsburgh would not be so great if it was not my friends who made my stay here so enjoyable. I need to mention Tomas Singliar and Zuzana Jurigova, Christopher Hughes, Mihai and Diana Rotaru, Roxana and Vlad Gheorgiou for marvelous times we spent together. I made great friends at Pitt, with whom I would like to keep in touch including Panickos Nephytou, Kiyeon Lee, Ryan Moore, Alexandre Ferreira, Yaw Gyamfi, Samah Mazraani, Weijia Li, Peter Djalaliev, Lory al Moakar, Shenoda Guirguis, Tatiana Ilina, and also many friends at CMU such as Miro Dudik, Mike Gamalinda, Polo Chau, Kiki Levanti, Michael Papamichael, Jose Gonzales-Brenes, Lucia Castellanos, Mladen Kolar, Stano Funiak, and others.

My time in Pittsburgh was fabulous also due to Pitt Men's Glee Club, where I sang Tenor 2 at many concerts, including the ones on our tours to Italy, Croatia, and Texas. I need to start with Richard Earl Teaster, the director of the group, who was one of the first people I met upon my arrival to Pittsburgh and over 6 years became one of my best friends.

Besides that he has been my private voice teacher for many of those years and raised me from somebody with almost no experience in singing to a singer in this exquisite ensemble. The glee club became a huge part of me, and my life often consisted of research, friends and glee club. Moreover, within the group I made great friends, such as Mike Pollock, Matt (and Kelly) Keeny, Dexter Gulick, Chad Slyman, Geoff Arnold, Paul Schillenger, Evan Pavloff, Joel Arter, Adam Sloan, Greg Hill, Phil Slane, Tyler Kirland, Ryan McGinnis, Ben Dichter, Josh Niznik, Matt Recker, Matt Cahalan, James Montgomery, Nick Czarnek, Erick Markley, Jared Wilson, Victor Bench, John Moriarty, Mark Ellenberger, Charlie Eichman, Evan McCullough, Evan Williams, and dozens of others with whom I shared the world of music, including my music teachers: Don Fellows, John Goldsmith, Claudia Pinza, Jim Ferla, Sister Maria Ozah, and Ben Harris.

For the most of my time at Pitt, I lived in a big house a few minutes away from my department. Since we often housed visiting students and scholars, during the five years I probably had more than 50 housemates. I will always remember the parental caring of Kevin and Elizabeth Leichbach, dancing robotic toys of David Palmer, delicious food of Az-zurra Missinato and Kikumi Ozaki, Sera Wang, Sonia Wu, Michael Wasilewski, and many others who lived at 307 Halket Street. Through Kevin and Elizabeth to have I met many nice people, such as Kirsten Ream, Kate Shaughnessy, Kelly Reed, George and Becky Mazagieros, and Bob Fratto. I made many friends at the Pittsburgh branch of Campus Crusade for Christ. The ones that stand out are Matt Budavich, TJ Laird, Zach Fogel, Joe Rathbun, Justin Cooper, and Evelyn Yarzebinski, who made sure that this dissertation is actually written in English.

I would also like to thank my friends in Slovakia, who were often welcoming me at home during my summer and winter breaks and spent time with me on hikes, travels and music festivals. Notably, I would to thank Michal Rjasko for the long years of great friendship. Finally, I am indebted to my family, in particular to my mom Maria, my dad Michal, and my sister Zuzka, who provided me with everything I needed and supported me throughout all my studies. I also thank my extended family, especially my only living grandparent, Anna, who has been praying for me every single day. Her prayers were definitely heard as God gave me the strength and grace I needed.

1.0 INTRODUCTION

1.1 MOTIVATION

If we want people to enjoy the benefits of machine learning, we should provide them with algorithms that do not require much training time before they can be useful. Therefore, we will investigate the algorithms that need only minimal feedback from the users. For example, in semi-supervised learning we assume that only very few examples from the data are labeled and we try to use the unlabeled examples to learn something about the structure of the data. In the area of conditional anomaly detection and in particular in medicine, a traditional approach is to ask experts to create a set of rules that would raise an alert if an adverse event is encountered. Since a manual creation of rules is very time consuming, we would rather like to learn what the adverse event might be from the collection of the past data.

In this dissertation, we will take advantage of using a similarity graph as the data representation. Similarity graphs help us model the relationship between the examples. However, graph-based algorithms, such as label propagation, do not scale well beyond several thousand examples. We will address this problem by data quantization, where unlike other approaches (k -means, subsampling) we consider the quality of the inference. Moreover, we investigate an online learning formulation of semi-supervised learning, which is suitable for adaptive machine learning systems when the data arrive in a stream.

Furthermore, we extend graph-based learning to conditional anomaly detection problem and apply it to clinical scenarios. Traditionally, anomaly detection techniques identify unusual patterns in data. In clinical settings, these may concern identification of unusual patients, unusual patient–state outcomes, or unusual patient-management decisions.

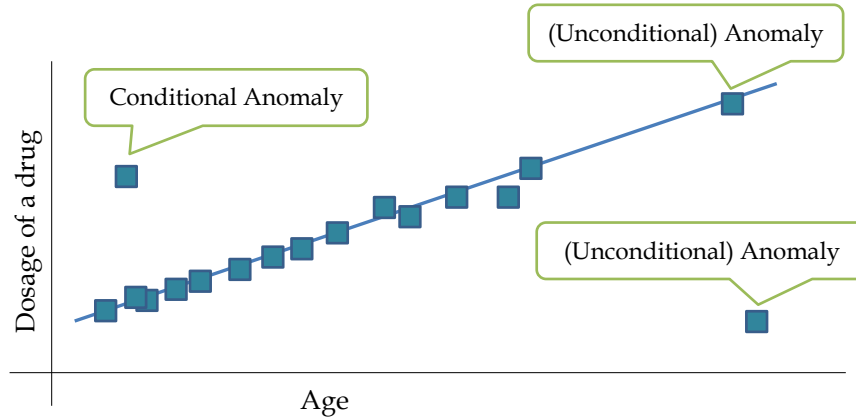


Figure 1: Conditional vs. unconditional anomalies

1

Our ability to detect unusual events in clinical data may have a tremendous impact on health care and its quality. First, the identification of an action that differs from an expected or usual pattern of care can aid in detection and prevention of the potential medical errors. According to the HealthGrades study (Wall Street Journal on July 27, 2004), medical errors account for 200,000 preventable deaths a year. Second, the identification of anomalous patient responses can help us to identify new promising treatments.

Typical anomaly detection methods used in data analysis are unconditional (with respect to the context) and look for outliers with respect to all data attributes. In the medical domain these methods would identify unusual patients, that is, patients suffering from a less frequent disease or patients with unusual collection of symptoms. Unfortunately, this does not fit the nature of the problem we want to solve in error detection: the identification of unusual patient management decisions with respect to past patients who suffer from the same or similar condition. To address this, we are developing a *qualitatively new conditional anomaly detection framework* where the decision event is judged anomalous with respect to the patient's symptoms, state, and demographics.

The conditional anomaly detection is the problem of detecting unusual values for a subset of variables given the values of the remaining variables. Figure 1 illustrates the concept of conditional anomaly: Assume that the dosage of a drug is a linear function of the age.

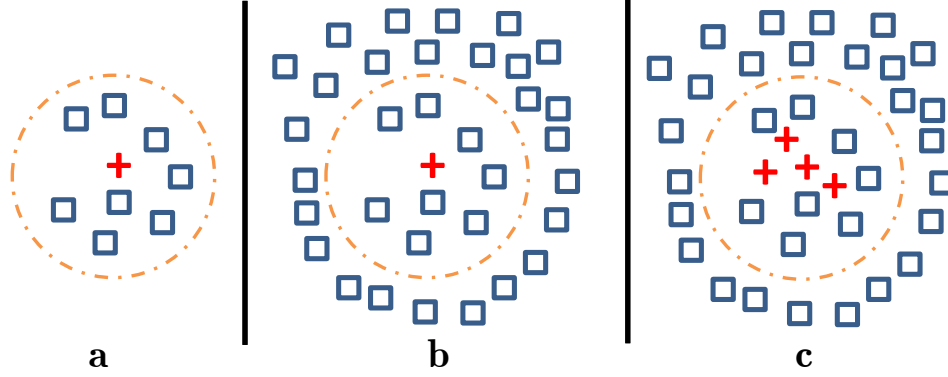


Figure 2: Disadvantages of nearest neighbor approach for conditional anomaly detection

Now imagine that we have a young patient that was given a higher dosage of a drug (Figure 1, top left). The amount of dosage is not unusual at all. Indeed, we have other patients with the same or similar dosage. What is unusual is the dosage with respect to his age; the patients that have similar ages were given lower dosages. We can say that this dosage was *conditionally anomalous* given a patient’s age.

Throughout this dissertation, we build on label propagation on a data similarity graph, which exploits the manifold assumption [Chapelle et al., 2006]. Unlike local neighborhood methods based on the nearest neighbors, it respects the structure of the manifold and lets us account for more complex interactions in the data. In other words, while the metric may provide a reasonable local similarity measure, it is frequently inadequate as a measure of global similarity [Szummer and Jaakkola, 2001]. Figure 2 illustrates a potential benefit of label propagation, where the goal is to detect that the positive (+) example has an anomalous label conditioned on its placement. The positive (+) label in 2b is more anomalous than the one in 2a, but nearest neighbor (NN) would consider them equal, because it only considers the points within the displayed circle. Moreover, the NN approach would find clustered (+) anomalies in 2c normal because it ignores the data beyond the nearest neighbors.

1.2 THESIS STATEMENT AND MAIN CONTRIBUTIONS

Although very popular, label propagation on a data similarity graph does not scale well beyond several thousand of examples, due to the following reasons:

1. The computation of the similarity matrix and the label propagation are $\Omega(n^2)$ where n is the number of examples. Label propagation itself requires the computation of the $n \times n$ matrix inverse or the solution of the system of n linear equations.
2. Current methods that reduce the size of the graph to form an approximate back-bone graph do not link the construction of this graph to the final inference task.
3. Despite the usefulness of the online semi-supervised learning paradigm for practical adaptive algorithms, there is not much success in applying this paradigm to realistic problems, especially when data arrive at a high rate.

Next, the problem of conditional anomaly detection could be approached by

1. extending one-class (unconditional) anomaly methods (Section 4.4)
2. classification and claiming misclassified examples as conditionally anomalous (Section 4.5)

Both of these approaches suffer from the problems of isolated and fringe points described in Section 4. In this dissertation we develop the methodology to address these problems. We take a graph-based approach, because it is non-parametric, incorporates the manifold assumption, and can also easily take advantage of unlabeled data. We present the following main contributions:

- We show how to combine max-margin and semi-supervised learning to **max-margin graph cuts** semi-supervised learning (Section 3.3).
- We show how to compute label propagation on a graph and the centroids of a backbone graph **jointly**. (Section 3.4)
- We propose the **online harmonic function** solution and show how to compute its approximation efficiently (Section 3.5).
- We prove **performance bounds** for our online algorithm in a semi-supervised setting on quantized graphs (Section 5.4).

- We introduce non-parametric **graph-based** methods and show how they can *handle unconditional outliers* (Section 4.6).
- We show how a **soft harmonic solution** on data similarity graphs can be used for conditional anomaly detection (Section 4.6.2).

In addition, we test the conditional anomaly detection methods by comparing them to the evaluations conducted with a panel of physicians and show the benefits of our methods (Section 6.2.5.1). Based on the aforementioned contributions, we claim the following:

Our graph-based methods can perform online semi-supervised learning with a constant per-step update and provable performance guarantees. Moreover, they can detect conditional anomalies and filter unconditional anomalies.

1.3 ORGANIZATION OF THE DISSERTATION

- In Chapter 2, we outline the related work in anomaly detection (Section 2.3), semi-supervised learning (Section 2.2), and graph quantization (Section 2.1).
- Chapter 3 presents new approaches for semi-supervised learning and the online semi-supervised learning (Section 3.5).
- Chapter 4 presents novel methods for conditional anomaly detection.
- Chapter 5 presents the theoretical analysis of the methods from Chapter 3 and Chapter 4. In particular, it presents the analysis of max-margin graph cuts (Section 5.2) and the analysis of the online semi-supervised learning on quantized graphs (Section 5.4).
- Chapter 6 presents the experimental results on various synthetic and real-world datasets, notably the face recognition video datasets and the medical datasets from University of Pittsburgh Medical Center.

Parts of this dissertation have previously appeared in [Hauskrecht et al., 2007, Hauskrecht et al., 2010, Valko et al., 2008, Valko and Hauskrecht, 2008, Valko and Hauskrecht, 2010, Valko et al., 2010, Valko et al., 2011, Kveton et al., 2010b, Kveton et al., 2010a].

2.0 RELATED WORK

In this chapter we review the relevant work on graph quantization, semi-supervised learning, and anomaly detection.

2.1 RELATED WORK IN GRAPH QUANTIZATION

Given n data points and a typical graph construction method, the exact computation of the harmonic solution has space and time complexity of $\Omega(n^2)$ in general due to the construction of an $n \times n$ similarity matrix. Furthermore, exact computation requires an inverse operation on an $n \times n$ similarity matrix which takes $O(n^3)$ in most practical implementations¹. For applications with large data size (e.g., exceeding thousands), the exact computation or even storage of the harmonic solution becomes infeasible, and problems with n in the millions are entirely out of reach.

An influential line of work in the related area of graph partitioning approaches the computation problem by reducing the size of the graph, collapsing vertices and edges, partitioning the smaller graph, and then uncoarsening to construct a partition for the original graph [Hendrickson and Leland, 1995, Karypis and Kumar, 1999]. Our work is similar in spirit but provides a theoretical analysis for a particular kind of coarsening and uncoarsening methodology.

Our aim is to find an effective *data preprocessing* technique that reduces the size of the data and coarsens the graph [Madigan et al., 2002, Mitra et al., 2002]. There are two types of approaches widely used in practice for data preprocessing:

¹The complexity can be further improved to $\mathcal{O}(n_u^{2.376})$ by using the Coppersmith-Winograd algorithm.

1. data quantization based methods, which aim to replace the original data set with a small number of high quality ‘representative’ points that capture relevant structure [Goldberg et al., 2008, Yan et al., 2009];
2. Nyström method based methods, which aim to explore low-rank matrix approximations to speed up the matrix operations [Fowlkes et al., 2004]).

While it is useful to define such preprocessors, it is not satisfactory to simply reduce the size of similarity matrix to speed up the matrix calculations. so that the related matrix operation can be performed in a desired time frame.

What is needed is an explicit connection between the amount of data reduction that is achieved by a preprocessor and the subsequent effect on the classification error. Some widely used data preprocessing approaches are based on data quantization, which replaces the original data set with a small number of high quality centroids that capture relevant structure [Goldberg et al., 2008, Yan et al., 2009].

Such approaches are often heuristic and do not quantify the relationship between the noise induced by the quantization and the final prediction risk. An alternative approach to the computation problem is the *Nyström method*, a low rank matrix approximation method that allows faster computation of the inverse. This method has been widely adopted, particularly in the context of approximations for SVMs [Drineas and Mahoney, 2005, Williams and Seeger, 2001, Fine and Scheinberg, 2001] and spectral clustering [Fowlkes et al., 2004].

However, since the Nyström method uses interactions between subsampled points and *all* other data points, storage of all points is required and thus, it becomes unsuitable for infinitely streamed data. To our best knowledge, we are not aware of any online version of Nyström method that could process an unbounded amount of streamed data. Additionally, in an offline setting, the approaches based on the Nyström method have inferior performance to the quantization-based methods, if both of them are given the same time budget for computation. This was shown in an early work on the spectral clustering [Yan et al., 2009].

Using incremental k -centers [Charikar et al., 1997] which has provable worst case bound on the distortion, we quantify the error introduced by quantization. Moreover, using regularization we show that the solution is stable, which gives the desired generalization bounds.

An interesting method is introduced in [Aggarwal et al., 2003], which addresses context drift, or *evolution* in the data streams. Clusters can emerge and die based on approximated recency. But again this method is a heuristic and comes with no guarantees on the quality of the quantization.

2.2 RELATED WORK IN SEMI-SUPERVISED LEARNING (SSL)

[Zhu et al., 2003] extend their previous work [Zhu et al., 2003] to Gaussian processes by no longer assuming that soft labels are fixed to the observed data. Instead they assume the data generation process $\mathbf{x} \rightarrow \mathbf{y} \rightarrow \mathbf{t}$, where $\mathbf{y} \rightarrow \mathbf{t}$ is a noisy label generation with process modeled by a sigmoid. The posterior is not Gaussian and the authors use Laplace approximation to compute $p(\mathbf{y}_L, \mathbf{y}_U | \mathbf{t}_L)$. They discuss using different kernels for the learning of graph weights, such as the tanh-weighted graph, and optimize it either by maximizing the likelihood of labeled data or maximizing the alignment to labeled data.

[Fergus et al., 2009] use the convergence of the eigenvectors of the normalized Laplacian to eigenfunctions of weighted Laplace-Beltrami operators to scale graph-based SSL to millions of examples. Assuming that the underlying distribution has a product form (which is a reasonable assumption after a PCA projection), they estimated the density using histograms for each dimension independently. Therefore, they only needed to solve d generalized eigenvector problems on the backbone graph, where d is the dimension of the data. Moreover, they only used the k smallest eigenvectors and subsequently needed to solve only one $k \times k$ least squares problem.

2.2.1 Semi-Supervised Max-Margin Learning

Most of the existing work on semi-supervised max-margin learning can be viewed as manifold regularization of SVMs [Belkin et al., 2006] or semi-supervised SVMs with the hat loss on unlabeled data [Bennett and Demiriz, 1999]. The two approaches are reviewed in the rest of this section. Let l and u be the sets of labeled and unlabeled data respectively. As-

sume that f is a function from some *reproducing kernel Hilbert space (RKHS)* \mathcal{H}_K , and $\|\cdot\|_K$ is the norm that measures the complexity of f .

2.2.1.1 Semi-supervised SVMs Semi-supervised support vector machines with the *hat loss* $\hat{V}(f, \mathbf{x}) = \max\{1 - |f(\mathbf{x})|, 0\}$ on unlabeled data [Bennett and Demiriz, 1999]:

$$\min_f \sum_{i \in l} V(f, \mathbf{x}_i, y_i) + \gamma \|f\|_K^2 + \gamma_u \sum_{i \in u} \hat{V}(f, \mathbf{x}_i) \quad (2.1)$$

compute max-margin decision boundaries that avoid dense regions of data. The hat loss makes the optimization problem non-convex. As a result, it is hard to solve the problem optimally and most of the work in this field has focused on approximations. A comprehensive review of these methods was done by [Zhu, 2008].

In comparison to semi-supervised SVMs, learning of max-margin graph cuts (3.7) is a convex problem. The convexity is achieved by having a two-stage learning algorithm. First, we infer labels of unlabeled examples using the regularized harmonic function solution, and then we minimize the corresponding convex losses.

2.2.1.2 Manifold regularization of SVMs Manifold regularization of SVMs [Belkin et al., 2006]:

$$\min_{f \in \mathcal{H}_K} \sum_{i \in l} V(f, \mathbf{x}_i, y_i) + \gamma \|f\|_K^2 + \gamma_u \mathbf{f}^\top L \mathbf{f}, \quad (2.2)$$

where $\mathbf{f} = (f(\mathbf{x}_1), \dots, f(\mathbf{x}_n))$, computes max-margin decision boundaries that are smooth in the feature space. The smoothness is achieved by the minimization of the regularization term $\mathbf{f}^\top L \mathbf{f}$. Intuitively, when two examples are close on a manifold, the minimization of $\mathbf{f}^\top L \mathbf{f}$ leads to assigning the same label to both examples.

2.2.2 Online Semi-Supervised Learning

The online learning formulation of SSL is suitable for *adaptive* machine learning systems. In this setting, a few labeled examples are provided in advance and set the initial bias of the system while unlabeled examples are gathered online and update the bias continuously. In the online setting, learning is viewed as a repeated game against a potentially adversarial nature. At each step t of this game, we observe an example \mathbf{x}_t , and then predict its label \hat{y}_t . The challenge of the game is that after it started we do not observe the true label y_t . Thus, if we want to adapt to changes in the environment, we have to rely on indirect forms of feedback, such as the structure of data.

Despite the usefulness of this paradigm for practical adaptive algorithms [Grabner et al., 2008, Goldberg et al., 2008], there is not much success in applying this paradigm to realistic problems, especially when data arrive at a high rate such as in video applications. [Grabner et al., 2008] applies online semi-supervised boosting to object tracking, but uses a heuristic method to greedily label the unlabeled examples. This method learns a binary classifier, where one of the classes explicitly models outliers. In comparison, our approach is multi-class and allows for implicit modeling of outliers. The two algorithms are compared empirically in Section 6.1.5. [Goldberg et al., 2008] develop an online version of manifold regularization of SVMs. Their method learns max-margin decision boundaries, which are additionally regularized by the manifold. Unfortunately, the approach was never applied to a naturally online learning problem, such as adaptive face recognition. Moreover, while the method is sound in principle, no theoretical guarantees are provided.

[Goldberg et al., 2011] combine semi-supervised learning and active learning in a unified framework. Unlike our work which builds on manifold assumption, they exploit cluster (or gap) assumption, [Chapelle et al., 2006]. The authors present a Bayesian model for this learning setting and use a sequential Monte Carlo approximation for efficient online Bayesian update.

2.3 RELATED WORK IN ANOMALY DETECTION (AD)

2.3.1 Unconditional Anomaly Detection

In this section we review previous approaches for traditional anomaly detection. Traditional anomaly detection looks for examples that deviate from the rest of the data if they are not expected from some underlying model. A comprehensive review of many anomaly detection approaches can be found in [Markou and Singh, 2003a] and [Markou and Singh, 2003b].

[Scholkopf et al., 1999] proposed the one-class SVM, that only needs positive (or non-anomalous) examples to learn the margin. The idea is that the space origin (zero) is treated as the only example of the ‘negative’ class. In that way, the learning essentially estimates the support of the distribution. The data that do not fall into this support have negative projections and can be considered anomalous.

[Eskin, 2000] assumes that the number of anomalies is significantly lower than the number of normal cases. The author defines a distribution for the data as a mixture of majority (M) and anomalous distribution(A): $D = (1 - \lambda)M + \lambda A$. He then iteratively partitions the dataset into the majority set M_t and the anomalous set A_t . At the beginning $A_0 = \emptyset, M_0 = D$. At each step t , it is determined whether the case x_t is an anomaly. x_t is considered anomalous if its displacement to the anomaly set ($M_t = M_{t-1} \setminus \{x\}$ and $A_t = A_{t-1} \cup \{x\}$) increases the log-likelihood LL_{t-1} of the dataset by a predefined threshold c . If $LL_t - LL_{t-1} \leq c$, x_t remains marked as a normal case ($M_t = M_{t-1}$ and $A_t = A_{t-1}$). At the end, we get the final partition of D into a normal set and an anomalous set.

The curse of high dimensionality is of concern in [Aggarwal and Yu, 2001]. The authors search for the abnormal lower dimensional projections by dividing each attribute into the equi-depth (the same range of f cases) ranges. Assuming statistical independence, each k -dimensional sub-cube in this grid should contain the fraction of f^k of total cases. The authors then search for k -dimensional sub-cubes, where the presence of points is significantly lower than expected. As the brute force search for projections is computationally infeasible, the authors use genetic algorithms to perform the search.

In [Breunig et al., 2000], the authors expand k -distance (distance to the k nearest

neighbor) to get the so-called reachability distance for the object O with respect to p as $\text{reach_dist}(O, p) = \max(k_distance(p), \text{dist}(O, p))$. Using this smoothed distance, they define the *local outlier factor* (LOF), which expresses the degree of the considered object being an outlier with respect to its neighborhood. LOF depends on *MinPts*, the number of nearest points to define a local neighborhood. Although this is data-dependent, the authors propose to calculate the maximum LOF for *MinPts* within a reasonable range (which was 30–50 in their experiments) and threshold. The bigger the LOF the more anomalous the object is. The authors give bounds for LOF and prove they are tight for important cases. For example, LOF is close to one for objects within the clusters. A useful property of LOFs is that it works well with cluster of different densities.

[Lazarevic and Kumar, 2005] applies a bagging approach to improve the performance of local (nearest neighbor) anomaly detectors. In every round of the algorithm a subset of features is selected and a local anomaly detector (such as LOF [Breunig et al., 2000]) is applied. Every round produces a scoring of all data, which is at the end merged to get a final score using either breadth-first or cumulative-sum approach.

[Syed and Rubinfeld, 2010] use a minimum enclosing ball approach to detect anomalies in clinical data similar to the data that we use in this work. The authors learn a minimum volume hypersphere that encloses the data for all patients. The anomaly score is defined as the distance from the center. They showed that this unsupervised approach performed similarly to the supervised approaches with prelabeled examples (Section 2.3.1.1).

[Akoglu et al., 2010] performs anomaly detection on weighted graphs when nodes do not follow discovered power laws between the number of neighbors and the properties of the local neighborhood subgraph (total number of edges, total weight, and the principal eigenvalue of the weighted adjacency graph). The outlier score is defined as a distance to the fitting line. To account for the points that fit the line but are far away from all other examples, the authors combine their methods with a density based method, such as LOF [Breunig et al., 2000].

[He et al., 2007] is a semi-supervised method that propagates the labels until a heuristic stopping criterion is reached. Moreover, it uses unlabeled data to better estimate the prior in the case that the empirical distribution is skewed from the true distribution.

[[Moonesignhe and Tan, 2006](#)] use random walks to detect outliers. They build their similarity matrix either by cosine similarity or by a number of shared neighbors after thresholded cosine similarity. Anomalous nodes are identified as those with low connectivity. Connectivity is calculated using the Markov chain with the similarity as a transition matrix. Starting from the uniform connectivity assigned at step 0, connectivity is spread according to the similarity matrix until convergence.

2.3.1.1 Approaches with prelabeled anomalies [[Chawla et al., 2003](#)] combine a boosting scheme with SMOTE (Synthetic Minority Over-sampling TEchnique). They do that in every iteration of smoothing. For continuous data, SMOTE generates a new sample by sampling a data point and one of its k nearest neighbors and taking a random point on segment between them in the space. For discrete data, a new point is created as a majority vote of the k nearest neighbors for each feature. The authors show improvement with this method over just smoothing, just SMOTE and applying SMOTE once before the boosting for a minority class. The SMOTEboost approach generally improves recall but does not cause significant degradation in precision, thus improving the F-measure.

[[Ma and Perkins, 2003](#)] use support vector regression to learn the underlying temporal model (time event is modeled as a linear regression function of the previous events). A surprise is defined as the value outside the tolerance range. Given the fixed length of the event, a probability of number of surprises actually happening is calculated. When that is too small, an anomaly is declared.

2.3.1.2 Rare category detection [[Pelleg and Moore, 2005](#)] aim to detect rare category which presumably correspond to the interesting anomalies in a pool-based active learning framework. After a human expert labels some examples, the Gaussian mixture is fit to the data. Different hinting heuristics are then used to propose the new examples to be labeled by the expert. The authors propose *interleave* heuristics which takes one example per mixture a time with low fit probability, not taking to account any mixture weight. This heuristic appears to be superior to the low-likelihood one (suggesting examples with the overall low fit probability) and ambiguous one (suggesting examples with uncertain class membership).

[He and Carbonell, 2008] attempt to detect rare categories in the data, assuming that examples from the rare category are self-similar, tightly grouped, and we have some knowledge about the class priors. The nearest neighbor based statistic is used to actively sample points corresponding to points with the maximum change in the local density.

2.3.2 Conditional Anomaly Detection (CAD)

We start with a short summary of our work. In [Hauskrecht et al., 2007], we introduce the concept of the conditional anomaly detection (CAD) and show its potential for the medical records. For each case, we take its nearest neighbors and learn a Bayesian belief network (BBN) or a naïve Bayes model (NB) from them. The cases with low class-conditional probabilities were deemed anomalous. We discovered that while for BBN it was better to use all the cases for learning, for a more restricted NB a small neighborhood was beneficial. The main problem with learning the structure of BBN is that it does not scale beyond a couple dozen features. In [Valko and Hauskrecht, 2008], we show the benefit of distance metric learning for the selection of closest cases. We also use the softmax model [McCullagh and Nelder, 1989] to calculate the class-conditional probability of a probabilistic one nearest neighbor (similar to [Goldberger et al., 2004]) for this purpose. In [Valko et al., 2008], we introduce a new anomaly measure based on the distance from the hyperplane learned by SVM [Vapnik, 1995] and perform the initial experiments on the PCP (Section 6.2.2) dataset. We later conduct an extensive human evaluation study with a panel of 15 physicians in [Hauskrecht et al., 2010]. Aside from our work which will be reviewed in more detail in later chapters, we also describe other early work along these lines.

[Valizadegan and Tan, 2007] use the kernel based weighted nearest neighbor approach to jointly estimate the probabilities of the examples being mislabeled. The joint estimation is posed as an optimization problem and solved with Newton methods. A regularization is needed to avoid one of the classes deemed to be completely mislabeled.

In [Song et al., 2007], a user defines a partitioning of the features into two groups: the **indicator** features — those that can be directly indicative of an anomaly and the **environmental** features, which cannot, but can influence the indicator features. The indicator (y)

and the environmental (x) variables are modeled separately both as the mixtures of multivariate Gaussians ($y \sim U$ and $x \sim V$). A mapping function is defined between those mixtures as the probability of choosing a Gaussian for an indicator variable given an environmental one $p(V_j|U_i)$. The authors assume the following generative process for a datapoint $\langle x, y \rangle$: If x is a sample from U_i then a die is tossed, according to $p(V_j|U_i)$, to determine which Gaussian from V will produce y and subsequently y is produced. Since it is not known, which U_i the x was sampled from, the likelihood of $f_{CAD}(y|\Theta, x)$ is computed as a weighted sum over Gaussians U_i . The model is learned via EM, either directly — optimizing all parameters at once (named as DIRECT), optimizing first parameters for Gaussians and then for the mapping function (FULL), or optimizing the indicator Gaussians, the environmental Gaussians and the mapping function separately (SPLIT).

The work on cross-outlier detection [Papadimitriou and Faloutsos, 2003] is also related to CAD. Papadimitriou and Faloutsos [Papadimitriou and Faloutsos, 2003] defined the notion of the cross-outliers as examples that seem normal when considering the distribution of examples from the assigned class, but are abnormal when considering the samples from the other class. For each sample (\mathbf{x}, y) , they compute two statistics based on the similarity of \mathbf{x} to its neighborhood from the samples belonging to class y and samples not belonging to class y . An example is considered anomalous if the first statistic is significantly smaller than the second statistic. Unfortunately, the method is not very robust to fringe points (Figure 5) [Papadimitriou and Faloutsos, 2003].

In his dissertation, [Das, 2009] aims to detect several kinds of individual and group anomalies. The approaches relevant to this work are *conditional* and *marginal* methods for individual record anomalies, ignoring rare values. For the data t and the subsets of attributes (A, B, C) he computes the ratios of the form $\frac{P(A, B)}{P(A)P(B)}$ for the marginal method and $\frac{P(A, B|C)}{P(A|C)P(B|C)}$ for the conditional method. The goal is to find unusual occurrences of the attribute values. The records that have low ratios are considered anomalous. The normalization of the joint probabilities by the marginal probabilities takes care of rare records, because those also have small marginals. The dissertation describes several speedups to compute the ratios for exponentially many subgroups to allow the methods to scale up.

3.0 SEMI-SUPERVISED LEARNING

Semi-supervised learning (SSL) is a field of machine learning that studies learning from both labeled and unlabeled examples. This learning paradigm is suitable for real-world problems, where data is often abundant but the resources to label them are limited. As a result, many semi-supervised learning algorithms have been proposed in the past few years [Zhu, 2008]. The closest to this work are semi-supervised support vector machines (S3VMs) [Bennett and Demiriz, 1999], manifold regularization of support vector machines (SVMs) [Belkin et al., 2006], and harmonic function solutions on data adjacency graphs [Zhu et al., 2003].

SSL is very closely related to transductive inference (Chapters 24 and 25 in [Chapelle et al., 2006]). In both approaches we have access to the unlabeled examples that we can take advantage of. Traditionally in SSL, we want to use the unlabeled data to learn a function f that can be later used to classify previously unseen examples. We present one such approach where we combine the harmonic solution on a data similarity graph with a max-margin inference in Section 3.3. In other scenarios, we may not need to learn such a function. In this case, we can focus just on classifying the unlabeled examples at hand. Even then, the prediction on unseen examples is still possible using out of sample extension methods [Bengio et al., 2004].

In this dissertation we study graph-based methods for SSL, because they can model complex interactions between the examples. However, graph-based methods (such as label propagation) do not scale beyond several thousand examples unless we use parallel architectures. One of the solutions is to reduce the number of nodes and create a representative back-bone graph. Typically, one can downsample the data or use some quantization technique (such as k -means) to come up with a smaller graph. Yet these approaches do

not consider the quality of semi-supervised learning inference for this backbone graph. In Section 3.4 we introduce a new objective function that lets us incorporate the quality of inferences into the construction of the backbone graph.

Furthermore, in Section 3.5 we investigate an online learning formulation of SSL, which is suitable for *adaptive* machine learning systems. In this setting, a few labeled examples are provided in advance and set the initial bias of the system, while unlabeled examples are gathered online and update the bias continuously. In the online setting, learning is viewed as a repeated game against a potentially adversarial nature. At each step t of this game, we observe an example \mathbf{x}_t and then predict its label \hat{y}_t . The challenge of the game is that after it started we do not observe the true label y_t . Thus, if we want to adapt to changes in the environment, we have to rely on indirect forms of feedback, such as the structure of data. When data arrive in a stream, the dual problems of computation and data storage arise for any SSL method. We therefore propose a fast approximate online SSL algorithm that solves for the harmonic solution on an approximate graph.

For all our methods, we introduce the regularized harmonic solution (Section 3.2) to achieve better stability properties. With such regularization, we can control the confidence of labeling unlabeled examples and discount the outliers in the data. In the following, we start with some needed background in graph theory and then continue with the just mentioned approaches for SSL.

3.1 GRAPHS AS DATA MODELS

Many of the methods presented here are based on a graph representation of the data. Having some data, we create a undirected weighted graph $G = (V, E)$ with set of vertices V and set of edges E , associating every data point with a graph vertex. Next, we define a non-negative weight function $V \times V \rightarrow \mathbb{R}$ such that $w_{ij} = w_{ji}$. In the case that $\{i, j\} \notin E(G)$, $w_{ij} = 0$. Let the similarity matrix $W = \{w_{ij}\}$ denote a matrix of all edge weights which encode how similar the vertices are to each other. We define degree d_i of the vertex i as the sum of all edges coinciding with i :

$$d_i = \sum_j w_{ij}$$

and the diagonal matrix D with $D_{ii} = d_i$. Let volume $\text{vol}(G)$ of graph G be the sum of all its weights:

$$\text{vol}(G) = \text{vol}(W) = \sum_i d_i = \sum_{i,j} w_{ij}$$

Now, let us define an unnormalized graph Laplacian L as

$$L(G) = L(W) = D - W$$

and the symmetric normalized graph Laplacian as

$$L_{\text{sym}}(G) = L_{\text{sym}}(W) = D^{-\frac{1}{2}} L D^{-\frac{1}{2}} = I - D^{-\frac{1}{2}} W D^{-\frac{1}{2}}.$$

It can be easily shown that for any $\mathbf{h} \in \mathbb{R}^n$:

$$\mathbf{h}^\top L \mathbf{h} = \frac{1}{2} \sum_{i,j} w_{ij} (h_i - h_j)^2.$$

3.1.1 Stationary Distribution of a Random Walk

Here we describe a way to compute a stationary distribution of a (non-absorbing) random walk on the data similarity graph in a closed form. Let us define the random walk as follows: In every step of a random walk, we jump from a node to its neighbors, proportionally to their mutual weight:

$$P(\mathbf{x}_i \rightarrow \mathbf{x}_j) = \frac{W_{ij}}{\sum_{j'} W_{ij'}}$$

Let D be the diagonal matrix with the sum of weights W on the diagonal: $D_{ii} = \sum_{j'} W_{ij'}$ for all i . The transition matrix of this random walk is $P = D^{-1}W$. The approximation we use here is that we estimate the class conditional probability with the proportion of the time that the random walk spends in the evaluated example [Lee and Wasserman, 2010]. We can calculate this proportion from the stationary distribution of this random walk [Chung,

1997]. Let s be a row vector of the stationary distribution of a random walk with the transition matrix P . For a stationary distribution s , it has to hold that $sP = s$. Note that $\mathbf{1}D = \mathbf{1}W$, where $\mathbf{1}$ is all one row vector. It is easy to verify that

$$s = \frac{\mathbf{1}W}{\text{vol}(W)} \quad (3.1)$$

satisfies the definition:

$$sP = \frac{\mathbf{1}WP}{\text{vol}(W)} = \frac{\mathbf{1}DP}{\text{vol}(W)} = \frac{\mathbf{1}DD^{-1}W}{\text{vol}(W)} = \frac{\mathbf{1}W}{\text{vol}(W)} = s$$

The equation (3.1) enables us to compute the stationary distribution in a closed form.

3.2 REGULARIZED HARMONIC FUNCTION

In this section, we build on the harmonic solution [Zhu et al., 2003]. Moreover, we show how to regularize it such that it can interpolate between semi-supervised learning (SSL) on labeled examples and SSL on all data. A standard approach to SSL on graphs is to minimize the quadratic objective function

$$\begin{aligned} \min_{\ell \in \mathbb{R}^n} \quad & \ell^\top L \ell \\ \text{s.t.} \quad & \ell_i = y_i \text{ for all } i \in l; \end{aligned} \quad (3.2)$$

where ℓ denotes the vector of predictions. Using the notation from Section 3.1, this problem has a closed-form solution:

$$\ell_u = (D_{uu} - W_{uu})^{-1} W_{ul} \ell_l,$$

which satisfies the *harmonic property* $\ell_i = \frac{1}{d_i} \sum_{j \sim i} w_{ij} \ell_j$ ($i \sim j$ denotes that i neighbors j), and therefore is commonly known as the *harmonic solution*.

Since the solution can be also computed as:

$$\ell_u = (I - P_{uu})^{-1} P_{ul} \ell_l,$$

it can be viewed as a product of a random walk on the graph W with the transition matrix $P = D^{-1}W$. The probability of moving between two arbitrary vertices i and j is w_{ij}/d_i , and the walk terminates when the reached vertex is labeled. Therefore, the harmonic solution is a form of *label propagation* on the data similarity graph. Each element of the solution is given by:

$$\begin{aligned}\ell_i &= (I - P_{uu})_{iu}^{-1} P_{ul} \ell_l \\ &= \underbrace{\sum_{j:y_j=1} (I - P_{uu})_{iu}^{-1} P_{uj}}_{p_i^{(+1)}} - \underbrace{\sum_{j:y_j=-1} (I - P_{uu})_{iu}^{-1} P_{uj}}_{p_i^{(-1)}} \\ &= p_i^{(+1)} - p_i^{(-1)},\end{aligned}$$

where p_i^{+1} and p_i^{-1} are probabilities by which the walk starting from the vertex i ends at vertices with labels $+1$ and -1 , respectively. Therefore, when ℓ_i is rewritten as $|\ell_i| \text{sgn}(\ell_i)$, $|\ell_i|$ can be interpreted as a *confidence* in assigning the label $\text{sgn}(\ell_i)$ to the vertex i . The maximum value of $|\ell_i|$ is 1, and it is achieved when either $p_i^{+1} = 1$ or $p_i^{-1} = 1$. The closer the confidence $|\ell_i|$ is to 0, the closer the probabilities p_i^{+1} and p_i^{-1} are to 0.5, and the more *uncertain* the label $\text{sgn}(\ell_i)$ is.

We propose to control the confidence of labeling by regularizing the Laplacian L as $L + \gamma_g I$, where γ_g is a scalar and I is the identity matrix. Similarly to (3.2), the corresponding problem

$$\begin{aligned}\min_{\ell \in \mathbb{R}^n} \quad & \ell^\top (L + \gamma_g I) \ell \\ \text{s.t.} \quad & \ell_i = y_i \text{ for all } i \in l;\end{aligned}\tag{3.3}$$

can be computed in a closed form

$$\ell_u = (L_{uu} + \gamma_g I)^{-1} W_{ul} \ell_l.\tag{3.4}$$

and we will refer to it as *regularized HS*. It can be also interpreted as a random walk on the graph W with an extra sink. At every step, a walk at node x_i may terminate at the sink with probability $\gamma_g/(d_i + \gamma_g)$ where d_i is the degree of the current node in the walk. Therefore, the scalar γ_g essentially controls how the ‘confidence’ $|\ell_i|$ of labeling unlabeled vertices

decreases with the number of hops from labeled vertices. The proposed regularization will essentially drive the confidence of distant vertices to zero.

3.2.1 Soft Harmonic Solution

A related problem to (3.2) is when the constraints representing the fit to the data are enforced in a soft manner [Cortes et al., 2008]. In such a case, we are able to bound the generalization error of the solution (Section 5.1). Moreover, the soft harmonic solution can be used for label propagation in case of noise labels (Section 4.6.2). One way of enforcing the fit constraints in a soft manner is by solving a following problem:

$$\ell^* = \min_{\ell \in \mathbb{R}^n} (\ell - \mathbf{y})^\top C (\ell - \mathbf{y}) + \ell^\top K \ell, \quad (3.5)$$

where $K = L + \gamma_g I$ is the regularized Laplacian of the similarity graph, C is a diagonal matrix such that $C_{ii} = c_l$ for all labeled examples, and $C_{ii} = c_u$ otherwise, and \mathbf{y} is a vector of pseudo-targets such that y_i is the label of the i -th example when the example is labeled, and $y_i = 0$ otherwise. The appealing property of (3.5) is that its solution can be computed in closed form as follows [Cortes et al., 2008]:

$$\ell^* = (C^{-1}K + I)^{-1} \mathbf{y} \quad (3.6)$$

We will use soft harmonic solution (3.5) particularly in the theoretical analysis in Chapter 5.

Several examples of how γ_g affects the regularized solution are shown in Figure 3. Figure 3a shows an example of a simple data adjacency graph. The vertices of the graph are depicted as dots. The bigger dots in the middle are labeled vertices. The edges of the graph are shown as dotted lines and weighted as $w_{ij} = \exp[-\|\mathbf{x}_i - \mathbf{x}_j\|_2^2/2]$. Figure 3b. shows three regularized harmonic function solutions on the data adjacency graph from Figure 3a. The plots are cubic interpolations of the solutions. The dark (or pink and blue) colors denote parts of the feature space \mathbf{x} where $\ell_i > 0$ and $\ell_i < 0$, respectively. The light (or yellow) color marks regions where the confidence $|\ell_i|$ is less than 0.05. When $\gamma_g = 0$, the solution turns into the ordinary harmonic function solution. When $\gamma_g = \infty$, the confidence of labeling unlabeled vertices decreases to zero. Finally, note that our regularization corresponds to in-

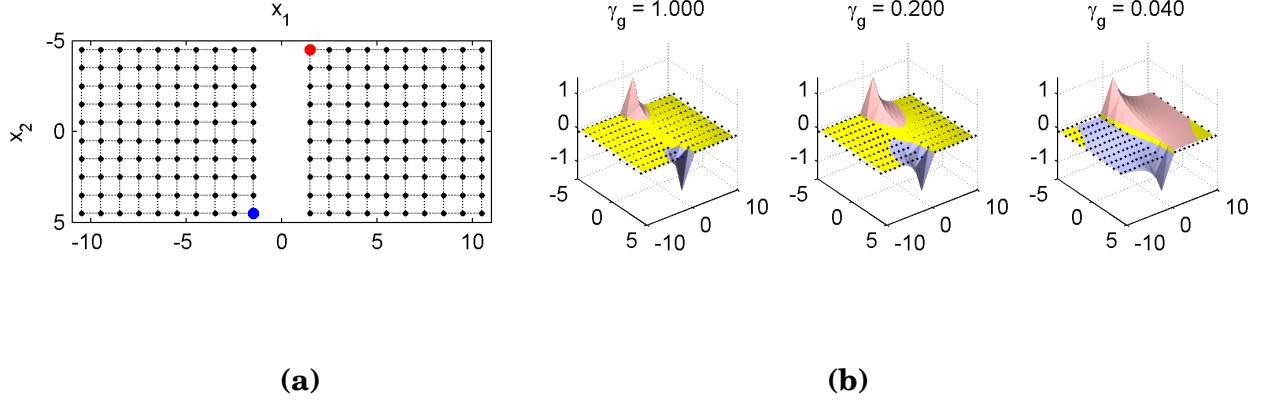


Figure 3: **a.** Similarity graph **b.** Three regularized harmonic solutions

creasing all eigenvalues of the Laplacian L by γ_g [Smola and Kondor, 2003]. In Section 5.2 we use this property to bound the generalization error of our solutions.

3.3 MAX-MARGIN GRAPH CUTS

In this part we present our algorithm that combines the harmonic solution with max-margin learning to learn a classifier f from some *reproducing kernel Hilbert space (RKHS)*. In the scenarios, where we do not want to store all the examples in the dataset and perform the inference transductively when the new data arrive, we may prefer to learn such f instead. Our semi-supervised learning algorithm involves two steps. First, we obtain the regularized harmonic function solution ℓ^* (3.4). The solution is computed from the system of linear equations $(L_{uu} + \gamma_g I)\ell_u = W_{ul}\ell_l$. This system of linear equations is sparse when the data adjacency graph W is sparse. Second, we learn a max-margin discriminator, which is conditioned on the labels induced by the harmonic solution. The optimization problem is given

by:

$$\begin{aligned}
& \min_{f \in \mathcal{H}_K} \sum_{i: |\ell_i^*| \geq \varepsilon} V(f, \mathbf{x}_i, \text{sgn}(\ell_i^*)) + \gamma \|f\|_K^2 \\
& \text{s.t. } \ell^* = \arg \min_{\ell \in \mathbb{R}^n} \ell^\top (L + \gamma_g I) \ell \\
& \text{s.t. } \ell_i = y_i \text{ for all } i \in l;
\end{aligned} \tag{3.7}$$

where $V(f, \mathbf{x}, y) = \max\{1 - yf(\mathbf{x}), 0\}$ denotes the *hinge loss*, \mathcal{H}_K , and $\|\cdot\|_K$ is the norm that measures the complexity of f .

The training examples $\{\mathbf{x}_i\}$ in our problem are selected based on our confidence into their labels. When the labels are highly *uncertain*, which means that $|\ell_i^*| < \varepsilon$ for some small $\varepsilon \geq 0$, the examples are excluded from learning. Note that as the regularizer γ_g increases, the values $|\ell_i^*|$ decrease towards 0 (Figure 3), and the ε thresholding allows for smooth interpolations between supervised learning on labeled examples and semi-supervised learning on all data. The trade-off between the regularization of f and the minimization of hinge losses $V(f, \mathbf{x}_i, \text{sgn}(\ell_i^*))$ is controlled by the parameter γ .

Due to the representer theorem [Wahba, 1999], the optimal solution f^* to our problem has a special form:

$$f^*(\mathbf{x}) = \sum_{i: |\ell_i^*| \geq \varepsilon} \alpha_i^* k(\mathbf{x}_i, \mathbf{x}),$$

where $k(\cdot, \cdot)$ is a Mercer kernel associated with the RKHS \mathcal{H}_K . Therefore, we can apply the kernel trick and optimize rich classes of discriminators in a finite-dimensional space of $\alpha = (\alpha_1, \dots, \alpha_n)$. Finally, note that when $\gamma_g = \infty$, our solution f^* corresponds to supervised learning with SVMs.

In some aspects, manifold regularization (Section 2.2.1.2) is similar to max-margin graph cuts. In particular, note that its objective (2.2) is similar to the regularized harmonic function solution (3.3). Both objectives involve regularization by a manifold, $\mathbf{f}^\top L \mathbf{f}$ and $\ell^\top L \ell$, regularization in the space of learned parameters, $\|f\|_K^2$ and $\ell^\top I \ell$, and some labeling constraints $V(f, \mathbf{x}_i, y_i)$ and $\ell_i = y_i$. Since max-margin graph cuts are learned conditionally on the harmonic function solution, the problems (3.7) and (2.2) may sometimes have similar solutions. A necessary condition is that the regularization terms in both objectives are

weighted in the same proportions, for instance, by setting $\gamma_g = \gamma/\gamma_u$. We adopt this setting when manifold regularization of SVMs is compared to max-margin graph cuts in Section 6.1.3.

3.4 JOINT QUANTIZATION AND LABEL PROPAGATION

Graph-based semi-supervised learning methods do not scale well to large data sets, mainly because their inference procedures require the computation of the inverse of an $n \times n$ matrix, where n is the size of the underlying graph that is equal to the size of the dataset. A typical solution to address this problem is to downsize the graph to a smaller *backbone* graph and perform the inference on this reduced representation. The key challenge is to decide on what elements should be included in the backbone graph. Typical solutions include sub-sampling, clustering, or a Nyström approximation. However, these techniques do not consider the quality of semi-supervised learning inferences for this backbone graph. We introduce a new objective function that lets us incorporate the quality of inferences into the construction of the backbone graph.

To reduce the computational complexity of (3.5), we replace all n nodes of the similarity graph G with a set $C = [\mathbf{c}_1, \dots, \mathbf{c}_m, \dots, \mathbf{c}_{m+k}]^\top$ of $(m+k) \ll n$ representative nodes to create a backbone graph \tilde{G} . Notice that $\mathbf{c}_i = \mathbf{x}_i$ for $i = 1, \dots, m$. We want to find \tilde{G} such that it is a good representation of G in constructing the manifold. Let us assume for a moment that we do know the best set of examples \tilde{G} . Then, Equation (3.5) becomes:

$$\ell^* = \operatorname{argmin}_{\ell \in \mathbb{R}^n} (\ell - \mathbf{y})^\top F^C (\ell - \mathbf{y}) + \ell^\top L^C \ell. \quad (3.8)$$

In general, $C \in \mathbb{R}^{(m+k) \times d}$ can be obtained by fixing the first m labeled examples and choosing k unlabeled points by subsampling the dataset, clustering or other means of quantization. As mentioned earlier, the common approach is to select the set C first and only then perform the inference (3.8). In this work, we will perform both the quantization and the inference jointly by adding the quantization penalty of the elastic nets to the objective function in (3.8). As we will see in Section 5.3, this simple joint approach will produce interesting properties.

The new objective function is:

$$[\ell^*, \{c_j\}_{j=m+1}^{m+k}] = \operatorname{argmin}_{\ell \in \mathbb{R}^n, \{c_j\}_{j=m+1}^{m+k}} (\ell - \mathbf{y})^\top F^C (\ell - \mathbf{y}) + \ell^\top L^C \ell \gamma_q \left(\frac{(m+k)^2}{n} \sum_{x_i \in K_j} \|c_j - x_i\|^2 \right) \quad (3.9)$$

where K_j is the set of examples for which c_j is the nearest centroid and γ_q is a cost parameter for the quantization penalty. We emphasize that we automatically consider all labeled examples as a fixed part of C and the optimization to learn the representing centroids are affected by the position of labeled examples. As we will see in Section 5.3, the above objective function has an interesting property: when optimized to find the centroids, it learns the principle manifold.

Adding the quantization penalty makes the objective function non-convex and hence difficult to optimize. To minimize (3.9), we propose to use an alternating optimization approach [Bezdek and Hathaway, 2002], where we alternate between 1) *label propagation* — inferring labels l on \tilde{G} , and 2) *quantization* — selecting the set C for \tilde{G} . Starting with random seeds of unlabeled examples (or the output of k -means algorithm) as the initial centroids, we iterate the following steps.

3.4.1 Label Propagation

Once C is fixed, the labels can be computed by solving the following convex optimization problem:

$$\ell^* = \operatorname{argmin}_{\ell \in \mathbb{R}^n} (\ell - \mathbf{y})^\top F^C (\ell - \mathbf{y}) + \ell^\top L^C \ell$$

This problem has a closed form solution: $\ell^* = ((F^C)^{-1} L^C + I)^{-1} \mathbf{y}$ (Section 3.2).

3.4.2 Quantization

To learn the centroids C when ℓ is fixed, first notice that:

$$\ell^\top L^C \ell = \sum_{i,j} \left(\frac{l_i}{n_i} - \frac{l_j}{n_j} \right)^2 W_{ij}^C$$

where $(n_i = 1)_{i=1}^{m+k}$ for unnormalized graph Laplacian $L = D^C - W^C$ [Luxburg, 2007] and $(n_i = \sqrt{d_i})_{i=1}^{m+k}$ for normalized graph Laplacian $L = I - D^{-1/2} W D^{-1/2}$ [Zhou et al., 2004]. Considering that $(\ell - \mathbf{y})^\top F^C (\ell - \mathbf{y})$ in (3.9) is not dependent on C , we have the following optimization problem to learn C if we use the widely used Gaussian kernel¹ as the similarity function W :

$$\{c_j\}_{j=m+1}^{m+k} = \operatorname{argmin}_{\{c_j\}_{j=m+1}^{m+k}} \sum_{i,j} \left(\frac{l_i}{n_i} - \frac{l_j}{n_j} \right)^2 \exp \left(\frac{-\|c_j - c_i\|^2}{2\sigma^2} \right) + \gamma_q \left(\frac{(m+k)^2}{n} \sum_{i \in K_j} \|c_j - x_i\|^2 \right) \quad (3.10)$$

To learn the centers by optimizing (3.10), we first approximate the exponential function using Taylor expansion²:

$$\exp \left(\frac{-\|c_j - c_i\|^2}{2\sigma^2} \right) \approx 1 - \frac{\|c_j - c_i\|^2}{2\sigma^2},$$

This results in the following optimization problem:

$$\{c_j\}_{j=m+1}^{m+k} = \operatorname{argmin}_{\{c_j\}_{j=m+1}^{m+k}} \frac{-1}{(m+k)^2} \sum_{i,j} \left(\frac{(l_i - l_j)^2}{2\sigma^2} \right) \|c_j - c_i\|^2 + \frac{\gamma_q}{n} \sum_{i \in K_j} \|c_j - x_i\|^2 \quad (3.11)$$

Taking derivatives of (3.11) with respect to $(c_j)_{j=m+1}^{m+k}$ and setting them to zero, we obtain the following system of k linear equations for $j = m+1, \dots, m+k$:

$$\sum_i c_i \frac{(l_i - l_j)^2}{(m+k)^2 \sigma^2} + c_j \left(2\gamma_q \frac{|K_j|}{n} - \sum_i \frac{(l_i - l_j)^2}{(m+k)^2 \sigma^2} \right) = \frac{2\gamma_q}{n} \sum_{i \in K_j} x_i, \quad (3.12)$$

where $|K_j|$ is the number of examples assigned to the center c_j . In order to optimize the system of linear equations in (3.12), we iterate between optimizing the centroids and the assignment of the examples to the centroids, a strategy similar to k -means.

Notice that the labeled examples c_1, \dots, c_m affect learning the centroids by

¹It is straightforward to apply similar derivation for other similarity functions.

²Notice we could also use the convexity of the exponential function to obtain an upper bound and have a more rigorous derivation. However, the results are very similar and we omit the details to simplify the description.

1. absorbing some of the unlabeled examples that are close to the labeled examples and do not need an unlabeled examples representative. In other words, in the quantization process, we remove those examples that are very close to the labeled examples;
2. controlling the position of unlabeled centers through the first term in (3.12).

Algorithm 1 outlines the *elastic-joint* algorithm.

Algorithm 1 Quantized semi-supervised learning with principal manifolds

Inputs:

examples $\{\mathbf{x}_i\}_{i=1}^n$
 labels l , such that $l_i = \pm 1$ for labeled and $l_i = 0$ for unlabeled examples
 k : number of centroids and size of the \tilde{G}
 regularizer γ_q for the quantization

Algorithm (elastic-joint):

randomly initialize the set of k centroids C
do until convergence
 infer labels on the graph:
 build a quantized data similarity graph \tilde{G} on C
 compute L^C as the graph Laplacian of \tilde{G}
 $\ell^* = \operatorname{argmin}_{\ell \in \mathbb{R}^n} (\ell - \mathbf{y})^\top F^C (\ell - \mathbf{y}) + \ell^\top L^C \ell$
 perform quantization
 calculate C by solving the following system of linear equations for $j = m+1, \dots, m+k$:

$$\sum_i c_i \frac{(l_i - l_j)^2}{(m+k)^2 \sigma^2} + c_j \left(2\gamma_q \frac{|K_j|}{n} - \sum_i \frac{(l_i - l_j)^2}{(m+k)^2 \sigma^2} \right) = \frac{2\gamma_q}{n} \sum_{i \in K_j} x_i$$

Outputs:

predictions $\hat{y} = |\ell^*|$

3.4.3 Final Inference Scheme for Unlabeled Examples

After solving the objective function in (3.9) using Algorithm 1, we need to infer the labels of unlabeled examples from the labels of the centroids. The common approach in the literature [Chapelle et al., 2006, Delalleau et al., 2005] is to use the weighted k -NN. The label of any new example x (including the unlabeled examples) is computed as follows:

$$\hat{y} = \frac{\sum_{i=1}^{m+k} W'(x, c_i) \ell_i}{\sum_{i=1}^{m+k} W'(x, c_i)} \quad (3.13)$$

where W' is a symmetric edge weighting function, such as Gaussian kernel [Chapelle et al., 2006]. We only use 1-NN for the inference, as we found that it produces the best results for the proposed method and the baselines.

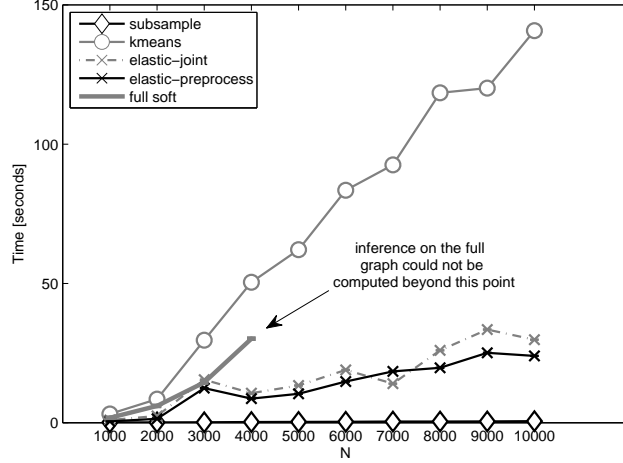


Figure 4: Running time for different methods on the SecStr dataset

3.4.4 Time Complexity

Suppose Algorithm 1 takes T iterations to converge. Each iteration has two optimization steps: 1) running SSL, and 2) constructing the backbone graph. Each run of the SSL algorithm needs the computation of the inverse of a matrix of size $n + k$ that takes $O((m + k)^3)$. Each run of the backbone graph construction iterates between two steps 1) assigning examples to centroids, and 2) solving the system of linear equations (3.11). The second step is the major step and takes $O(k^3)$ which results in $O(tk^3)$ time complexity for t iterations. Since $(m + k)^3 \geq tk^3$ for even a small number of labeled examples, the complexity of the proposed method is $O(T(m + k)^3)$. In our experiments, we found that T is usually very small; i.e. less than 10. Figure 4 shows the running time of different methods on SecStr dataset [Chapelle et al., 2006] by changing the total number of unlabeled examples from 1000 to 10000. Different quantization approaches are described in Section 6.1.4. We fixed the number of labeled examples to $m = 10$, the number of centroids to $k = 100$, and varied the number of sampled points N from the original 83679 examples. This plot clearly shows that the proposed method scales very well with the large number of examples. Also note that we used the k -means function in MATLAB, which seems extremely slow.

3.5 ONLINE SEMI-SUPERVISED LEARNING WITH QUANTIZED GRAPHS

The regularized HS (Section 3.2) is an offline learning algorithm. This algorithm can be made naïvely online by taking each new example, connecting it to its neighbors, and re-computing the HS. Unfortunately, this naïve implementation has computational complexity $O(t^3)$ at step t , and computation becomes infeasible as more examples are added to the graph.

To address the problem, we use *data quantization* [Gray and Neuhoff, 1998] and substitute the vertices in the graph with a smaller set of k distinct centroids. The resulting $t \times t$ similarity matrix W has many identical rows/columns. We will show that the *exact* HS using W may be reconstructed from a much smaller $k \times k$ matrix \tilde{W}^q , where \tilde{W}_{ij}^q contains the similarity between the i^{th} and j^{th} centroids, and a vector \mathbf{v} of length k , where v_i denotes the number of points collapsed into the i^{th} centroid. To show this, we introduce the matrix $W^q = V\tilde{W}^qV$ where V is a diagonal matrix containing the counts in \mathbf{v} on the diagonal.

Proposition 1. *The harmonic solution (3.3) using W can be computed compactly as*

$$\ell^q = (L_{uu}^q + \gamma_g V)^{-1} W_{ul}^q \ell_l,$$

where L^q is the Laplacian of W^q .

Proof: Our proof uses the electric circuit interpretation of a random walk [Zhu et al., 2003]. More specifically, we show that W and W^q represent identical electric circuits and, therefore, their harmonic solutions are the same.

In the electric circuit formulation of W , the edges of the graph are resistors with the conductance w_{ij} . If two vertices i and j are identical, then by symmetry, the HS must assign the same value to both vertices, and we may replace them with a single vertex. Furthermore, they correspond to the ends of resistors in parallel. The total conductance of two resistors in parallel is equal to the sum of their conductances. Therefore, the two resistors can be replaced by a single resistor with the conductance of the sum. A repetitive application of this rule gives $W^q = V\tilde{W}^qV$, which yields the same HS as W . In Section 3.2, we showed that the regularized HS can be interpreted as having an extra sink in a graph.

Therefore, when two vertices i and j are merged, we also need to sum up their sinks. A repetitive application of this rule yields the term $\gamma_g V$ in our closed-form solution. ■

We note that Proposition 1 may be applied whenever the similarity matrix has identical rows/columns, not just when quantization is applied. However, when the data points are quantized into a fixed number of centroids k , it shows that we may compute the HS for the t^{th} point in $O(k^3)$ time. Since the time complexity of computation on the quantized graph is independent of t , it gives a suitable algorithm for online learning.

We now describe how to perform incremental quantization with provably nearly-optimal distortion.

Algorithm 2 Online quantized harmonic solution

Inputs:

an unlabeled example \mathbf{x}_t
a set of centroids C_{t-1}
vertex multiplicities \mathbf{v}_{t-1}

Algorithm:

```

if ( $|C_{t-1}| = k + 1$ )
   $R \leftarrow mR$ 
  greedily repartition  $C_{t-1}$  into  $C_t$  such that:
    no two vertices in  $C_t$  are closer than  $R$ 
    for any  $\mathbf{c}_i \in C_{t-1}$  exists  $\mathbf{c}_j \in C_t$  such that  $d(\mathbf{c}_i, \mathbf{c}_j) < R$ 
  update  $\mathbf{v}_t$  to reflect the new partitioning
else
   $C_t \leftarrow C_{t-1}$ 
   $\mathbf{v}_t \leftarrow \mathbf{v}_{t-1}$ 
if  $\mathbf{x}_t$  is closer than  $R$  to any  $\mathbf{c}_i \in C_t$ 
   $\mathbf{v}_t(i) \leftarrow \mathbf{v}_t(i) + 1$ 
else
   $\mathbf{v}_t(|C_t| + 1) \leftarrow 1$ 
   $C_t(|C_t| + 1) \leftarrow \mathbf{x}_t$ 
build a similarity matrix  $\tilde{W}_t^q$  over the vertices  $C_t$ 
build a matrix  $V_t$  whose diagonal elements are  $\mathbf{v}_t$ 
 $W_t^q = V_t \tilde{W}_t^q V_t$ 
compute the Laplacian  $L^q$  of the graph  $W_t^q$ 
infer labels on the graph:
   $\ell^q[t] \leftarrow \operatorname{argmin}_{\ell} \ell^\top (L^q + \gamma_g V_t) \ell$ 
  s.t.  $\ell_i = y_i$  for all labeled examples up to time  $t$ 
make a prediction  $\hat{y}_t = \operatorname{sgn}(\ell_t^q[t])$ 

```

Outputs:

a prediction \hat{y}_t
a set of centroids C_t
vertex multiplicities \mathbf{v}_t

3.5.1 Incremental k -centers

We make use of the *doubling algorithm* for incremental k -center clustering [Charikar et al., 1997] which assigns points to centroids in a near optimal way. In particular, it is a $(1 + \epsilon)$ -approximation with cost measured by the maximum quantization error over all points. In Section 5.4.3, we show that under reasonable assumptions, the quantization error goes to zero as the number of centroids increases.

The algorithm of [Charikar et al., 1997] maintains a set of centroids $C_t = \{\mathbf{c}_1, \mathbf{c}_2, \dots\}$ such that the distance between any two vertices in C_t is at least R and $|C_t| \leq k$ at the end of each iteration. For each new point \mathbf{x}_t , if its distance to some $\mathbf{c}_i \in C_t$ is less than R , the point is assigned to \mathbf{c}_i . Otherwise, the distance of \mathbf{x}_t to $\mathbf{c}_i \in C_t$ is at least R and \mathbf{x}_t is added to the set of centroids C_t . If adding \mathbf{x}_t to C_t results in $|C_t| > k$, the scalar R is doubled and C_t is greedily repartitioned such that no two vertices in C_t are closer than R . The doubling of R also ensures that $|C_t| < k$.

Pseudocode of our algorithm is given in Algorithm 2. We make a small modification to the original quantization algorithm in that, instead of doubling R , we multiply it with some $m > 1$. This still yields a $(1 + \epsilon)$ -approximation algorithm as it still obeys the invariants given in Lemma 3.4 in [Charikar et al., 1997]. We also maintain a vector of multiplicities \mathbf{v} , which contains the number of vertices that each centroid represents. At each time step, the HS is calculated using the updated quantized graph, and a prediction is made.

The incremental k -centers algorithm also has the advantage that it provides a variable R , which may be used to bound the maximum quantization error. In particular, at any point in time t , the distance of any example from its centroid is at most $Rm/(m - 1)$. To see this, consider the following: As the new data arrive we keep increasing R by multiplying it by some $m > 1$. But for any point at any time, the centroid assigned to a vertex is at most R apart from the previously assigned centroid, which is at most R/m apart from the centroid assigned before, etc. Summing up, at any time, any point is at most

$$R + \frac{R}{m} + \frac{R}{m^2} + \dots = R \left(1 + \frac{1}{m} + \frac{1}{m^2} + \dots \right) = \frac{Rm}{m - 1}$$

apart from its assigned centroid, where R is the most recent one.

3.6 PARALLEL MULTI-MANIFOLD LEARNING

Most of the SSL methods that exploit the manifold assumption (such as graph-based SSL methods) assume that the data lie on a single manifold. A more plausible setting, however, is that the data lie on a mixture of manifolds [Goldberg et al., 2009]. For example, in digit recognition each digit lies on its own manifold in the feature space [Goldberg et al., 2009].

In this work, we use the multi-manifold idea from a different perspective. We assume no or little interaction between the manifolds and learn the manifolds *in parallel* to achieve a speedup in computation. The speedup is accomplished in two ways:

1. Assuming independence between the manifolds, we can solve several smaller problems instead. For example, in the ideal case (Section 5.5), the similarity matrix will consist of b block-diagonal blocks of the equal size. Therefore, to approximate the harmonic solution (HS) on a graph with n nodes which takes $\mathcal{O}(n^3)$ time, we can instead solve b HS problems on b graph with n/b nodes, each taking only $\mathcal{O}((n/b)^3)$ and achieve a polynomial speedup.
2. Using multi-core and/or multi-processor architectures, we can solve the smaller problems in parallel and achieve additional, potentially linear speedup, up to the number of cores.

Assuming the independence of the manifolds may come with a cost in accuracy when the manifolds are not independent. We study this theoretically in Section 5.5 and empirically in Section 6.1.6, where we measure the trade-off between the computational speedup and decrease in prediction accuracy.

4.0 CONDITONAL ANOMALY DETECTION

4.1 INTRODUCTION TO CONDITONAL ANOMALY DETECTION

Anomaly detection is the task of finding unusual elements in a set of observations. Most existing anomaly detection methods in data analysis are unconditional and look for outliers with respect to all data attributes [Breunig et al., 2000, Akoglu et al., 2010, Markou and Singh, 2003a, Markou and Singh, 2003b, Chandola et al., 2009]. *Conditional anomaly detection* (CAD) [Chandola et al., 2009] is the problem of detecting unusual values for a subset of variables given the values of the remaining variables. In other words, one set of variables defines the context in which the other set is examined for anomalous values.

CAD can be extremely useful for detecting unusual behaviors, outcomes, or unusual attribute pairings in many domains [Das et al., 2008]. Examples of such problems are the detection of unusual actions or outcomes in medicine [Hauskrecht et al., 2007], investments [Rubin et al., 2005], law [Aktolga et al., 2010], social networks [Heard et al., 2010], politics [Kolar et al., 2010], and other fields [Das et al., 2008]. In all these domains, the outcome strongly depends on the context (patient conditions, economy and market, case circumstances, etc.), hence the outcome is unusual only if it is compared to the examples with the same context.

In this work, we study a special case of CAD that tries to identify the unusual values for just one target variable given the values of the remaining variables (attributes). The target variable is assumed to take on a finite set of values, which we also refer to as labels, because of its similarity to the classification problems. Therefore, we refer to conditional anomalies as mislabelings [Valizadegan and Tan, 2007] or cross-outliers [Papadimitriou and Faloutsos, 2003]. Our objective is to develop robust conditional anomaly methods that

work well for high-dimensional datasets and let us capture various non-linearities in the underlying space. This work is motivated primarily by clinical and biomedical datasets and applications. These datasets are highly heterogeneous, and may include hundreds of lab results of different nature, medications, and procedures performed during hospital stay. In general, the distributions are multi-modal, reflecting many different patients' conditions [Hauskrecht et al., 2010].

4.2 DEFINITION OF CONDITIONAL ANOMALY

In general, the concept of (conditional) anomaly in data in the existing literature is somewhat ambiguous and several definitions have been proposed in the past [Markou and Singh, 2003a, Markou and Singh, 2003b]. Typically, an example is considered anomalous when it is not expected from some underlying model. A number of anomaly detection methods have been developed for this purpose (Section 2.3.1). The conditional anomaly detection (CAD) problem (Section 2.3.2) is different, but equally useful in practice. It seeks to detect unusual values for a subset of variables \mathcal{Y} given the values for the remaining variables \mathcal{X} . Since in this dissertation we focus on CAD in one variable, we provide the definition for this case only.

Intuitively, we can define a conditional anomaly as follows: Given a set of n past observed examples $(\mathbf{x}_i, y_i)_{i=1}^n$ (with possible label noise), a *conditional anomaly* is any instance i among recent m examples $(\mathbf{x}_i, y_i)_{i=n+1}^{n+m}$ for which y_i is unusual. In this statement, we assume that the past observed examples $(\mathbf{x}_i, y_i)_{i=1}^n$ are given. We do not assume that their labels are perfect; they may also be subject to the label noise.

Let us motivate a formal definition of conditional anomaly by assuming that the y_i is a continuous variable and has a standard normal distribution:

$$y_i | \mathbf{x}_i \sim \mathcal{N}(0, 1).$$

As the standard normal distribution is a unimodal distribution with zero mean, the most anomalous values are the ones with the largest absolute value. Assuming a random sample

of the size n , $Y^{(n)} = y_1, y_2, \dots, y_n$, the extreme values for this distribution correspond to the first and the n -th order statistic. The expected n -th order statistic for the standard normal can be approximated as $n \rightarrow \infty$ as [Cramér, 1999]:

$$Y_{(n)}^{(n)} \approx \sqrt{2 \ln n} \quad (4.1)$$

Therefore, the more samples we have, the larger extreme values we are likely to see and the less we should be surprised by them. This motivates our definition, which assumes some probabilistic model of data (not necessarily normal) and depends on the sample size n :

Definition 1. *Given any probabilistic model P and a random sample $(\mathbf{x}_i, y_i)_{i=1}^n$, a **conditional anomaly** of the c -level in the value y_i given \mathbf{x}_i is any instance i , such that $P(y_i|\mathbf{x}_i) = O(e^{-cn})$.*

It is not common that we would have access to such a model or that we would be able to estimate the class conditional probabilities reliably (especially in high dimensions). Therefore, in practice we may need to assess the anomalies otherwise (e.g., using human experts).

Not knowing the underlying model, which generates the (attribute, label) pairs, may lead to two major complications illustrated in Figure 5. First, a given instance may be far from the past observed data points (e.g. patient cases). Because of the lack of the support for alternative responses, it is difficult to assess the anomalousness of these instances. We refer to these instances as *isolated points*. Second, the examples on the boundary of the class distribution support may look anomalous due to their low likelihood. These boundary examples are also known as *fringe points* [Papadimitriou and Faloutsos, 2003]. We aim to avoid both of those when we look for conditional anomalies.

4.3 RELATIONSHIP TO MISLABELING DETECTION

The work on CAD, when the target variable is restricted to discrete values only, is closely related to the problem of mislabeling detection [Brodley and Friedl, 1999]. The objective in this line of work is to 1) to make a yes/no decision on whether the examples are mislabeled,

and 2) to improve the classification accuracy by removing the mislabeled examples. [Jiang and Zhou, 2004] use an ensemble of neural nets to remove suspicious samples to create a k -NN classifier. [Sanchez et al., 2003] introduce several k -NN based approaches including *Depuration*, *Nearest Centroid Neighborhood* (NCN), and *Iterative k -NCN*. [Brodley and Friedl, 1999] tried different approaches to remove the mislabeled samples, including single and ensemble classifiers. Bagging and boosting are applied in [Verbaeten and Assche., 2003] to detect and remove mislabeled examples. [Valizadegan and Tan, 2007] introduce an objective function based on the weighted k -NN approach to identify the mislabeled examples and solve it with the Newton method.

While the objective of mislabeling detection research is to improve the classification accuracy by removing or correcting mislabeled examples, the objective of CAD is different: CAD is interested in ranking examples according to the severity of conditional anomalies in the data. This is the main reason our evaluations of CAD in Chapter 6 measure the rankings of the cases being anomalous, not the improved classification accuracy when we remove them. Nevertheless, we do compare (Section 6.2) to the methods typically used in mislabeling detection.

There are various solutions to implement the conditional anomaly detection. We continue by outlining two baseline approaches.

4.4 CLASS-OUTLIER APPROACH

The simplest approach is to use one of the unconditional anomaly detection methods: For every possible class value y we learn a separate anomaly detection model M_y using only the values of \mathbf{x} attributes in the data. An example (\mathbf{x}_i, y_i) is anomalous if \mathbf{x}_i is anomalous in $M_{y=y_i}$. We refer to this approach as the *class-outlier* approach. The anomaly detection model M_y can be implemented with any unconditional anomaly detection model, such as the one-class SVM [Scholkopf et al., 1999], local outlier factor [Breunig et al., 2000] and many others [Chandola et al., 2009, Markou and Singh, 2003a, Markou and Singh, 2003b].

The class-outlier approach comes with some limitations. Such an approach detects

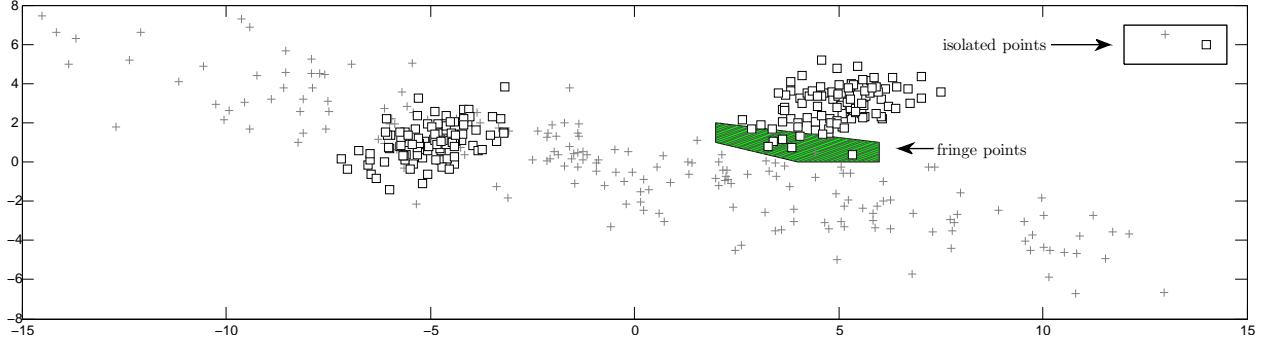


Figure 5: Challenges for CAD: 1) **fringe** and 2) **isolated** points

anomalies with respect to its class label and ignores the examples from the other classes. This may not work well for those examples for which \mathbf{x} is away from all of the classes and hence \mathbf{x} is an anomaly itself. To illustrate this, let us assume we have two classes (-1 and $+1$) and an example $(\mathbf{x}, -1)$, such that \mathbf{x} is an anomaly in $M_{y=-1}$. The class-outlier approach compares this example to all examples with the same label (-1) and declares it to be an anomaly. However, the problem is when \mathbf{x} is also an anomaly with respect to $M_{y=+1}$. In such a case it is unclear whether y should be -1 or $+1$ and hence the conclusion stating that $(\mathbf{x}, -1)$ is a conditional anomaly may be incorrect.

The other problem with class-outlier approach is that those methods often declare *fringe* points (Figure 5) as anomalies. Fringe points [Papadimitriou and Faloutsos, 2003] are points on the outer boundary of a distribution support for a specific class.

4.5 DISCRIMINATIVE APPROACH

Another approach to detect conditional anomalies is to estimate the posterior $P(y_i|\mathbf{x}_i)$ for the observed example (\mathbf{x}_i, y_i) and to use the posterior to measure how anomalous the data example is [Song et al., 2007, Hauskrecht et al., 2007, Hauskrecht et al., 2010, Valko et al., 2008]. According to Definition 1, an example is conditionally anomalous if the probability of

the opposite label for this example is high. Various classification machine learning models can be used to estimate the posterior from the past data. For example, one can use the logistic regression model or generative probabilistic models such as probabilistic graphical models that come with an immediate probabilistic interpretation. However, the output of other classification models, such as SVM, can be modified and transformed to produce a probabilistic output. For example, for the non-parametric Parzen window, the posterior probability can be estimated by summing the kernel weights for all examples with the same class label and by normalizing it with the sum of weights for all examples.

$$P(y = y_i | \mathbf{x}_i) = \frac{\sum_{y_j=y_i} K(\mathbf{x}_j, \mathbf{x}_i)}{\sum_j K(\mathbf{x}_j, \mathbf{x}_i)}$$

We will assume $y \in \{-1, +1\}$ from now on, but the generalization to the multi-class case is straightforward. Without loss of generality, we assume that the testing example \mathbf{x}_i has $y_i = +1$. We want to compute $P(y_i \neq +1 | \mathbf{x}_i)$ to see whether this quantity is not too high, which would mean that y_i is conditionally anomalous given \mathbf{x}_i . Using Bayes theorem we get:

$$P(y \neq +1 | \mathbf{x}_i) = \frac{P(\mathbf{x}_i | y = -1)P(y = -1)}{\sum_{c \in \{-1, +1\}} P(\mathbf{x}_i | y = c)P(y = c)} \quad (4.2)$$

Since we model both prior and class-conditional density, this is a generative model. In the following we present a new discriminative method that uses random walks on the data similarity graph. We then modify it to address the problem of isolated and fringe points.

4.5.1 CAD with Random Walks

The following method is an example of the discriminative approach. Let (\mathbf{x}_i, y_i) be the new example that we want to evaluate and $P(\mathbf{x}_i | y = +1)$ and $P(\mathbf{x}_i | y = -1)$ be the probabilities we want to compute for (4.2). In this part we show how we can estimate $P(\mathbf{x}_i | y)$ from the similarity graphs constructed separately for each class. A similarity graph for a set of examples is built by assigning each example to a node in the graph. The edges between the nodes and their weights represent the similarities between the examples.

To explain our method, let us consider (again, without the loss of generality) the problem of estimating $P(\mathbf{x}_i | y = +1)$. First, we take all \mathbf{x}_i from the training set such that $y_i = +1$ and

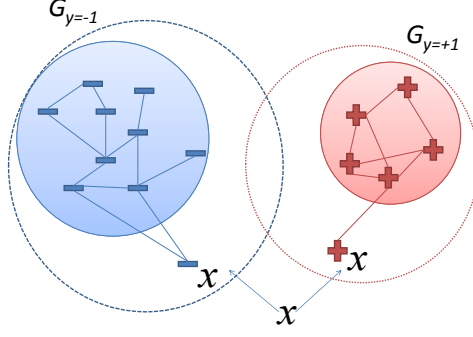


Figure 6: Estimating class-conditional probabilities from two similarity graphs

form a similarity graph using these examples. We then add the new example \mathbf{x}_i pretending that its label is $y = +1$. Let $G_{y=+1}$ be the graph we get (Figure 6). In the following we describe how we can use the stationary distribution of a random walk on $G_{y=+1}$ and use the local connectivity as an *approximation* for a density estimate [Lee and Wasserman, 2010] for $P(\mathbf{x}_i|y = +1)$. We do the same for $P(\mathbf{x}_i|y = -1)$ and plug the both estimates into (4.2) to get an estimate for $P(y \neq +1|\mathbf{x})$.

The equation (3.1) enables us to compute the stationary distribution in a closed form and ultimately allows us to compute (4.2) efficiently. Once we have the stationary distribution s of the random walk on $G_{y=+1}$ we approximate $P(\mathbf{x}_i|y = +1)$ with s_i .

4.6 REGULARIZED DISCRIMINATIVE APPROACH

We now describe how to avoid detecting the fringe and isolated points using regularization. Again, our approach considers both classes and y becomes an anomaly if its posterior probability given \mathbf{x} is small. We stress again that in this work we are not interested in isolated or fringe points. Let us consider the case of isolated points. Imagine the scenario that we get such an anomaly (\mathbf{x}_a, y_a) . If we take the approach we just described, \mathbf{x}_a will be far from $G_{y=c}$

for all c . Intuitively, the posterior (4.2) compares the weighted likelihoods of \mathbf{x}_a given the class, where weight is the class prior. If these likelihoods are estimated from the training data (and possibly from a small sample size), the estimates of $P(\mathbf{x}_a|y = -1)$ and $P(\mathbf{x}_a|y = +1)$ may become unreliable. Consequently, the relative difference between these likelihoods can strongly favor one class. Our model would then become overly confident in that \mathbf{x}_a belongs to that class. We illustrate this behavior in Section 6.2.4.3.

To alleviate these problems, we propose a new discriminative approach that penalizes instances of \mathbf{x} that are anomalies themselves. We do it by regularizing the model as follows:

$$P(y \neq +1|\mathbf{x}) = \frac{P(\mathbf{x}|y = -1)P(y = -1)}{\lambda + \sum_{c \in \{-1, +1\}} P(\mathbf{x}|y = c)P(y = c)} \quad (4.3)$$

Intuitively, λ is a placeholder for the ‘everything else’ class. We point out that this is different from the Laplace correction, which is used to smooth out probability estimates derived from the empirical counts¹. First, this regularization is applied directly to Bayes theorem and not to a probability estimate. Second, this regularization only changes the denominator of the Bayes theorem and effectively creates the aforementioned ‘everything else’ class. The λ is data dependent and can be set for example by cross-validation.

4.6.1 Regularized Random Walk CAD

We will refer to the recently proposed algorithm as the λ -regularized random walk CAD algorithm (λ -RWCAD). Algorithm 3 displays the pseudo-code of the λ -RWCAD algorithm. Notice that $\text{vol}(W^+)$ and $\text{vol}(W^-)$ are constants and can be precomputed. One of the benefits of the λ -RWCAD algorithm is that it does not require us to store the whole $n \times n$ similarity matrix. Moreover, the method requires only a nearest neighbor type of a computation, and therefore it has $O(n^2)$ time and $O(n)$ space requirements. For sparse representations of the graph, the time is reduced to $O(|E|)$, where $|E|$ is the number of edges in the graph. On the other hand, many other graph-based algorithms require quadratic space, and their time complexity is related to the computation of the inverse of $n \times n$ matrix which is $\Omega(n^2)$ and $O(n^{2.807})$ in most practical implementations². Finally, modeling the data distribution with a

¹ $P(y = k) = (N_k + \lambda) / (\sum_k N_k + K\lambda)$, where K is the number of classes and N_k are the corresponding counts.

²The complexity can be improved to $O(n^{2.376})$ by using the Coppersmith-Winograd algorithm.

graph can be extended to online learning [Kivinen et al., 2002]. Unlike the label propagation methods that require us to store the whole $O(n^2)$ weight matrix ($O(|E|)$ when it is sparse) for the future computations, our method requires only a summary statistic for each vertex, which is $O(n)$.

Algorithm 3 RWCAD that calculates the anomaly score

Inputs:

new example (\mathbf{x}_e, y_e)
similarity metric $K(\cdot, \cdot)$
 $\text{vol}(W^+) = \sum_{y_i=y_j=+1} W_{ij}$
 $\text{vol}(W^-) = \sum_{y_i=y_j=-1} W_{ij}$
regularization coefficient λ

Algorithm:

$W_{i\mathbf{x}_e}^+ = K(\mathbf{x}_i, \mathbf{x}_e), \forall i \text{ positive}$
 $W_{i\mathbf{x}_e}^- = K(\mathbf{x}_i, \mathbf{x}_e), \forall i \text{ negative}$
 $P(\mathbf{x}_e | y = +1) = \sum_i W_{i\mathbf{x}_e}^+ / \left(\text{vol}(W^+) + 2 \times \sum_i W_{i\mathbf{x}_e}^+ \right)$
 $P(\mathbf{x}_e | y = -1) = \sum_i W_{i\mathbf{x}_e}^- / \left(\text{vol}(W^-) + 2 \times \sum_i W_{i\mathbf{x}_e}^- \right)$
 $P(y \neq y_e | \mathbf{x}_e) = \frac{P(\mathbf{x}_e | y \neq y_e) P(y \neq y_e)}{\lambda + \sum_{c \in \{-1, +1\}} P(\mathbf{x}_e | y=c) P(y=c)}$

Outputs:

$P(y \neq y_e | \mathbf{x}_e)$

4.6.2 Conditional Anomaly Detection with Soft Harmonic Functions

In this section we show how to solve the CAD problem using label propagation on the data similarity graph and how to compute the anomaly score. In particular, we will build on the harmonic solution approach (Section 3.2.1) and adopt it for CAD in the following ways: 1) show how to compute the confidence of mislabeling, 2) add a regularizer to address the problem of isolated and fringe points, 3) use soft constraints to account for a fully labeled setting, and 4) describe a compact computation of the solution from a quantized backbone graph.

The label propagation method described in Section 3.2.1 can be applied to CAD by considering all observed data as labeled examples with no unlabeled examples. The setting for matrix C is dependent on the quality of the past observed data. If the labels of the past observed data (or any example from the recent sample) are guaranteed to be correct, we set the corresponding diagonal elements of C to a large value to make their labels fixed. Notice

that specific domain techniques can be utilized to make sure that the collected examples from the past observed data have correct labels. We assume that we do not have the access to such prior knowledge and therefore, the observed data are also subject to label noise.

We now propose a way to compute the anomaly score from (3.6). The output ℓ^\star of (3.5) for the example i can be rewritten as:

$$\ell_i^\star = |\ell_i^\star| \times \text{sgn}(\ell_i^\star) \quad (4.4)$$

SSL methods use $\text{sgn}(\ell_i^\star)$ in (4.4) as the predicted label for i . For an unlabeled example, when the value of ℓ_i is close to ± 1 , then the labeling information that was propagated to it is more consistent. Typically, that means that the example is close to the labeled examples of the respective class. The key observation, which we exploit here, is that we can interpret $|\ell_i^\star|$ as the confidence in the label. Our situation differs from SSL, as all our examples are labeled and we aim to assess the confidence of *already labeled* example. Therefore, we define the *anomaly score* as the absolute difference between the actual label y_i and the inferred soft label ℓ_i :

$$s_i = |\ell_i^\star - y_i|. \quad (4.5)$$

We will now address the problems illustrated in Figure 5. Recall that the isolated points are the examples that are (with respect to some metric) far from the majority of the data. Consequently, they are surrounded by few or no nearby points. Therefore, no matter what their label is, we do not want to report them as conditional anomalies. In other words, we want CAD methods to assign them a low anomaly score. Even when the isolated points are far from the majority data, they still can be orders of magnitudes closer to the data points with the opposite label. This can make a label propagation approach falsely confident about that example being a conditional anomaly. In the same way, we do not want to assign a high anomaly score to fringe points just because they lie on the distribution boundary. To tackle these problems we set $K = L + \gamma_g I$, where we diagonally regularize the graph Laplacian. Intuitively, such a regularization lowers the confidence value $|\ell^\star|$ of all examples; however it reduces the confidence score of far outlier points relatively more. To see this, notice (Section 6.2.3.5) that the similarity weight metric is an exponentially decreasing function of

the Euclidean distance. In other words, such a regularization can be interpreted as a label propagation on the graph with an extra sink. The sink is an extra node in G with label 0 and every other node connected to it with the same small weight γ_g . The edge weight of γ_g affects the isolated points more than other points, because their connections to other nodes are small.

In the fully labeled setting, the *hard* harmonic solution degenerates to the weighted k -NN. In particular, the hard constraints of the harmonic solution do not allow the labels to spread beyond other labeled examples. However, despite the fully labeled case, we still want to take the advantage of the manifold structure. To alleviate this problem we allow labels to spread on the graph by using soft constraints in the unconstrained regularization problem (3.5). In particular, instead of $c_l = \infty$ we set c_l to a finite constant and we set $C = c_l I$. With such a setting of K and C , we can solve (3.5) using (3.6) to get:

$$\ell^* = ((c_l I)^{-1} (L + \gamma_g) + I)^{-1} \mathbf{y} = \left(c_l^{-1} L + \left(1 + \frac{\gamma_g}{c_l} \right) I \right)^{-1} \mathbf{y}. \quad (4.6)$$

To avoid computation of the inverse,³ we calculate (4.6) using the following system of linear equations:

$$\left(c_l^{-1} L + \left(1 + \frac{\gamma_g}{c_l} \right) I \right) \ell^* = \mathbf{y} \quad (4.7)$$

We then plug the output of (4.7) into (4.5) to get the anomaly score. We will refer to this score as the SoftHAD score. Intuitively, when the confidence is high but $\text{sign}(\ell_i^*) \neq y_i$, we will consider the label y_i of the case (\mathbf{x}_i, y_i) conditionally anomalous.

Backbone graph The computation of the system of linear equations (4.7) scales with complexity⁴ $O(n^3)$. This is not feasible for a graph with more than several thousand nodes. To address the problem, we use *data quantization* [Gray and Neuhoff, 1998] and sample a set of nodes from the training data to create G . We then substitute the nodes in the graph with a smaller set of $k \ll n$ distinct centroids, which results in $O(k^3)$ computation.

We improve the approximation of the original graph with the backbone graph, by assigning different weights to the centroids. We do it by computing the multiplicities (i.e. how

³due to numerical instability

⁴The complexity can be further improved to $O(n_u^{2.376})$ with the Coppersmith-Winograd algorithm.

many nodes each centroid represents). In the following we will describe how to modify (4.7) to allow for the computation with multiplicities.

Let V be the diagonal matrix of multiplicities with v_{ii} being the number of nodes that centroid \mathbf{x}_i represents. We will set the multiplicities according to the empirical prior.

Let W^V be the compact representation of the matrix W on G , where each node \mathbf{x}_i is replicated v_{ii} times. Let L^V and K^V be the graph Laplacian and regularized graph Laplacian of W^V . Finally, let C^V be the C in (3.5) with the adjustment for the multiplicities. C^V accounts for the fact that we care about ‘fitting’ to train data according to the multiplicities. Then:

$$\begin{aligned} W^V &= VWV \\ L^V &= L(W^V) \\ K^V &= L^V + \gamma_g V \\ C^V &= V^{1/2} C V^{1/2} \end{aligned}$$

The unconstrained regularization (3.5) now becomes:

$$\ell^{V\star} = \min_{\ell \in \mathbb{R}^n} (\ell - \mathbf{y})^\top C^V (\ell - \mathbf{y}) + \ell^\top K^V \ell \quad (4.8)$$

and subsequently (4.6) becomes:

$$\begin{aligned} \ell^{V\star} &= \left((C^V)^{-1} K^V + I \right)^{-1} \mathbf{y} \\ &= \left(V^{-1/2} C^{-1} V^{-1/2} (L^V + \gamma_g V) + I \right)^{-1} \mathbf{y} \\ &= \left((c_l V)^{-1} (L^V + \gamma_g V) + I \right)^{-1} \mathbf{y} \\ &= \left(1/c_l V^{-1} L^V + c_l \gamma_g + I \right)^{-1} \mathbf{y} \end{aligned}$$

With these adjustments the anomaly score that accounts for the multiplicities is equal to $|\ell^{V\star} - \mathbf{y}|$.

5.0 THEORETICAL ANALYSIS

In this chapter, we analyze the methods proposed in Chapter 3 and Chapter 4. We will analyze mostly:

- **generalization** errors induced by harmonic solutions on the graph,
- errors induced by **quantization** of the graph to accommodate online learning, and
- errors due to the **online** setting.

5.1 SOFT HARMONIC SOLUTION

In this section we prove a bound on the generalization error of our transductive learner. The generalization error of the solution to the problem (3.6) (and also (3.5)) is bounded in Lemma 1.

Lemma 1. *Let ℓ^* be a solution to the problem:*

$$\min_{\ell \in \mathbb{R}^n} (\ell - \mathbf{y})^\top C(\ell - \mathbf{y}) + \ell^\top Q \ell,$$

where $Q = L + \gamma_g I$ and all labeled examples l are selected i.i.d. Then the inequality:

$$R_P^W(\ell^*) \leq \underbrace{\hat{R}_P^W(\ell^*) + \beta + \sqrt{\frac{2 \ln(2/\delta)}{n_l}} (n_l \beta + 4)}_{\text{transductive error } \Delta_T(\beta, n_l, \delta)}$$

$$\beta \leq 2 \left[\frac{\sqrt{2}}{\gamma_g + 1} + \sqrt{2n_l} \frac{1 - \sqrt{c_u}}{\sqrt{c_u}} \frac{\lambda_M(L) + \gamma_g}{\gamma_g^2 + 1} \right]$$

holds with probability $1 - \delta$, where:

$$R_P^w(\ell^*) = \frac{1}{n} \sum_i (\ell_i^* - y_i)^2$$

$$\hat{R}_P^w(\ell^*) = \frac{1}{n_l} \sum_{i \in l} (\ell_i^* - y_i)^2$$

are risk terms for all vertices and labeled vertices, respectively, and β is the stability coefficient of the solution ℓ^* .

Proof: To simplify the proof, we assume that $c_l = 1$ and $c_l > c_u$. Our risk bound follows from combining Theorem 1 of [Belkin et al., 2004] with the assumptions $|y_i| \leq 1$ and $|\ell_i^*| \leq 1$. The coefficient β is derived based on Section 5 of [Cortes et al., 2008]. In particular, based on the properties of the matrix C and Proposition 1 [Cortes et al., 2008], we conclude:

$$\beta = 2 \left[\frac{\sqrt{2}}{\lambda_m(Q) + 1} + \sqrt{2n_l} \frac{1 - \sqrt{c_u}}{\sqrt{c_u}} \frac{\lambda_M(Q)}{(\lambda_m(Q) + 1)^2} \right],$$

where $\lambda_m(Q)$ and $\lambda_M(Q)$ refer to the smallest and largest eigenvalues of Q , respectively, and can be further rewritten as $\lambda_m(Q) = \lambda_m(L) + \gamma_g$ and $\lambda_M(Q) = \lambda_M(L) + \gamma_g$. Our final claim directly follows from applying the lower bounds $\lambda_m(L) \geq 0$ and $(\lambda_m(L) + \gamma_g + 1)^2 \geq \gamma_g^2 + 1$. ■

Lemma 1 is practical when the error $\Delta_T(\beta, n_l, \delta)$ decreases at the rate of $O(n_l^{-\frac{1}{2}})$. This is achieved when $\beta = O(1/n_l)$, which corresponds to $\gamma_g = \Omega(n_l^{\frac{3}{2}})$. Thus, when the problem (3.5) is sufficiently regularized, its solution is stable, and the generalization error of the solution is bounded.

5.2 ANALYSIS OF MAX-MARGIN GRAPH CUTS

5.2.1 When Manifold Regularization Fails

The major difference between manifold regularization (2.2) and the regularized harmonic function solution (3.3) is in the space of optimized parameters. In particular, manifold regularization is performed on a class of functions \mathcal{H}_K . When this class is severely restricted,

such as with linear functions, the minimization of $\mathbf{f}^\top L \mathbf{f}$ may lead to results which are significantly worse than the harmonic function solution.

This issue can be illustrated on the problem from Figure 3, where we learn a linear decision boundary $f(\mathbf{x}) = \alpha_1 x_1 + \alpha_2 x_2$ through manifold regularization of linear SVMs:

$$\min_{\alpha_1, \alpha_2} \sum_{i \in l} V(f, \mathbf{x}_i, y_i) + \gamma[\alpha_1^2 + \alpha_2^2] + \gamma_u \mathbf{f}^\top L \mathbf{f}. \quad (5.1)$$

The structure of our problem simplifies the computation of the regularization term $\mathbf{f}^\top L \mathbf{f}$. In particular, since all edges in the data adjacency graph are either horizontal or vertical, the term $\mathbf{f}^\top L \mathbf{f}$ can be expressed as a function of α_1^2 and α_2^2 . Therefore, for this particular problem we have:

$$\begin{aligned} \mathbf{f}^\top L \mathbf{f} &= \frac{1}{2} \sum_{i,j} w_{ij} (f(\mathbf{x}_i) - f(\mathbf{x}_j))^2 \\ &= \frac{1}{2} \sum_{i,j} w_{ij} (\alpha_1(\mathbf{x}_{i1} - \mathbf{x}_{j1}) + \alpha_2(\mathbf{x}_{i2} - \mathbf{x}_{j2}))^2 \\ &= \frac{\alpha_1^2}{2} \underbrace{\sum_{i,j} w_{ij} (\mathbf{x}_{i1} - \mathbf{x}_{j1})^2}_{\Delta=218.351} + \\ &\quad \frac{\alpha_2^2}{2} \underbrace{\sum_{i,j} w_{ij} (\mathbf{x}_{i2} - \mathbf{x}_{j2})^2}_{\Delta=218.351}. \end{aligned} \quad (5.2)$$

After we incorporate (5.2) to our objective function (5.2), we get (5.2) as an additional weight at the regularizer $[\alpha_1^2 + \alpha_2^2]$:

$$\min_{\alpha_1, \alpha_2} \sum_{i \in l} V(f, \mathbf{x}_i, y_i) + \left(\gamma + \frac{\gamma_u \Delta}{2} \right) [\alpha_1^2 + \alpha_2^2] = \min_{\alpha_1, \alpha_2} \sum_{i \in l} V(f, \mathbf{x}_i, y_i) + \gamma^* [\alpha_1^2 + \alpha_2^2], \quad (5.3)$$

where $\gamma^* = \left(\gamma + \frac{\gamma_u \Delta}{2} \right)$. Thus, manifold regularization of linear SVMs on our problem can be viewed as supervised learning with linear SVMs with a varying weight at the regularizer. In other words, in this particular problem, the unlabeled examples only influence the solution through the regularizer γ^* on $f(\mathbf{x})$. That means we can get the same $f(\mathbf{x})$ for a different γ^* if the unlabeled examples were not present at all. Since the problem involves only two labeled examples, changes in the weight γ^* do not affect the direction of the discriminator $f^*(\mathbf{x}) = 0$, because the margin is maximized by the hyperplane between them. Therefore,

different settings of the regularizer only change the slope of f^* (Figure 7, second row). The above analysis shows that the discriminator $f^*(\mathbf{x}) = 0$ does not change with γ_u . As a result, all discriminators are equal to the discriminator for $\gamma_u = 0$, which can be learned by linear SVMs, yet none of them solves our problem optimally. Max-margin graph cuts solve the problem optimally for small values of γ_g . If we included more unlabeled examples, we could get the error arbitrarily large, assuming our problems would consist of two coherent square-shaped classes, as in 3. Figure 7 shows linear, cubic, and RBF decision boundaries, obtained by manifold regularization of SVMs (MR) and max-margin graph cuts (GC) on the problem from Figure 3. The regularization parameter $\gamma_g = \gamma/\gamma_u$ is set as suggested in Section 2.2.1.2, $\gamma=0.1$, and $\varepsilon=0.01$. The pink and blue colors denote parts of the feature space \mathbf{x} where the discriminators f are positive and negative, respectively. The yellow color marks the regions where $|f(\mathbf{x})| < 0.05$.

A similar line of reasoning can be used to extend our results to polynomial kernels. Figure 7 indicates that max-margin learning with the cubic kernel exhibits trends similar to the linear case.

The notion of algorithmic stability can be used to bound the generalization error of many learning algorithms [Bousquet and Elisseeff, 2002]. In this section, we discuss how to make the harmonic function solution stable and prove a bound on the generalization error of max-margin cuts (3.7). Our bound combines existing transductive [Belkin et al., 2004, Cortes et al., 2008] and inductive [Vapnik, 1995] bounds.

5.2.2 Generalization Error

Our objective is to show that the *risk* of our solution f :

$$R_P(f) = \mathbb{E} P(\mathbf{x}) \mathcal{L}(f(\mathbf{x}), y(\mathbf{x})) \quad (5.4)$$

is bounded by the *empirical risk* on graph-induced labels:

$$\frac{1}{n} \sum_i \mathcal{L}(f(\mathbf{x}_i), \text{sgn}(\ell_i^*)) \quad (5.5)$$

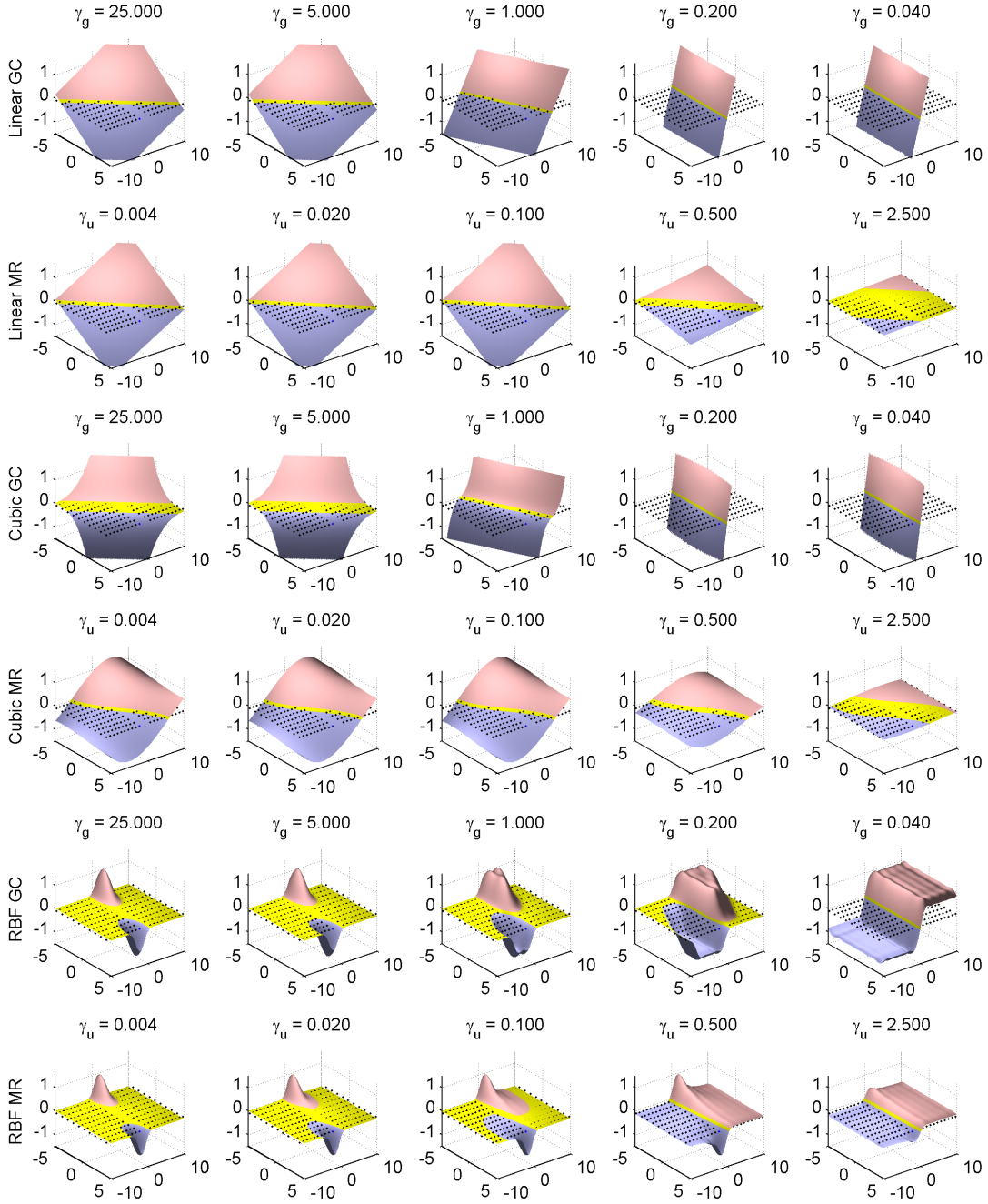


Figure 7: Linear, cubic, and RBF decision boundaries for different methods

and error terms, which can be computed from training data. The function $\mathcal{L}(y', y) = 1\{\text{sgn}(y') \neq y\}$ computes the zero-one loss of the prediction $\text{sgn}(y')$ given the ground truth y . $P(\mathbf{x})$ is the distribution of our data. For simplicity, we assume that the label y is a deterministic function of \mathbf{x} . Our proof starts by relating $R_P(f)$ and graph-induced labels ℓ_i^* .

Lemma 2. *Let f be from a function class with the VC dimension h and \mathbf{x}_i be n examples, which are sampled i.i.d. with respect to the distribution $P(\mathbf{x})$. Then the inequality:*

$$R_P(f) \leq \frac{1}{n} \sum_i \mathcal{L}(f(\mathbf{x}_i), \text{sgn}(\ell_i^*)) + \frac{1}{n} \sum_i (\ell_i^* - y_i)^2 + \underbrace{\sqrt{\frac{h(\ln(2n/h) + 1) - \ln(\eta/4)}{n}}}_{\text{inductive error } \Delta_I(h, n, \eta)}$$

holds with the probability of $1 - \eta$, where y_i and ℓ_i^* represent the true and graph-induced soft labels, respectively.

Proof: Based on Equations 3.15 and 3.24 [Vapnik, 1995], the inequality:

$$R_P(f) \leq \frac{1}{n} \sum_i \mathcal{L}(f(\mathbf{x}_i), y_i) + \Delta_I(h, n, \eta)$$

holds with the probability of $1 - \eta$. Our final claim follows from bounding all terms $\mathcal{L}(f(\mathbf{x}_i), y_i)$ as:

$$\mathcal{L}(f(\mathbf{x}_i), y_i) \leq \mathcal{L}(f(\mathbf{x}_i), \text{sgn}(\ell_i^*)) + (\ell_i^* - y_i)^2.$$

The above bound holds for any $y_i \in \{-1, 1\}$ and ℓ_i^* . ■

It is hard to bound the error term $\frac{1}{n} \sum_i (\ell_i^* - y_i)^2$ when the constraints $\ell_i = y_i$ (3.3) are enforced in a hard manner. Thus, in the rest of our analysis, we consider a relaxed version of the harmonic function solution (Section 3.2.1). Lemma 1 and its proof can be found in Section 5.1. Lemmas 1 and 2 can be combined using the union bound.

Proposition 2. *Let f be from a function class with the VC dimension h . Then the inequality:*

$$R_P(f) \leq \frac{1}{n} \sum_i \mathcal{L}(f(\mathbf{x}_i), \text{sgn}(\ell_i^*)) + \widehat{R}_P^w(\ell^*) + \Delta_T(\beta, n_l, \delta) + \Delta_I(h, n, \eta)$$

holds with probability $1 - (\eta + \delta)$.

The above result can be viewed as follows. If both n and n_l are large, the sum of $\frac{1}{n} \sum_i \mathcal{L}(f(\mathbf{x}_i), \text{sgn}(\ell_i^*))$ and $\widehat{R}_P^w(\ell^*)$ provides a good estimate of the risk $R_P(f)$. Unfortunately, our bound is not practical for setting γ_g , because it is hard to find a γ_g that minimizes both $\widehat{R}_P^w(\ell^*)$ and $\Delta_T(\beta, n_l, \delta)$. The same phenomenon was observed by [Belkin et al., 2004] in a similar context. To solve our problem, we suggest setting γ_g based on the validation set. This methodology is used in the experimental section.

5.2.3 Threshold epsilon

Finally, note that when $|\ell_i^*| < \varepsilon$, where ε is a small number, $|\ell_i^* - y_i|$ is close to 1 irrespective of y_i , and a trivial upper bound $\mathcal{L}(f(\mathbf{x}_i), y_i) \leq 1$ is almost as good as $\mathcal{L}(f(\mathbf{x}_i), \text{sgn}(\ell_i^*)) + (\ell_i^* - y_i)^2$ for any f . This allows us to justify the ε threshold in the problem (3.7). In particular, note that $\mathcal{L}(f(\mathbf{x}_i), y_i)$ is bounded by $1 - (\ell_i^* - y_i)^2 + (\ell_i^* - y_i)^2$. When $|\ell_i^*| < \varepsilon$, $1 - (\ell_i^* - y_i)^2 < 2\varepsilon - \varepsilon^2$, we conclude the following:

Proposition 3. *Let f be from a function class with the VC dimension h and n_ε be the number of examples such that $|\ell_i^*| < \varepsilon$. Then the inequality:*

$$R_P(f) \leq \frac{1}{n_{i:|\ell_i^*| \geq \varepsilon}} \sum \mathcal{L}(f(\mathbf{x}_i), \text{sgn}(\ell_i^*)) + \frac{2\varepsilon n_\varepsilon}{n} + \widehat{R}_P^w(\ell^*) + \Delta_T(\beta, n_l, \delta) + \Delta_I(h, n, \eta)$$

holds with probability $1 - (\eta + \delta)$.

Proof: The generalization bound is proved as:

$$\begin{aligned}
R_P(f) &\leq \widehat{R}_P(f) + \Delta_I(h, n, \eta) \\
&= \frac{1}{n_{i:|\ell_i^*| \geq \varepsilon}} \sum \mathcal{L}(f(\mathbf{x}_i), y_i) + \frac{1}{n_{i:|\ell_i^*| < \varepsilon}} \sum \mathcal{L}(f(\mathbf{x}_i), y_i) + \\
&\quad \Delta_I(h, n, \eta) \\
&\leq \frac{1}{n_{i:|\ell_i^*| \geq \varepsilon}} \sum [\mathcal{L}(f(\mathbf{x}_i), \text{sgn}(\ell_i^*)) + (\ell_i^* - y_i)^2] + \\
&\quad \frac{1}{n_{i:|\ell_i^*| < \varepsilon}} \sum [1 - (\ell_i^* - y_i)^2 + (\ell_i^* - y_i)^2] + \\
&\quad \Delta_I(h, n, \eta) \\
&= \frac{1}{n_{i:|\ell_i^*| \geq \varepsilon}} \sum \mathcal{L}(f(\mathbf{x}_i), \text{sgn}(\ell_i^*)) + \\
&\quad \frac{1}{n_{i:|\ell_i^*| < \varepsilon}} \sum [1 - (\ell_i^* - y_i)^2] + \frac{1}{n} \sum_i (\ell_i^* - y_i)^2 + \\
&\quad \Delta_I(h, n, \eta) \\
&\leq \frac{1}{n_{i:|\ell_i^*| \geq \varepsilon}} \sum \mathcal{L}(f(\mathbf{x}_i), \text{sgn}(\ell_i^*)) + \frac{2\varepsilon n_\varepsilon}{n} + \\
&\quad \widehat{R}_P(\ell^*) + \Delta_T(\beta, n_l, \delta) + \Delta_I(h, n, \eta).
\end{aligned}$$

The last step follows from the inequality $1 - (\ell_i^* - y_i)^2 < 2\varepsilon$ and Lemma 1. ■

When $\varepsilon \leq n_l^{-\frac{1}{2}}$, the new upper bound is asymptotically as good as the bound in Proposition 2. As a result, we get the same convergence guarantees, although highly-uncertain labels $|\ell_i^*| < \varepsilon$ are excluded from our optimization.

In practice, optimization of the thresholded objective often yields a lower risk

$$\frac{1}{n} \sum_{i:|\ell_i^*| \geq \varepsilon} \mathcal{L}(f^*(\mathbf{x}_i), \text{sgn}(\ell_i^*)) + \frac{2\varepsilon n_\varepsilon}{n},$$

and also lower training and test errors. This is a result of excluding the most uncertain examples $|\ell_i^*| < \varepsilon$ from learning. Figure 8 illustrates these trends on three learning problems. In particular it shows the thresholded empirical risk $\frac{1}{n} \sum_{i:|\ell_i^*| \geq \varepsilon} \mathcal{L}(f^*(\mathbf{x}_i), \text{sgn}(\ell_i^*)) + \frac{2\varepsilon n_\varepsilon}{n}$ of the optimal max-margin graph cut f^* (3.7), its training and test errors, and the percentage

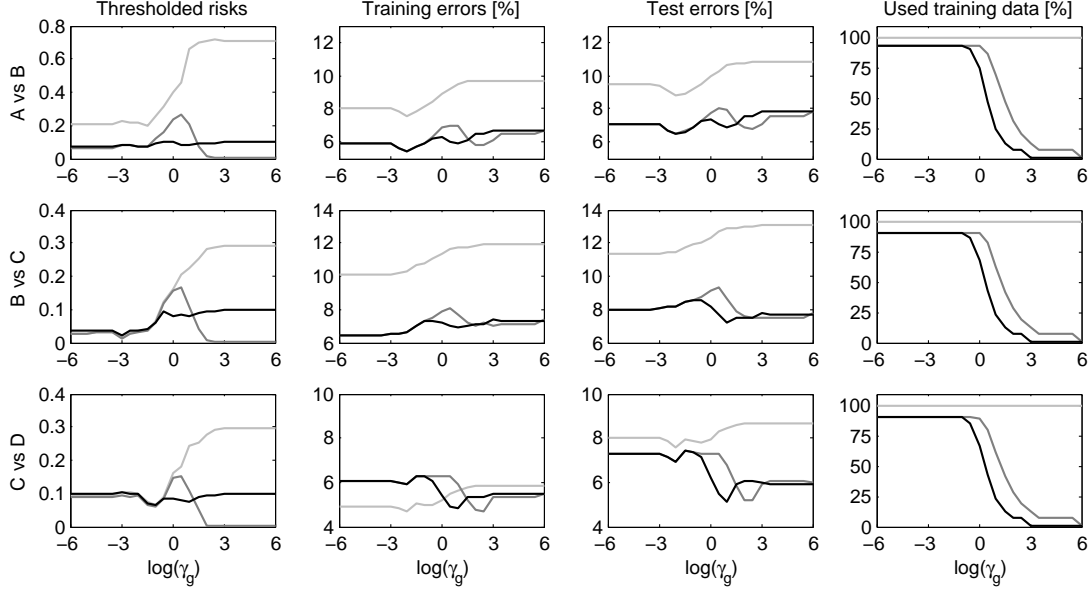


Figure 8: The thresholded empirical risk

of training examples such that $|\ell_i^*| \geq \varepsilon$, on 3 letter recognition problems from the UCI ML repository. The plots are shown as functions of the parameter γ_g and correspond to the thresholds $\varepsilon = 0$ (light gray lines), $\varepsilon = 10^{-6}$ (dark gray lines), and $\varepsilon = 10^{-3}$ (black lines). All results are averaged over 50 random choices of 1 percent of labeled examples.

Note that the parameters γ_g and ε are redundant in the sense that the same result is often achieved by different combinations of parameter values. This problem is addressed in the experimental section by fixing ε and optimizing γ_g only.

5.3 ANALYSIS OF JOINT QUANTIZATION AND LABEL PROPAGATION

In this section we analyze our method of jointly optimizing for the backbone graph and the harmonic solution (Section 3.4) by showing its connection to the principal manifold approach. One interesting property of the objective function in (3.11) for learning the centroids is that it has a similar form to the objective function of the elastic net model [Gorban and

[Zinovyev, 2009]. The elastic net is a well-known technique based on an analogy between principle manifolds and an elastic membrane. It is a fast approximation of the principle manifolds and produces results similar to Kohonen's self-organized maps (SOM) [Haykin, 1994]. Given a set of initial centroids and a given connectivity between the centroids (just like SOM), the elastic net has the following form:

$$U = \gamma_q \sum_{i \in K_j} \|x_i - c_j\|^2 + \sum_{i,j \in \tilde{G}} \lambda_{ij} \|c_i - c_j\|^2 + \sum_{i,j,k \in \tilde{G}} \mu_{ijk} \|c_i + c_k - 2c_j\|^2 \quad (5.6)$$

where \tilde{G} is the graph connectivity between centroids and is assumed to be given. The objective function of the elastic net model consists of three terms: the k-means term $U^Y = \gamma_q \sum_{i \in K_j} \|x_i - c_j\|^2$, the term $U^E = \sum_{i,j \in \tilde{G}} \lambda_{ij} \|c_i - c_j\|^2$ for stretching elasticity, and the term $U^R = \sum_{i,j,k \in \tilde{G}} \mu_{ijk} \|c_i + c_k - 2c_j\|^2$ for bending elasticity. λ_{ij} and μ_{ijk} are the coefficients of stretching elasticity of edge between nodes i and j and the coefficients of bending elasticity of edge between nodes i, j , and k , respectively.

Notice that U^Y is equivalent to the quantization penalty (3.9) for $\gamma_q = 1$. Moreover, if we set $\lambda_{ij} = -(l_i - l_j)^2 / 2\sigma^2$, then U^E approximates $\ell^\top L^C \ell$. Therefore, the objective function in (3.11) is the Elastic net with no bending term and with stretching coefficients dependent on the labels of the centroids; if the labels of two centroids are similar, the objective function tries to keep them close to each other and if the labels of two centroids are different, the objective function keeps them apart.

5.4 ANALYSIS OF ONLINE SSL ON QUANTIZED GRAPHS

In the rest of this section, W denotes the full data similarity matrix, W_t^o its observed portion up to time t and W_t^q the quantized version of W_t^o . For simplicity, we do not consider the compact version of quantized matrix. In other words, W_t^q is $t \times t$ matrix with at most k distinct rows/columns. The Laplacians and regularized Laplacians of these matrices are denoted as L, L^o, L^q and K, K^o, K^q respectively. Similarly, we use ℓ^* , $\ell^o[t]$, and $\ell^q[t]$ to refer to the harmonic solutions on W , W_t^o , and W_t^q respectively. Finally, ℓ_t^* , $\ell_t^o[t]$, and $\ell_t^q[t]$ refer

to the predicted label of the example \mathbf{x}_t .

In this section, we use a stability argument to bound quality of the predictions. We note that the derived bounds are not tight. Our online learner (Figure 2) solves an online regression problem. As a result, it should ideally minimize the error of the form $\sum_t (\ell_t^q[t] - y_t)^2$, where $\ell_t^q[t]$ is the prediction at the time step t (again, time is denoted in the square brackets). In the following proposition we decompose this error into three terms. The first term (5.7) corresponds to the generalization error of the HS and is bounded by the algorithm stability argument. The second term (5.8) appears in our online setting because the similarity graph is only partially revealed. Finally, the third term (5.9) quantifies the error introduced due to quantization of the similarity matrix.

Proposition 4. *Let $\ell_t^q[t]$, $\ell_t^o[t]$, ℓ_t^* be the predictions as defined above and let y_t be the true labels. Then the error of our predictions $\ell_t^q[t]$ is bounded as*

$$\frac{1}{n} \sum_{t=1}^n (\ell_t^q[t] - y_t)^2 \leq \frac{9}{2n} \sum_{t=1}^n (\ell_t^* - y_t)^2 \quad (5.7)$$

$$+ \frac{9}{2n} \sum_{t=1}^n (\ell_t^o[t] - \ell_t^*)^2 \quad (5.8)$$

$$+ \frac{9}{2n} \sum_{t=1}^n (\ell_t^q[t] - \ell_t^o[t])^2. \quad (5.9)$$

Proof: Our bound follows from the inequality

$$(a - b)^2 \leq \frac{9}{2} [(a - c)^2 + (c - d)^2 + (d - b)^2],$$

which holds for $a, b, c, d \in [-1, 1]$. ■

We continue by bounding all the three sums in Proposition 4. These sums can be bounded if the constraints $\ell_i = y_i$ are enforced in a soft manner [Cortes et al., 2008]. One way of achieving this is by solving the related problem

$$\min_{\ell \in \mathbb{R}^n} (\ell - \mathbf{y})^\top C(\ell - \mathbf{y}) + \ell^\top K \ell,$$

where $K = L + \gamma_g I$ is the regularized Laplacian of the similarity graph, C is a diagonal matrix such that $C_{ii} = c_l$ for all labeled examples, and $C_{ii} = c_u$ otherwise, and \mathbf{y} is a vector of pseudo-targets such that y_i is the label of the i -th example when the example is labeled, and $y_i = 0$ otherwise.

5.4.1 Bounding Transduction Error (5.7)

The following proposition bounds the generalization error of the solution to the problem (3.5). We then use it to bound the HS part (5.7) of Proposition 4.

Proposition 5. *Let ℓ^* be a solution to the problem (3.5), where all labeled examples l are selected i.i.d. If we assume that $c_l = 1$ and $c_l \gg c_u$, then the inequality*

$$R(\ell^*) \leq \underbrace{\widehat{R}(\ell^*) + \beta + \sqrt{\frac{2\ln(2/\delta)}{n_l}}(n_l\beta + 4)}_{\text{transductive error } \Delta_T(\beta, n_l, \delta)}$$

$$\beta \leq 2 \left[\frac{\sqrt{2}}{\gamma_g + 1} + \sqrt{2n_l} \frac{1 - \sqrt{c_u}}{\sqrt{c_u}} \frac{\lambda_M(L) + \gamma_g}{\gamma_g^2 + 1} \right]$$

holds with the probability of $1 - \delta$, where

$$R(\ell^*) = \frac{1}{n} \sum_t (\ell_t^* - y_t)^2 \text{ and } \widehat{R}(\ell^*) = \frac{1}{n_l} \sum_{t \in l} (\ell_t^* - y_t)^2$$

are risk terms for both all and labeled vertices, respectively, and β is the stability coefficient of the solution ℓ^* .

The proof can be found in Section 5.2.2. Proposition 5 shows that when $\Delta_T(\beta, n_l, \delta) = o(1)$, the true risk is not much different from the empirical risk on the labeled points which bounds the generalization error. This occurs when $\beta = o(n_l^{-1/2})$, which corresponds to setting $\gamma_g = \Omega(n_l^{1+\alpha})$ for any $\alpha > 0$.

5.4.2 Bounding Online Error (5.8)

In the following, we will bound the difference between the online and offline HS and use it to bound (5.8) of the Proposition 4. The idea is that when Laplacians L and L^o are regularized enough by γ_g , the resulting harmonic solutions are close to zero and therefore close to each other. We first show that any regularized HS can be bounded as follows:

Lemma 3. *Let ℓ be a regularized harmonic solution, i.e. $\ell = (C^{-1}K + I)^{-1}\mathbf{y}$ where $K = L + \gamma_g I$.*

Then

$$\|\ell\|_2 \leq \frac{\sqrt{n_l}}{\gamma_g + 1}.$$

Proof: If $A \in \mathbb{R}^{n \times n}$ is a symmetric matrix and $\lambda_m(A)$ and $\lambda_M(A)$ are its smallest and largest eigenvalues, then for any $\mathbf{v} \in \mathbb{R}^{n \times 1}$, $\lambda_m(A)\|\mathbf{v}\|_2 \leq \|A\mathbf{v}\|_2 \leq \lambda_M(A)\|\mathbf{v}\|_2$. Then

$$\|\ell\|_2 \leq \frac{\|\mathbf{y}\|_2}{\lambda_m(C^{-1}K + I)} = \frac{\|\mathbf{y}\|_2}{\frac{\lambda_m(K)}{\lambda_M(C)} + 1} \leq \frac{\sqrt{n_l}}{\gamma_g + 1}. \quad \blacksquare$$

The straightforward implication of Lemma 3 is that any 2 regularized harmonic solutions can be bounded as in the following proposition:

Proposition 6. *Let $\ell^o[t]$ be the predictions of the online HS, and ℓ^* be the predictions of the offline HS. Then*

$$\frac{1}{n} \sum_{t=1}^n (\ell_t^o[t] - \ell^*[t])^2 \leq \frac{4n_l}{(\gamma_g + 1)^2}. \quad (5.10)$$

Proof: We use the fact that $\|\cdot\|_2$ is an upper bound on $\|\cdot\|_\infty$. Therefore, for any t

$$\begin{aligned} (\ell_t^o[t] - \ell_t^*)^2 &\leq \|\ell^o[t] - \ell^*\|_\infty^2 \leq \|\ell^o[t] - \ell^*\|_2^2 \\ &\leq \left(\frac{2\sqrt{n_l}}{\gamma_g + 1} \right)^2, \end{aligned}$$

where in the last step we used Lemma 3 twice. By summing over n and dividing by n we get (5.10). \blacksquare

From Proposition 6 we see that we can achieve convergence of the term (5.8) at the rate of $O(n^{-1/2})$ with $\gamma_g = \Omega(n^{1/4})$.

5.4.3 Bounding Quantization Error (5.9)

In this section, we show in Proposition 7 how to bound the error for the HS between the full and quantized graph, and then use it to bound the difference between the *online* and *online quantized* HS in (5.9). Let us consider the perturbed version of the problem (3.5), where we replace the regularized Laplacian K^o with K^q ; i.e., K^q corresponds to the regularized Laplacian of the quantized graph. Let ℓ^o and ℓ^q minimize (3.5) and its perturbed version respectively. Their closed-form solutions are given by $\ell^o = (C^{-1}K^o + I)^{-1}\mathbf{y}$ and $\ell^q = (C^{-1}K^q + I)^{-1}\mathbf{y}$ respectively. We now follow the derivation of [Cortes et al., 2008] that derives stability coefficients for unconstrained regularization algorithms. Instead of considering perturbation

on C , we consider the perturbation on K^0 . Our goal is to derive a bound on a difference in HS when we use K^q instead of K^0 .

Lemma 4. *Let ℓ^0 and ℓ^q minimize (3.5) and its perturbed version respectively. Then*

$$\|\ell^q - \ell^0\|_2 \leq \frac{\sqrt{n_l}}{c_u \gamma_g^2} \|K^q - K^0\|_F.$$

Proof: Let $Z^q = C^{-1}K^q + I$ and $Z^0 = C^{-1}K^0 + I$. By definition

$$\begin{aligned} \ell^q - \ell^0 &= (Z^q)^{-1}\mathbf{y} - (Z^0)^{-1}\mathbf{y} = (Z^q Z^0)^{-1}(Z^0 - Z^q)\mathbf{y} \\ &= (Z^q Z^0)^{-1}C^{-1}(K^0 - K^q)\mathbf{y}. \end{aligned}$$

Using the eigenvalue inequalities from the proof of Lemma 3 we get

$$\|\ell^q - \ell^0\|_2 \leq \frac{\lambda_M(C^{-1})\|(K^q - K^0)\mathbf{y}\|_2}{\lambda_m(Z^q)\lambda_m(Z^0)}. \quad (5.11)$$

By the compatibility of $\|\cdot\|_F$ and $\|\cdot\|_2$ and since \mathbf{y} is zero on unlabeled points, we have

$$\|(K^q - K^0)\mathbf{y}\|_2 \leq \|K^q - K^0\|_F \cdot \|\mathbf{y}\|_2 \leq \sqrt{n_l} \|K^q - K^0\|_F.$$

Furthermore,

$$\lambda_m(Z^0) \geq \frac{\lambda_m(K^0)}{\lambda_M(C)} + 1 \geq \gamma_g \quad \text{and} \quad \lambda_M(C^{-1}) \leq c_u^{-1},$$

where c_u is a small constant as defined in (3.5). By plugging these inequalities into (5.11) we get the desired bound. ■

Proposition 7. *Let $\ell_t^q[t]$ be the predictions of the online harmonic solution on the quantized graph at the time step t and $\ell_t^0[t]$ be predictions of the online harmonic solution at the time step t . Then*

$$\frac{1}{n} \sum_{t=1}^n (\ell_t^q[t] - \ell_t^0[t])^2 \leq \frac{n_l}{c_u^2 \gamma_g^4} \|L^q - L^0\|_F^2. \quad (5.12)$$

Proof: Similarly as in Proposition 6, we get

$$\begin{aligned} (\ell_t^q[t] - \ell_t^o[t])^2 &\leq \|\ell_t^q[t] - \ell_t^o[t]\|_\infty^2 \leq \|\ell_t^q[t] - \ell_t^o[t]\|_2^2 \\ &\leq \left(\frac{\sqrt{n_l}}{c_u \gamma_g^2} \|K^q - K^o\|_F \right)^2, \end{aligned}$$

where we used (5.11) the last step. We also note that

$$K^q - K^o = L^q + \gamma_g I - (L^o + \gamma_g I) = L^q - L^o,$$

which gives us $(\ell_t^q[t] - \ell_t^o[t])^2 \leq \|L^q - L^o\|_F^2 \cdot n_l / (c_u^2 \gamma_g^4)$. By summing over n and dividing by n we get (5.12). ■

If $\|L^q - L^o\|_F^2 = O(1)$, the left-hand side of (5.12) converges to zero at the rate of $O(n^{-1/2})$ with $\gamma_g = \Omega(n^{1/8})$. We show this condition is achievable whenever the Laplacian is scaled appropriately. Specifically, we demonstrate that normalized Laplacian achieves this bound when the quantization is performed using incremental k -center clustering in Section 3.5, and when the weight function obeys a Lipschitz condition (e.g. the Gaussian kernel). We also show that this error goes to zero as the number of center points k goes to infinity.

Suppose the data $\{\mathbf{x}_i\}_{i=1,\dots,n}$ lie on a smooth d -dimensional compact manifold \mathcal{M} with boundary of bounded geometry as defined in Definition 11 (Manifold with boundary of bounded geometry) in [Hein et al., 2007]. Intuitively, the manifold should not intersect itself or fold back onto itself. We first demonstrate that the distortion introduced by quantization is small, and then show that small distortion gives a small error in the Frobenius norm.

Proposition 8. *Using incremental k -center clustering for quantization has maximum distortion $Rm/(m-1) = \max_{i=1,\dots,n} \|\mathbf{x}_i - \mathbf{c}\|_2 = O(k^{-1/d})$, where \mathbf{c} is the closest centroid to \mathbf{x}_i .*

Proof: Consider a sphere packing with k centers contained in \mathcal{M} and each with radius r . Since the manifold is compact and the boundary has bounded geometry, it has finite volume V and finite surface area A . The maximum volume that the packing can occupy obeys the inequality $k c_d r^d \leq V + A c_{\mathcal{M}} r$ for some constants $c_d, c_{\mathcal{M}}$ that only depend on the dimension and the manifold. For a sufficiently large k , r will be smaller than the *injectivity radius* of \mathcal{M} [Hein et al., 2007]. Moreover, if k is sufficiently large, then $r < 1$, and we have an

upper bound $r < ((V + Ac_{\mathcal{M}})/(kc_d))^{1/d} = O(k^{-1/d})$. An r -packing is a $2r$ -covering, so we have an upper bound on the distortion of the optimal k -centers solution. Since the incremental k -centers algorithm is a $(1 + \epsilon)$ -approximation algorithm [Charikar et al., 1997], it follows that the maximum distortion returned by the algorithm is $Rm/(m - 1) = 2(1 + \epsilon)O(k^{-1/d})$. ■

We now show that with appropriate normalization, the error $\|L^q - L^o\|_F^2 = O(k^{-2/d})$. If L^q and L^o are normalized Laplacians, then this bound holds if the underlying density is bounded away from 0. Note that since we use the Gaussian kernel, the Lipschitz condition is satisfied.

Proposition 9. *Let W_{ij}^o be a weight matrix constructed from $\{x_i\}_{i=1,\dots,n}$ and a bounded, Lipschitz function $\omega(\cdot, \cdot)$ with Lipschitz constant M . Let D^o be the corresponding degree matrix and $L_{ij}^o = (D_{ij}^o - W_{ij}^o)/c_{ij}^o$ be the normalized Laplacian. Suppose $c_{ij}^o = \sqrt{D_{ii}^o D_{jj}^o} > c_{\min} n$ for some constant $c_{\min} > 0$ that does not depend on k . Likewise define W^q, L^q, D^q on the quantized points. Let the maximum distortion be $Rm/(m - 1) = O(k^{-1/d})$. Then $\|L^q - L^o\|_F^2 = O(k^{-2/d})$.*

Proof: Since ω is Lipschitz, we have that $|W_{ij}^q - W_{ij}^o| < 2MRm/(m - 1)$ and $|c_{ij}^q - c_{ij}^o| < 2nMRm/(m - 1)$. The error of a single off-diagonal entry of the Laplacian matrix is

$$\begin{aligned} L_{ij}^q - L_{ij}^o &= \frac{W_{ij}^q}{c_{ij}^q} - \frac{W_{ij}^o}{c_{ij}^o} \\ &\leq \frac{W_{ij}^q - W_{ij}^o}{c_{ij}^q} + \frac{W_{ij}^q(c_{ij}^q - c_{ij}^o)}{c_{ij}^o c_{ij}^q} \\ &\leq \frac{4MRm}{(m - 1)c_{\min} n} + \frac{4M(nMRm)}{((m - 1)c_{\min} n)^2} \\ &= O\left(\frac{R}{n}\right). \end{aligned}$$

The error on the diagonal entries is 0 since the diagonal entries of L^q and L^o are all 1. Thus $\|L^q - L^o\|_F^2 \leq n^2 O(R^2/n^2) = O(k^{-2/d})$. ■

Here we showed the asymptotic behavior $\|L^q - L^o\|_F$ in term of the number of vertices used in the quantized graph. In Section 6.1.5.1, we empirically show that $\|L^q - L^o\|_F$ vanishes quickly as the number of vertices increases (Figure 15). Moreover, with a fixed number of vertices, $\|L^q - L^o\|_F$ quickly flattens out even when the data size (time) keeps increasing (Figure 14).

5.4.4 Discussion

Our goal in this section is to show how much of regularization γ_g is needed for the error of our predictions to reasonably decrease over time. We point out that in Proposition 1 the lower bound for γ_g for reasonable convergence is a function of n_l labeled examples. On the other hand, in Propositions 6 and 7 those lower bounds are the functions of all n examples.

In particular, Proposition 1 requires $\gamma_g = \Omega(n_l^{1+\alpha})$, $\alpha > 0$ for the true risk not to be much different from the empirical risk on the labeled points. Next, Propositions 6 and 7 require $\gamma_g = \Omega(n^{1/4})$ and $\gamma_g = \Omega(n^{1/8})$, respectively, for the terms (5.8) and (5.9) to be $O(n^{-1/2})$.

For many applications of online SSL, a small set of n_l labeled example is given in advance, the rest of the examples are unlabeled. That means we usually expect $n \gg n_l$. Therefore, if we regard n_l as a constant, we need to regularize as much as $\gamma_g = \Omega(n^{1/4})$. For such a setting of γ_g we have that for n approaching infinity, the error of our predictions is getting close to the empirical risk on labeled examples with the rate of $O(n^{-1/2})$.

5.5 PARALLEL MULTI-MANIFOLD LEARNING

In this section we analyze the approximation proposed in Section 3.6, when instead of computing the harmonic solution (HS) on the whole graph, we

1. decompose the graph into several smaller subgraphs,
2. compute the HSs on the smaller graphs *in parallel*, and
3. aggregate the partial HSs.

In the ideal case, the similarity matrix has a block-diagonal (BD) structure, which corresponds to the graph with disconnected components. In this case, such an approximation is exact. Since the harmonic solution for n nodes of the graph has computational complexity of $\mathcal{O}(n^3)$, the time savings can be significant (Section 5.5).

In the rest of this section we analyze the general case, when the similarity matrix does not have BD structure. Intuitively, the closer the similarity matrix resembles BD structure, the smaller decrease in prediction accuracy we expect.

Again, if similarity and its Laplacian are BD, then HS calculated per block and as a whole are identical (even with the regularization), because it can be rewritten as solving two independent systems of linear equations. On the other hand, an *impurity* of BD structure can change HS a lot (think of the case when we merge blocks with labeled examples from different classes). We continue by extending the analysis in Section 5.4 and follow Proposition 7:

Lemma 5. *Let ℓ^o and ℓ^q minimize (3.5) and its perturbed version, respectively. Then*

$$\|\ell^q - \ell^o\|_2 \leq \frac{\sqrt{n_l}}{c_u \gamma_g^2} \|K^q - K^o\|_F.$$

The proof is in Section 5.4.3. The question now is how to bound $\|K^q - K^o\|_F$ or $\|L^q - L^o\|_F$ if the same regularization is used. Let L^{bd} denote general block-diagonal approximation of L^q , where the entries outside the BD structure are ignored (ie. are assumed to be zero). Then

$$\|L^{\text{bd}} - L^o\|_F \leq \|L^{\text{bd}} - L^q\|_F + \|L^q - L^o\|_F. \quad (5.13)$$

Let d_{\max} be the value of the maximum entry in K^q , which is ignored when the approximation is performed. In general, for a BD setting, we can have $n^2/2$ to n^2 ignored entries. Therefore,

$$n\sqrt{d_{\max}/2} \leq \|L^{\text{bd}} - L^q\|_F \leq n\sqrt{d_{\max}}. \quad (5.14)$$

This approximation adds a factor of $\Theta(n)$ to the quantization bound (Section 5.4.3). To maintain the overall convergence of $O(n^{-1/2})$ we need to have $\gamma_g = \Omega(n^{3/8})$, along with the discussion in Section 5.4.4.

5.6 ANALYSIS OF CONDITIONAL ANOMALY DETECTION

In this part we show that the weighed k -NN is a special case of λ -RWCAD for $\lambda = 0$ and $n \rightarrow \infty$. Rewriting (4.2) we get:

$$P(y \neq +1 | \mathbf{x}_i) = \frac{1}{1 + \frac{P(\mathbf{x}_i | y=+1)P(y=+1)}{P(\mathbf{x}_i | y=-1)P(y=-1)}} \quad (5.15)$$

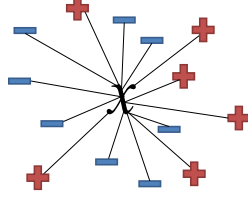


Figure 9: Estimating the likelihood ratio from a single graph

Let us estimate $P(\mathbf{x}_i|y = +1)/P(\mathbf{x}_i|y = -1)$ – *conditional likelihood* – in (5.15) also from a stationary distribution of a random walk shown in Figure 9, where we connect the node representing \mathbf{x}_i with all examples in the training set (from all classes) and define the likelihood ratio as the ratio between the time spent in the nodes with the respective labels:

$$\frac{P(\mathbf{x}_i|y = +1)}{P(\mathbf{x}_i|y = -1)} = \frac{\#T(y = +1)}{\#T(y = -1)}, \quad (5.16)$$

where $\#T(y = c)$ is the time spent in the nodes of class c during the random walk. Let W , W^+ , W^- be the weight matrices for all, just the positive, and just the negative nodes, respectively. Combining (5.16) and (3.1), we get:

$$\frac{P(\mathbf{x}_i|y = +1)}{P(\mathbf{x}_i|y = -1)} = \frac{\sum_j W_{j\mathbf{x}_i}^+}{\sum_j W_{j\mathbf{x}_i}^-} \quad (5.17)$$

which is equal to the weighted k -NN method. Now, let $T^+ = \text{vol}(W^+)$ and $T^- = \text{vol}(W^-)$ be the sums of all weights in W^+ and W^- . Moreover, let $T_{\mathbf{x}_i}^+$, $T_{\mathbf{x}_i}^-$ be the total edge sums of the respective graphs including the node \mathbf{x}_i . The conditional likelihood of the λ -RWCAD for $\lambda = 0$ can be derived combining (4.2) and (3.1) to get:

$$\frac{P(\mathbf{x}_i|y = +1)}{P(\mathbf{x}_i|y = -1)} = \frac{\sum_j W_{j\mathbf{x}_i}^+}{\sum_j W_{j\mathbf{x}_i}^-} \times \frac{T_{\mathbf{x}_i}^-}{T_{\mathbf{x}_i}^+} \quad (5.18)$$

Equations (5.17) and (5.18) are the conditional likelihoods for the weighted k -NN and RW-CAD for $\lambda = 0$, respectively. Notice that as the number of nodes increases, $T_{\mathbf{x}_i}^-/T_{\mathbf{x}_i}^+$ approaches T^-/T^+ , which is a constant. Therefore, the influence of one node (\mathbf{x}_i) in the ratio becomes negligible. In that case, both methods will yield comparable results.

6.0 EXPERIMENTS

This chapter presents the set of experiments we performed for semi-supervised learning (SSL) and conditional anomaly detection (CAD). We present our SSL results in Section 6.1 and our CAD results in Section 6.2. We start each of these sections with the descriptions of the data. We used medical, vision, the UCI ML repository, and synthetic datasets.

6.1 EVALUATIONS OF SEMI-SUPERVISED LEARNING MODELS

In this section we evaluate the predictive performance of our graph-based model on semi-supervised tasks. Our goal is to demonstrate that graph-based methods can yield predictors that outperform the current state-of-the-art methods. We continue with the description of the datasets we used.

6.1.1 UCI ML Datasets

In this part we describe the datasets from the UCI ML Repository [Asuncion and Newman, 2011] that we used to test our semi-supervised algorithms. We used *Digit*, *Letter*, and *Image segmentation* as the benchmark datasets to compare our max-margin graph cuts to manifold regularization of SVMs. Moreover, we used *Digit* and *Letter*, due to their small size, to compare the performance of our online semi-supervised algorithm on quantized graphs to the performance of a full offline non-quantized harmonic solution. Finally, we used *COIL*, *Car*, and *SecStr* as the benchmark datasets for large scale semi-supervised learning, as suggested by [Chapelle et al., 2006].

6.1.1.1 Digit recognition This dataset was preprocessed by programs made available by NIST to extract normalized bitmaps of handwritten digits from a preprinted form. From a total of 43 people, 30 contributed to the training set and the remaining 13 contributed to the test set. 32x32 bitmaps are divided into non-overlapping blocks of 4x4, and the number of on pixels are counted in each block. This generates an input matrix of 8x8, where each element is an integer in the range 0–16. This reduces dimensionality and gives invariance to small distortions.

6.1.1.2 Letter recognition The objective is to identify each of a large number of black-and-white rectangular pixel displays as one of the 26 capital letters in the English alphabet. The character images were based on 20 different fonts and each letter within these 20 fonts was randomly distorted to produce a file of 20,000 unique stimuli. Each stimulus was converted into 16 primitive numerical attributes (statistical moments and edge counts), which were then scaled to fit into a range of integer values from 0 through 15.

6.1.1.3 Image segmentation The Segmentation dataset, created in 1990 by the Vision Group, University of Massachusetts, consists of 2310 instances. Each instance was drawn randomly from a database of seven outdoor images. The image, a 3×3 region, was hand-segmented to create a classification for each pixel. The seven classes are brickface, sky, foliage, cement, window, path, and grass. Each of the 7 images is represented by 330 instances. The extracted features are 19 continuous attributes that describe the position of extracted image, line densities, edges, and color values.

6.1.1.4 COIL The Columbia object image library (COIL-100) is a set of color images of 100 different objects taken from different angles (in steps of 5 degrees) at a resolution of 128×128 pixels [Nene et al., 1996]. We use the binary version of this dataset as preprocessed by [Chapelle et al., 2006].

6.1.1.5 Car The Car evaluation data set classifies cars into four categories using 6 features including buying price, number of doors, etc. We converted the Car dataset into a

binary problem to classify first two vs. the second two car categories.

6.1.1.6 SecStr The SecStr is a benchmark data set designed by [Chapelle et al., 2006] to investigate how far current methods can cope with large-scale application. The task is to predict the secondary structure of a given amino acid in a protein, based on a sequence window centered around that amino acid.

For the multi-class datasets we sometimes transformed them into a set of binary problems.

6.1.2 Vision Datasets

In this section, we describe several face recognition datasets that we recorded to evaluate the performance of online semi-supervised learning algorithms on noisy real world data that involve outliers.

The *environment adaptation* dataset consists of faces of a single person, which are captured at various locations, such as a cubicle, a conference room, and a corner with a couch (Figure 10). The first four faces in the cubicle are labeled, and we want to learn a face recognizer for all locations. To test the sensitivity of the recognizer to outliers, we augmented the dataset with random faces. The *office space* dataset (Figure 10) is multi-class and involves 8 people who walk in front of a camera and make funny faces. When a person shows up on the camera for the first time, we label four faces of the person. Our goal is to learn good face recognizers for all 8 people.

Another vision dataset is a *face-based authentication* dataset of 16 people (Figure 11). The people try to log into a tablet PC with their face, while being recorded by its embedded camera. The data are collected at 10 indoor locations, which differ by backgrounds and lighting conditions. In short, we recorded 20 10-second videos per person, each at 10 fps. Therefore, our face-based authentication dataset contains a total of $16 \times 20 = 32000$ images. Faces in the images are detected using OpenCV [Bradski, 2000], converted to grayscale, resized to 96×96 , smoothed using the 3×3 Gaussian kernel, and equalized by the histogram of their pixel intensities.



Figure 10: Snapshots from the environment adaptation and office space datasets

6.1.3 Max-margin Graph Cuts Experiments

The experiments with max-margin graph cuts are divided into two parts. The first part compares max-margin graph cuts to manifold regularization of SVMs on the problem from Figure 3. The second part compares max-margin graph cuts, manifold regularization of SVMs, and supervised learning with SVMs on three UCI ML repository datasets [Asuncion and Newman, 2011]. Manifold regularization of SVMs is evaluated based on the implementation of [Belkin et al., 2006]. Max-margin graph cuts and SVMs are implemented using LIBSVM [Chang and Lin, 2001].

6.1.3.1 Synthetic problem The first experiment (Figure 7) illustrates linear, cubic, and RBF graph cuts (3.7) on the synthetic problem from Figure 3. The cuts are shown for various settings of the regularization parameter γ_g . As γ_g decreases, note that the cuts gradually interpolate between supervised learning on just two labeled examples and semi-supervised learning on all data. The resulting discriminators are max-margin decision boundaries that separate the corresponding colored regions in Figure 3.

Figure 7 also shows that the manifold regularization of SVMs (2.2) with linear and cubic kernels cannot perfectly separate the two clusters in Figure 3 for any setting of the parameter γ_u . The reason for this problem is discussed in Section 5.2.1. Finally, note the similarity between max-margin graph cuts and manifold regularization of SVMs with the RBF kernel.

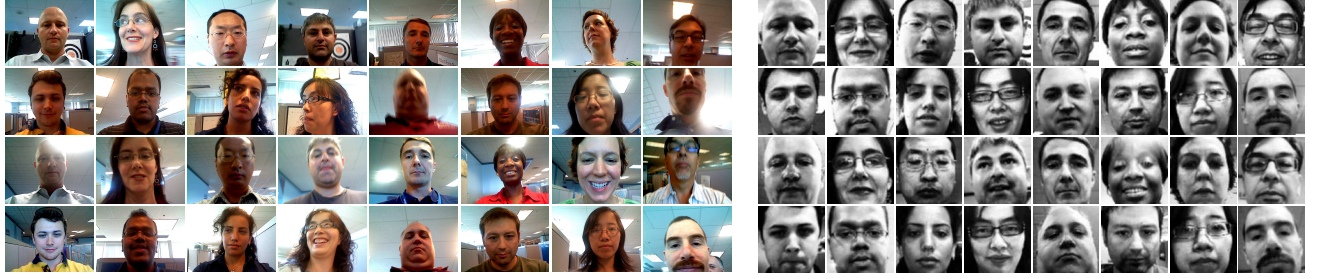


Figure 11: Face-based authentication dataset (left) and examples of labeled faces (right)

This similarity was suggested in Section 2.2.1.2.

Dataset	L	Misclassification errors [%]								
		Linear kernel			Cubic kernel			RBF kernel		
		SVM	MR	GC	SVM	MR	GC	SVM	MR	GC
Letter recognition	1	18.90	30.94	15.79	20.54	25.96	17.45	20.06	17.61	16.01
	2	12.92	28.45	10.79	12.18	18.34	10.90	13.52	13.10	11.83
	5	8.21	27.13	5.65	5.49	18.77	4.80	6.81	8.06	5.65
	10	6.51	25.45	3.96	4.17	14.03	2.96	4.95	6.14	3.32
Digit recognition	1	7.06	9.59	6.88	9.62	5.29	8.55	8.22	6.36	7.65
	2	4.87	7.97	4.60	6.06	5.06	5.09	6.17	4.21	5.61
	5	2.97	3.68	2.29	3.04	2.27	2.36	2.74	2.29	2.19
	10	1.70	2.86	1.59	1.87	1.60	1.74	1.68	1.75	1.35
Image segmentation	1	14.02	11.81	10.27	23.30	12.02	14.10	14.02	11.60	9.51
	2	8.54	10.87	7.69	14.28	13.07	7.73	9.06	8.93	7.34
	5	4.73	7.83	4.49	8.32	8.79	7.17	5.87	5.43	5.31
	10	3.30	6.26	3.28	3.65	6.64	3.60	3.84	4.81	3.73

Figure 12: Comparison of SVMs, GC and MR on 3 datasets from the UCI ML repository

6.1.3.2 UCI ML repository datasets The second experiment (Figure 12) shows that max-margin graph cuts (3.7) typically outperform manifold regularization of SVMs (2.2) and supervised learning with SVMs. In particular it shows the comparison of SVMs, max-margin graph cuts (GC), and manifold regularization of SVMs (MR) on three datasets from the UCI ML repository. The fraction of labeled examples L varies from 1 to 10 percent.

The experiment is done on three UCI ML repository datasets: letter recognition, digit recognition, and image segmentation. The datasets are multi-class and thus, we transform each of them into a set of binary classification problems. The digit recognition and image segmentation datasets are converted into 45 and 15 problems, respectively, where all classes are discriminated against every other class. The letter recognition dataset is turned into 25 problems that involve pairs of consecutive letters. Each dataset is divided into three folds. The first fold is used for training, the second one for selecting the parameters $\gamma \in [0.01, 0.1]n_l$, $\gamma_u \in [10^{-3}, 10^3]\gamma$, and $\gamma_g = \gamma/\gamma_u$, and the last fold is used for testing.¹ The fraction of labeled examples in the training set is varied from 1 to 10 percent. All examples in the validation set are labeled, and its size is limited to the number of labeled examples in the training set.

In all experiments, we use 5-nearest neighbor graphs whose edges are weighted as $w_{ij} = \exp[-\|\mathbf{x}_i - \mathbf{x}_j\|_2^2 / (2K\sigma^2)]$, where K is the number of features, and σ denotes the mean of their standard deviations. The width of radial basis functions (RBFs) is set accordingly to $\sqrt{K}\sigma$, and the threshold ε for choosing training examples (3.7) is 10^{-6} .

The test errors of all compared algorithms are averaged over all binary problems within each dataset and shown in Figure 12. Max-margin graph cuts outperform manifold regularization of SVMs in 29 out of 36 experiments. Note that the lowest errors are usually obtained for linear and cubic kernels, and our method improves the most over manifold regularization of SVMs in these settings.

6.1.4 Joint Quantization and Label Propagation Experiments

In this part, we evaluate the method we proposed in Section 3.4 that combines the creation of a backbone graph with label propagation. The benefit of our algorithm comes when the data lies on a low dimensional manifold. In this section, we show the 2 data sets when this is the case. For data sets without a manifold structure or for the data sets where a cluster assumption holds, the performance of our method is comparable to the case when k -means is used as a preprocessing step. We compare our algorithm to several quantization approaches:

¹Alternatively, the regularization parameters γ , γ_u , and γ_g can be set using leave-one-out cross-validation on labeled examples.

1. *random subsampling*: We randomly sample k examples from the unlabeled data. Then we apply SSL method on the selected samples.
2. *k-means*: We cluster the unlabeled data using k -means [Hastie et al., 2001] to get k cluster centers and then apply SSL algorithms to get their labels.
3. *elastic nets*: We use elastic net [Gorban and Zinovyev, 2009] as a preprocessing to get k cluster centers. We then apply SSL to get their labels.
4. *elastic-joint*: We apply the proposed algorithm in this dissertation to get both the centroids and their labels.
5. *full-soft*: We apply SSL algorithm on the full set of examples as a reference point.

After obtaining the labels of the centroids using items 1-4 above, we apply the approximation in Section 3.4.3 to get the labels for unlabeled examples.

6.1.4.1 Experimental setup We use a small subset of examples as labeled examples. To see the sensitivity of the method on a different number of labeled examples, we try $m = 2, 10, 20$, and 50 as the number of labeled examples. To allow for the fair comparison between the methods, we run all the algorithms on the same set of labeled examples. Moreover, all the approximation methods are initialized with the same cluster centers (seeds) as the ones that were drawn by random subsampling.

Finally, we fix all the parameters for the semi-supervised prediction in Equation (3.5) to the same settings as follows. We create a 3-nearest neighbors similarity graph, and we use the Gaussian kernel with the kernel width σ equal to 10% of the standard deviation of the distances as suggested in [Luxburg, 2007].

For each of the methods we compute the regularized graph Laplacian, where we add $\gamma_g = 10^{-6}$ to the diagonal. For the diagonal matrix F of empirical weights we set $f_l = 10$ for the labeled and $f_u = 0.1$ for the unlabeled examples. We set parameter γ_q in our method to 10^5 . Finally, we vary the number of cluster centers as $k = 15, 20, 25, 30, 60$, and 90.

6.1.4.2 Results The results are shown in Figure 13 for the varying number of labeled examples m and centroids k . Error bars show the 95% confidence intervals over 50 runs.

The 5 compared methods are 1) subsample — random subsampling, 2) k -means as a pre-processing, 3) our method: elastic-joint, 4) elastic net as a preprocessing, and 5) full soft — harmonic solution using all unlabeled examples to create the full graph. For the Car dataset and $m = 2$ unlabeled examples, our method outperforms the other baselines for the different number of cluster centers up to $k = 60$, where all the methods achieved the performance of the full non-approximated graph. For $m = 10, 20$, and 50 , all the subsampling methods are comparable. For the COIL dataset, $m = 2$ of labeled examples was not sufficient for learning, as the classes are perfectly balanced and all the methods produced a trivial classifier comparable to a random one, including the SSL on the full graph with all the examples. For $m = 10, 20$, and 50 , our method significantly outperforms all the other approximation methods. The result for SecStr (Figure 4) is similar for all the baselines. We utilize this data set to show the time complexity of different methods. Notice that the same observation and setup is used in [Chapelle et al., 2006].

6.1.5 Online Quantized SSL Experiments

The experimental section is divided into two parts. In the first part, we evaluate our online learner (Figure 2) on UCI ML repository datasets (Section 6.1.1). In the second part, we apply our learner to solve two face recognition problems. In all experiments, the multiplicative parameter m of the k -centers algorithm is set to 1.5.

6.1.5.1 UCI ML Repository Experiments In the first experiment, we study the online quantization error $\|L_t^q - L_t^o\|_F$ and its relation to the HS on the quantized graphs W_t^q . This experiment is performed on two datasets from the UCI ML repository: letter and optical digit recognition. The datasets are converted into a set of binary problems, where each class is discriminated against every other class. The similarity weights are computed as $w_{ij} = \exp[-\|\mathbf{x}_i - \mathbf{x}_j\|_2^2 / (2p\sigma^2)]$, where p is the number of features and σ denotes the mean of their standard deviations. Our results are averaged over 10 problems from each dataset and shown in Figures 14 and 15.

In Figure 14, we fix the number of centroids at $k = 200$ and study how the quality of

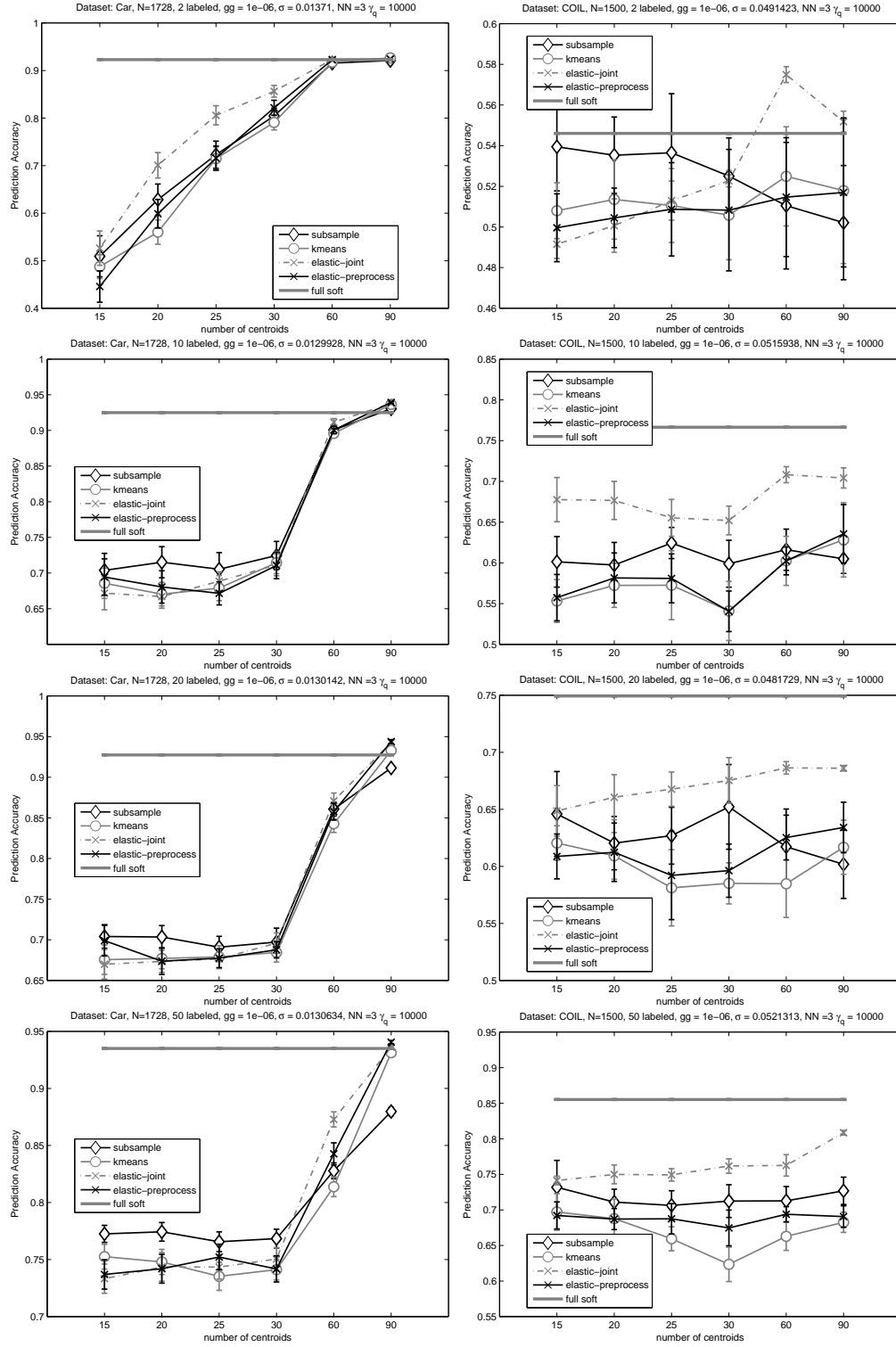


Figure 13: Coil and Car datasets from UCI ML Repository

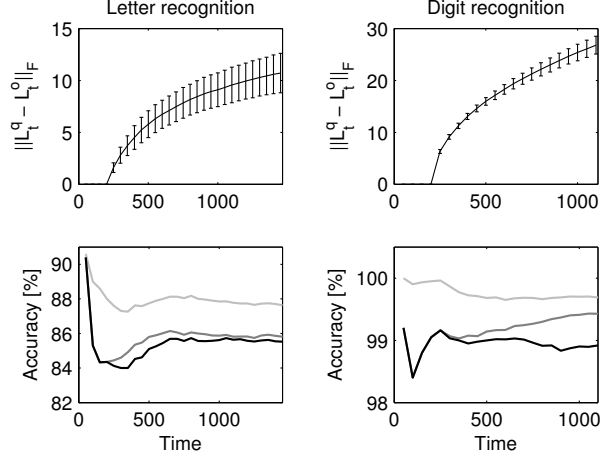


Figure 14: UCI ML: Quality of approximation as a function of time

our solution changes with the learning time t . The upper plots show the difference between the normalized Laplacian L_t^o and its approximation L_t^q at time t . The bottom plots show the cumulative accuracy of the harmonic solutions on W (light gray lines), W_t^o (dark gray lines), and W_t^q (black lines) for various times t . Two trends are apparent. First, as time t increases, the error $\|L_t^q - L_t^o\|_F$ slowly levels off. Second, the accuracy of the harmonic solutions on W_t^q changes little with t . These trends indicate that a fixed number of centroids k may be sufficient for quantizing similarity graphs that grow with time. In Figure 15, we fix the learning time at $t = n$ and vary the number of centroids k . The upper plots show the difference between the normalized Laplacian L and its approximation L_n^q . The difference is plotted as a function of the number of centroids k . The bottom plots compare the cumulative accuracy of the harmonic solutions up to time n on W (light gray lines), W_t^o (dark gray lines), and W_t^q (black lines). Note that as k increases, the quantization error decreases and the quality of the solutions on W_t^q improves. This trend is consistent with the theoretical results in our work (Section 5.4.3).

6.1.5.2 Face recognition In the second experiment, we evaluate our learner on 2 face recognition datasets: office space and environment adaptation. (Section 6.1.2).

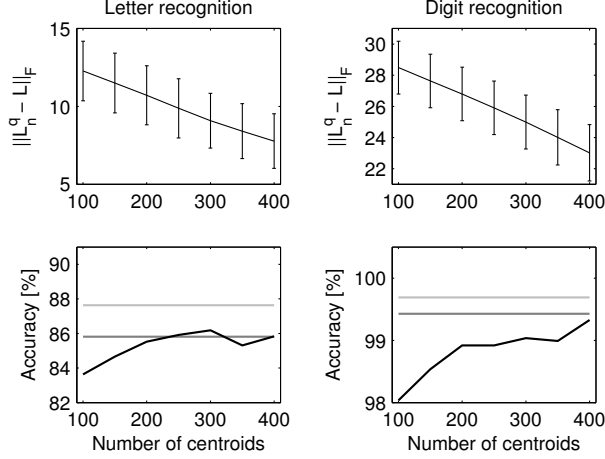


Figure 15: UCI ML: Quality of approximation as a function of number of centroids

The similarity of faces \mathbf{x}_i and \mathbf{x}_j is computed as $w_{ij} = \exp[-d(\mathbf{x}_i, \mathbf{x}_j)^2/2\sigma^2]$, where σ is a heat parameter, which is set to $\sigma = 0.025$, and $d(\mathbf{x}_i, \mathbf{x}_j)$ is the distance of the faces in the feature space. To make the graph W sparse, we treat it as an ε -neighborhood graph and set w_{ij} to 0 when $w_{ij} < \varepsilon$. The scalar ε is set as $\varepsilon = 0.1\gamma_g$. As a result, the lower the regularization parameter γ_g , the higher the number of edges in the graph W and our learner extrapolates to more unlabeled examples. If an example is disconnected from the rest of the graph W , we treat it as an outlier and neither predict the label of the example, nor use it to update the quantized graph. This setup makes our algorithm robust to outliers and allows for controlling its precision and recall by a single parameter γ_g . In the rest of the section, the number of centroids k is fixed at 500. More details are provided in Section 6.1.3.2.

In Figure 16, we compare our online algorithm to online semi-supervised boosting [Grabner et al., 2008] and a k -NN classifier, which is trained on all labeled faces. The recognizers are trained by a NN classifier (gray lines with circles), online semi-supervised boosting (thin gray lines), and our online learner (black lines with diamonds). The plots are generated by varying the parameters ε and γ_g . From left to right, the points on the plots correspond to decreasing values of the parameters. Online semi-supervised boosting is performed on 500 weak NN learners, which are sampled at random from the whole environment adaptation

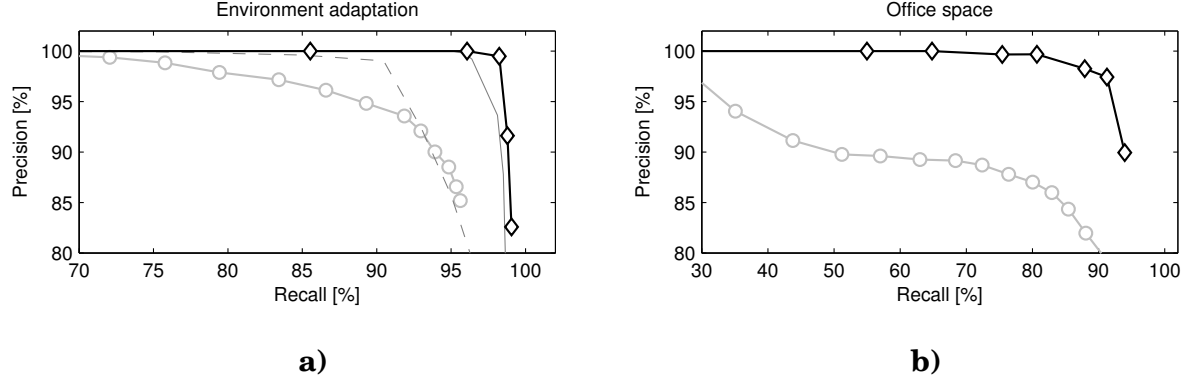


Figure 16: Comparison of 3 face recognizers on 2 face recognition datasets

dataset (solid line), and its first and last quarters (dashed line). The algorithm of [Grabner et al., 2008] is modified to allow for a fair comparison to our method. First, all weak learners have the nearest neighbor form $h_i(\mathbf{x}_t) = \mathbb{1}\{w_{it} \geq \varepsilon\}$, where ε is the radius of the neighborhood. Second, outliers are modeled implicitly. The new algorithm learns a regressor $H(\mathbf{x}_t) = \sum_i \alpha_i h_i(\mathbf{x}_t)$, which yields $H(\mathbf{x}_t) = 0$ for outliers and $H(\mathbf{x}_t) > 0$ when the detected face is recognized.

Figure 16a clearly shows that our learner is better than the nearest neighbor classifier. Furthermore, note that online semi-supervised boosting yields results as good as our method when given a good set of weak learners. However, future data are rarely known in advance, and when the weak learners are chosen using only a part of the dataset, the quality of the boosted results degrades significantly (Figure 16a). In comparison, our algorithm constantly adapts its representation of the world. How to incorporate a similar adaptation step in online semi-supervised boosting is not obvious.

In Figure 16b, we evaluate our learner on an 8-class face recognition problem. Despite the fact that only 4 faces of each person are labeled, we can identify people with 95 percent precision and 90 percent recall. In general, our precision is 10 percent higher than the precision of the NN classifier at the same recall level.

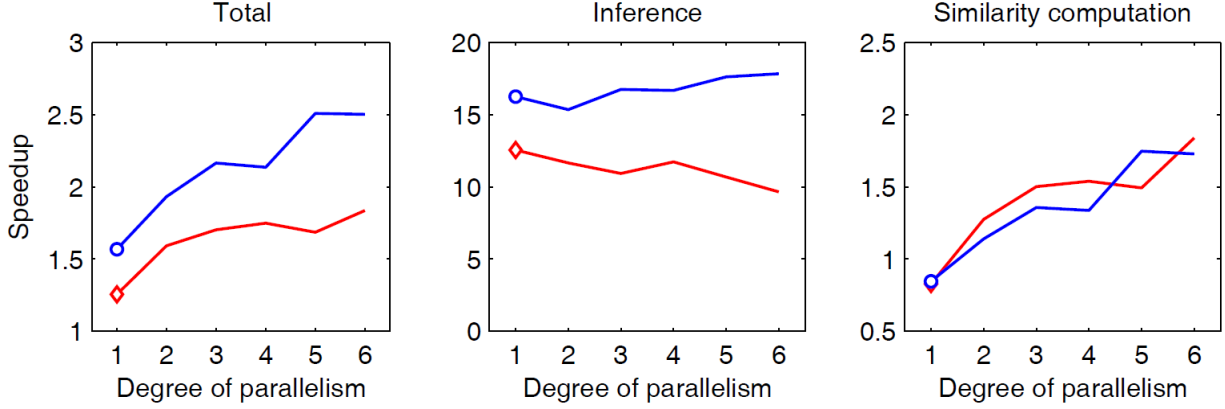


Figure 17: Speedups in the total, inference, and similarity computation times

6.1.6 Parallel SSL

In this experiment, we demonstrate how to speed up the online HS on a graph using an additional structure and parallelization (Section 3.6). Therefore, we perform our experiments on an Intel Xeon workstation with six cores. The experimental setup is the same as in Section 6.1.5. The number of labeled examples used for training models of Person 1 and 13 (from Figure 11) is 5 and 6, respectively. Figure 17 reports speedups due to decomposing the online HFS on 300 vertices into n_l smaller graphs of 50 vertices. The plots correspond to Person 1 (red lines) and 13 (blue lines) in our dataset. The diamonds and circles mark speedups that are obtained by the decomposition alone. We observe two main trends. First, the decomposition alone yields a modest speedup of 35% on average. The speedup is due to 15 times faster inference, which is a result of solving n_l smaller systems of linear equations, each with 50 variables, instead of a bigger one with 300. Second, we parallelize the online HS on the n_l smaller graphs using OpenMP [OpenMP, 2008]. The problem is trivially parallelizable because the graphs can be updated independently. Figure 17 shows that as the number of used cores increases, the online HFS can be sped up more than two times on average. The speedup is due to parallelizing the computation of similarities w_{ij} , which at this point consumes much more time than inference. Finally, note that the proposed decom-

position has almost no impact on the quality of our solutions. For Person 1 and Person 13, the loss in accuracy is 2.5% and 1%, respectively.

6.1.7 Conclusions

In this section, we have evaluated our algorithms for the semi-supervised learning tasks. Max-margin graph cuts algorithm learns max-margin graph cuts that are conditioned on the labels induced by the harmonic function solution. The approach is evaluated on a synthetic problem and three UCI ML repository datasets, and we have showed that it usually outperforms manifold regularization of SVMs. Next, we have evaluated our joint optimization approach for graph quantization and label propagation. We have experimentally showed that this approach can lead to a significant gain in classification accuracy over the competing quantization approaches. In the online SSL experiments we approximated a similarity graph for a harmonic solution. This algorithm significantly reduces the expense of the matrix computation in the harmonic solution, while retaining good control on the classification accuracy. Our evaluation shows that a significant speedup for semi-supervised learning can be achieved with little degradation in classification accuracy. We have further approximated the computation by decomposing the graph into several smaller graphs, thereby performing parallel multi-manifold learning. With such a decomposition we were able to speed up the computation even more with almost no loss in accuracy.

6.2 EVALUATIONS OF CONDITIONAL ANOMALY DETECTION METHODS

In this section we present the experiments using the CAD methods from Chapter 4. In all our experiments, we focus on the conditional anomalies in the class labels with respect to the features. In general, in the whole field of anomaly detection and in medical domain especially, the evaluation is extremely challenging. Most of time, it is subjective. The most veracious evaluations would have human experts judging the goodness of the methods. Since this is a very expensive way, most researchers resort to some surrogate measures. In the

area of mislabel detection, the most common surrogate measure is to change the labels of a fraction of the dataset and observe how many of those were detected as mislabeled. The problem with this measure is that the anomalies in the real life datasets are really *sam-pled* randomly. We describe the data we use in Sections 6.2.1 and 6.2.2 and the algorithms we use for the comparison in Section 6.2.3. We then provide two kinds of evaluations: the evaluation when the ground truth is known or can be computed (Section 6.2.4) and then the evaluation with human experts (Section 6.2.5).

6.2.1 Synthetic Datasets

We use two synthetic datasets for the evaluation of conditional anomaly detection methods where we know or can compute the true conditional anomaly score.

6.2.1.1 Core dataset Inspired by [Papadimitriou and Faloutsos, 2003], we generate a synthetic *Core* dataset, which consists of two overlapping squares from two uniform distributions. We extend this dataset with two tiny squares (Figure 23, top left). These 2 tiny squares may be considered anomalous, but not conditionally anomalous. The goal is to detect 12 conditional anomalies that are located in the middle square (Figure 23, top middle). We also use this dataset to demonstrate the challenges for conditional anomaly detectors, namely fringe and isolated points.

6.2.1.2 Mixtures of gaussians We generated three synthetic datasets (D1, D2, and D3) with known underlying distributions that let us compute the true anomaly scores.

We show the three datasets we used in our experiments in Figure 18. Each dataset consists of an equal number of samples from the class +1 and class -1. The class densities we use to generate these datasets are modeled with mixtures of multivariate Gaussians and vary in locations, shapes, and mutual overlaps.

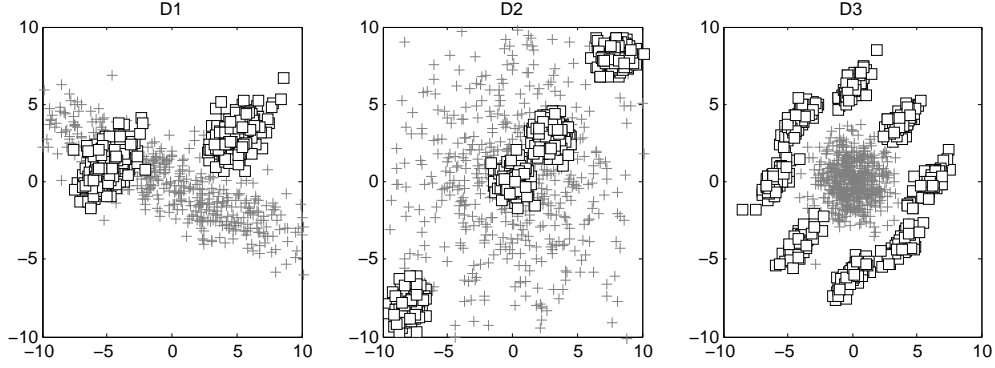


Figure 18: The three synthetic datasets with known underlying distributions

6.2.2 Post-surgical cardiac patients (PCP)

For the evaluation of our conditional anomaly detection methods on the real world medical data, we use the post-surgical cardiac patients (PCP) dataset. PCP is a database of de-identified records for 4486 post-surgical cardiac patients treated at one of the University of Pittsburgh Medical Center (UPMC) teaching hospitals. The entries in the database were populated from data from the MARS² system, which serves as an archive for much of the data collected at UPMC. The records for individual patients include discharge records, demographics, progress notes, all labs and tests (including standard and all special tests), two medication databases, microbiology labs, EKG, radiology and special procedures reports, and a financial charges database. The data in the PCP database were cleaned, cross-mapped, and stored in a local MySQL database with protected access. The cohort of the patient data we use in this dissertation consists of 4486 patients that underwent cardiac surgery from 2002 to 2007. The database is very heterogeneous and has many variables in different formats. It has also a fair amount of missing data.

The EHRs were first divided into two groups: a training set that included 2646 patients, and a test set that included 1840 patients. We use the time-stamped data in each EHR to segment the record at 8:00am every day to obtain multiple patient case instances, as

²MARS stands for Medical Archival System, and it is a medical record system that has been storing clinical and financial information from UPMC since 1980.

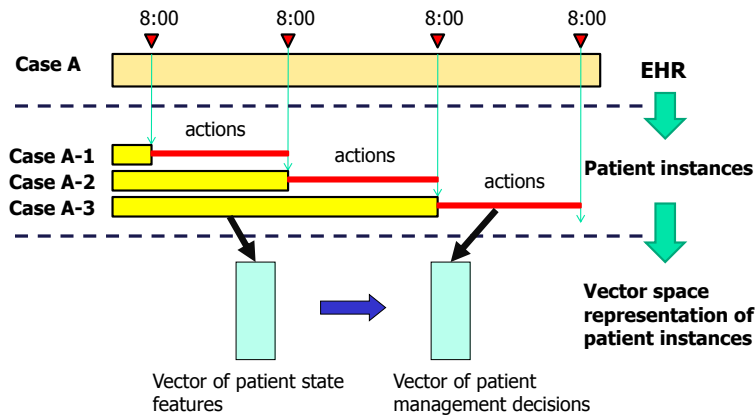


Figure 19: Processing of data in the electronic health record

illustrated in Figure 19: 1) segmentation of an EHR into multiple patient-state/decision instances, and 2) transformation of these instances into a vector space representation of patient states and their follow-up decisions. The segmentation led to 51,492 patient-state instances, such that 30,828 were used for training the model, and 20,664 were used in the evaluation.

To represent a patient state we adopt a vector space representation that is suitable for machine learning approaches. In this representation a patient state is represented by a set of features characterizing the patient at a specific point in time and their corresponding feature values. Features represent and summarize the information in the medical record such as last blood glucose measurement, last glucose trend, or the time the patient is on heparin.

The features used in our experiment were generated from a time series associated with different clinical variables, such as blood glucose measurement, platelet measurement, and Amiodarone medication. The clinical variables used in this study were from the following five sources:

1. Laboratory tests (LABs)
2. Medications (MEDs)

3. Visit features/demographics
4. Procedures
5. Heart support devices

Altogether, our dataset consists of 9,223 different features. We now briefly describe the features generated for clinical variables in each of these categories.

6.2.2.1 Visit/Demographic Features We only have 3 features in this category: age, sex and race. These are static and the same for every time point we generate.

6.2.2.2 Lab features For the categorical labs, for example the ones with POS/NEG results, we use the following features: last value, second to last value, first value, time since the last order, is the order pending, is the value known, and is the trend known. For the labs with continuous or ordinal values we use a richer set of features, including features as difference between the last two values, the slope of last 2 values, and their percentage drop/increase. We use the same kind of features for the following pairs of lab values: (last value, first value), (last value, nadir value), and (last value, horizon value). Nadir and horizon values are the lab values with the smallest and the greatest value recorded up to that point. Figure 20 illustrates a subset of features generated for labs with continuous values. The total number of features generated for such a lab is 28. Some of the features here that can be derived from Figure 20 are:

- Last value: A
- Last value difference = B-A
- Last percentage change = $(B-A)/B$
- Last slope = $(B-A) / (t_B - t_A)$
- Nadir = D
- Nadir difference = A-D
- Nadir percentage difference = $(A-D)/D$
- Baseline = F
- Drop from baseline = F-A

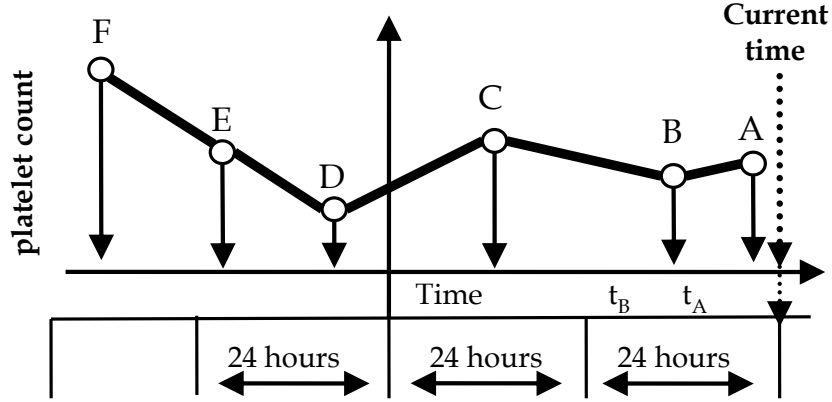


Figure 20: Examples of temporal features for continuous lab values

- Percentage drop from baseline = $(F-A)/F$
- 24 hour average = $(A+B)/2$

6.2.2.3 Medication features For each medication we used four features: 1) an indicator if the patient is currently on the medication, 2) the time since the patient was first put on that medication, 3) the time since the patient was last on that medication, and 4) the time since last change in the order of the medication.

6.2.2.4 Procedure features The procedure features capture the information about procedures, such as *Heart valve repair*, that were performed either in operating room (OR) or at the bedside. In our data we distinguish 36 different procedures that are performed on cardiac patients. We record four features per procedure: 1) the time since the procedure was done the last time 2) the time since the procedure was done the first time 3) an indicator of whether the procedure was done in the last 24 hours and 4) an indicator of if the procedure was done.

6.2.2.5 Heart support device features Finally, we describe the status of 4 different heart support devices: an extra-corporeal membrane oxygenation (ECMO), a balloon counter

pulsation, a pacemaker, and other heart assist devices. For each of them we record a single feature which describes whether the device is currently used to support the patient’s heart function.

6.2.2.6 Orders/labels Labels in this case correspond to patient-management decisions. In addition to feature generation, every patient-state example in the dataset that was generated by the above segmentation process was linked to lab order decisions and medication decisions that were made for the patient within next 24 hours. Patient management decisions considered were:

- lab order decisions with (true/false) values reflecting whether the lab was ordered within the next 24 hours or not
- medication decisions with (true/false) values reflecting if the patient was given a medication within the next 24 hours or not.

A total of 335 lab order decisions and 407 medication decisions were recorded and linked to every patient-state example in the dataset.

6.2.3 Algorithms for Comparison

In this section we review the CAD algorithms chosen for the comparison with our CAD methods.

6.2.3.1 Discriminative SVM anomaly detection For the baseline method we use an SVM based method [Valko et al., 2008, Hauskrecht et al., 2010], that computes an anomaly score from the distance from the hyperplane. SVM [Vapnik, 1995, Burges, 1998] is a discriminative method that learns the decision boundary as

$$\mathbf{w}^T \mathbf{x} + w_0 = \sum_{i \in SV} \hat{\alpha}_i y_i (\mathbf{x}_i^T \mathbf{x}) + w_0,$$

where only samples in the support vector set (SV) contribute to the computation of the decision boundary. To support classification tasks, the projection defining the decision boundary

is used to determine the class of a new example. That is, if the value

$$\mathbf{w}^T \mathbf{x} + w_0 \geq 0$$

is positive, then $C(\mathbf{x})$ belong to one class, but if it is negative it belongs to the other class. However, for conditional anomaly detection we use the projection itself for the positive class and the negated projection for the negative class to measure the deviation:

$$d(y|\mathbf{x}) = y(\mathbf{w}^T \mathbf{x} + w_0), \text{ where } y \in \{-1, 1\}$$

In other words, the smaller the projection is the more likely the example is anomalous. We note that the negative projections correspond to misclassified examples.

6.2.3.2 One-class SVM As an example of a classical anomaly detection method converted to the CAD method we compare to the one-class SVM [Manevitz and Yousef, 2002]. Originally proposed in [Scholkopf et al., 1999], the method only needs positive examples to learn the margin. The idea is that the space origin (zero) is treated as the only example of the ‘negative’ class. In that way the learning essentially estimates the support of the distribution. The data that do not fall into this support have negative projections and can be considered anomalous. In our scenario, we will learn one one-class SVM for each of the classes and based on the test label (which is known) we calculate the anomaly score. The more negative the score the higher the rank of the anomaly.

6.2.3.3 Quadratic discriminant analysis In the quadratic discriminant analysis (QDA) model [Hastie et al., 2001], we model each class by a multivariate Gaussian, and the anomaly score is the class posterior of the opposite class.

6.2.3.4 Weighted NN We also use the weighted k -NN approach [Hastie et al., 2001] that uses the same weight metric W as SoftHAD, but relies on only on the labels in the local neighborhood and does not account for the manifold structure.

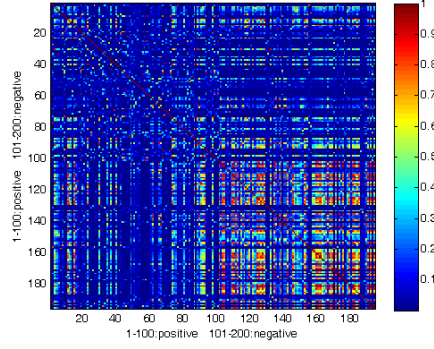


Figure 21: The weight matrix for 100 negative and 100 positive cases of HPF4 order

6.2.3.5 Parameters for the graph-based algorithms The similarity weights are computed as

$$w_{ij} = \exp \left[-\frac{\|\mathbf{x}_i - \mathbf{x}_j\|_{2,\psi}^2}{p\sigma^2} \right],$$

where p is the number of features and $\psi = (p \times 1)$ is a weighing of the features based on their discriminative power. Including p in the weight metric allows us to control the connectivity of the graph. Next, σ is chosen so that the graph is reasonably sparse [Luxburg, 2007]. We follow [Valizadegan and Tan, 2007] and chose σ as 10% of the mean of empirical standard deviations of all features. Based on the experiments, our algorithm is not sensitive to the small perturbations of σ ; what is important is that the graph does not become disconnected by having all edges of several nodes with weights close to zero.

For the feature weights ψ for PCP data we used the univariate Wilcoxon (ROC) score [Hanley and Mcneil, 1982], which is typically used for medical data [Hauskrecht et al., 2006]. Since this score ranges from 0.5 to 1, we modify the score by subtracting 0.5 and raising it to a power of 5 to make the differences between the weights larger. We use to same metric for the weighted NN anomaly detection from Section 5.6. We vary the regularization parameter as $\lambda \in \{10^{-5}, 10^{-9}, \dots, 10^5\}$. Figure 21 illustrates this metric on a binary classification task for the heparin induced thrombocytopenia (a life threatening condition that may occur with prolonged heparin treatments). One hundred negative and one hun-

dred positive cases and their mutual similarities are shown. We can see that the positive cases are much closer to each other (bottom right part in Figure 21) than the negatives. For the other datasets, we used a uniform ψ for all features.

6.2.4 Evaluation of CAD with Known Ground Truth

6.2.4.1 CAD on synthetic datasets with known distribution The evaluation of a CAD is a very challenging task when the true model is not known. Therefore, we first evaluate and compare the results of different CAD methods on three synthetic datasets (D1, D2, and D3) with known underlying distributions that let us compute the true anomaly scores (Section 6.2.1.2). Then, we show the advantage of regularizing a discriminative approach on a synthetic dataset. We will use a 2D synthetic dataset, where we can demonstrate the ability to tackle fringe and isolated points as described in Section 4.6.

For each experiment we sample the datasets 10 times. After the sampling, we randomly switch the class labels for three percent of examples. We then calculate the true anomaly score as $P(y \neq y_i | \mathbf{x}_i)$, reflecting how anomalous the label of the example is with respect to the true model.

Each of the methods outputs a score which orders the examples according to the belief of the anomalous labeling. For each of the CAD methods, we assess how much this ordering is consistent with the ordering of the true anomaly score. In particular, we calculated the area under the receiver operating characteristic (AUROC), which is inversely proportional to the number of swaps between the ordering induced by the evaluated method and the true ordering.

Table 1 compares the AUROCs of the experiment for all methods for 1000 samples per dataset. The results demonstrate that our λ -RWCAD method outperforms the weighted k -NN, the one-class SVM, and the discriminative SVM with the RBF kernel³, and it is comparable to our label propagation SoftHAD algorithm on D2 and D3. SoftHAD seems to be the best choice overall because it takes advantage of both local and global consistency. However, it is computationally more expensive.

³We also evaluated the linear versions of SVM and the one-class SVM, but the results were inferior to the ones with the RBF kernel.

	Dataset D1	Dataset D2	Dataset D3
<i>SVM RBF</i>	58.4% (7.4)	49.3% (2.1)	51.7% (1.9)
<i>1cSVM RBF</i>	51.5% (0.8)	47.4% (0.6)	59.1% (0.6)
<i>SoftHAD</i>	82.8% (1.3)	63.9% (2.3)	63.5% (3.3)
<i>weighted k-NN</i>	64.3% (2.2)	45.6% (1.6)	62.5% (1.5)
<i>λ-RWCAD</i>	64.7% (0.8)	68.9% (1.1)	67.4% (1.9)

Table 1: Mean anomaly AUROC and variance on three synthetic datasets

In the next experiment we evaluate the scalability of the graph-based methods as we increase the number of examples. All of the graph methods were given the same graph (with the same weight matrix). Figure 22 compares the running times of these algorithms. We see that while the running time of the SoftHAD algorithm becomes prohibitive once the number of examples gets into thousands, our algorithm scales similarly to the k -NN method. Figure 22 also shows the time spent in constructing the graph from the data, which is the same among all the graph-based methods. Observe that both the weighted k -NN and our λ -RWCAD algorithm take very little time over the necessary graph construction time to do their calculations.

6.2.4.2 CAD on UCI ML datasets with ordinal response variable We also evaluated our method on the three UCI ML datasets [Asuncion and Newman, 2011], for which an ordinal response variable was available to calculate the true anomaly score. In particular, we selected 1) *Wine Quality* dataset with the response variable *quality*, 2) *Housing* dataset with the response variable *median value of owner-occupied homes*, and 3) *Auto MPG* dataset the response variable *miles per gallon*. In each of the datasets we scaled the response variable y_r to the $[-1, +1]$ interval and set the class label as $y := y_r \geq 0$. As with the synthetic datasets, we randomly switched the class labels for three percent of examples. The true anomaly score was computed as the absolute difference between the original response variable y_r and the

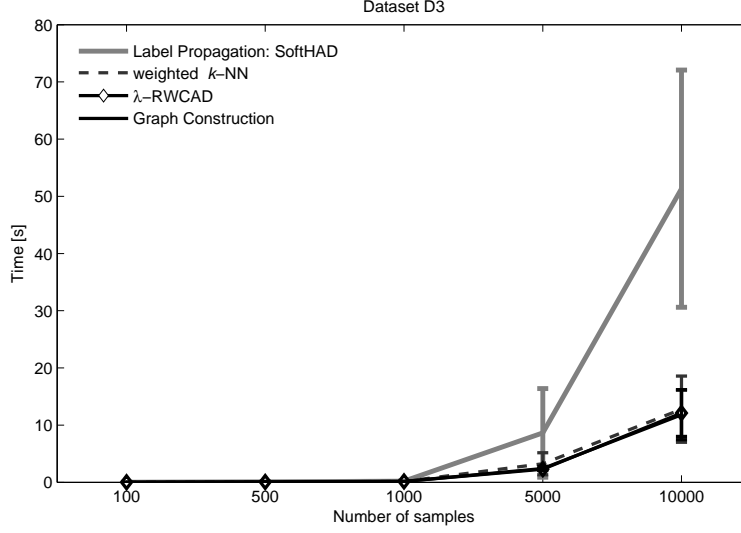


Figure 22: Computation time comparison for the three graph-based methods

(possibly switched) label. Table 2 compares the agreement scores (over 100 runs) to the true score for all methods on (2/3, 1/3) train-test split. The results in bold show when a method significantly outperforms the rest. Again, we see that SoftHAD either performed the best or was close to the best method.

	Wine Quality	Housing	Auto MPG
<i>QDA</i>	75.1% (1.3)	56.7% (1.5)	65.9% (2.9)
<i>SVM</i>	75.0% (9.3)	58.5% (4.4)	37.1% (8.6)
<i>one-class SVM</i>	44.2% (1.9)	27.2% (0.5)	50.1% (3.5)
<i>weighted k-NN</i>	67.6% (1.4)	44.4% (2.0)	61.4% (2.3)
<i>SoftHAD</i>	74.5% (1.5)	71.3% (3.2)	72.6% (1.7)

Table 2: Mean anomaly agreement score and variance on 3 UCI ML datasets

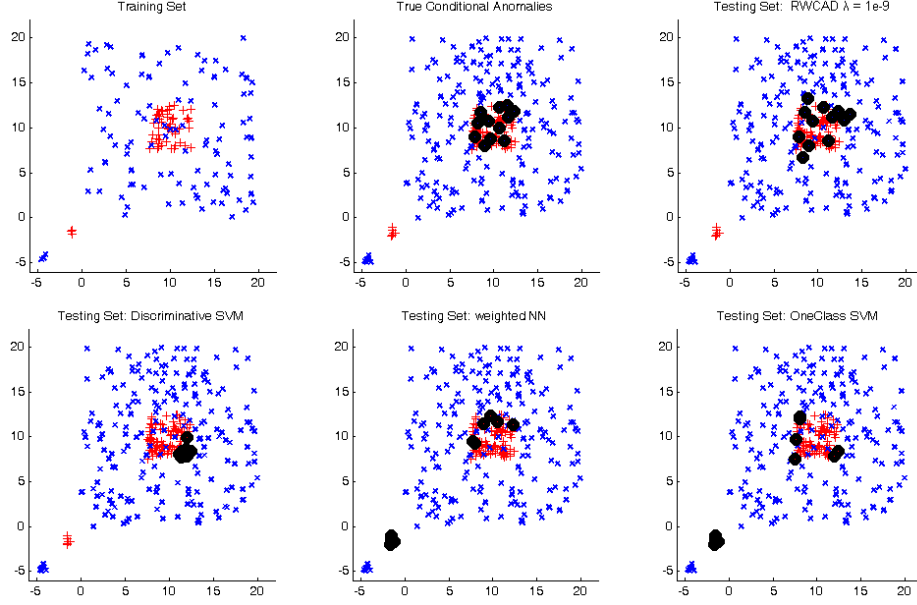


Figure 23: Conditional anomaly detection on a synthetic *Core* dataset

6.2.4.3 CAD on Core dataset with fringe points In this part we tested our CAD method on the synthetic Core dataset (Section 6.2.1.1). Besides the one-class SVM (Section 6.2.3.2), we also compared to the weighted k -NN described in Section 5.6 and to the cross-outlier method [Papadimitriou and Faloutsos, 2003] described in Section 2.3.2.

In Figure 23, the training data consists of a bigger square of 100 uniformly distributed points (blue ‘x’), a smaller square of 50 uniformly distributed points (red ‘+’), and 2 small groups of points (3 points from each class). The testing dataset is twice as big sampled from the same distribution. The big black dots display true conditional anomalies and the top 12 highest ranked conditional anomalies for 1) our λ -RWCAD method, 2) the discriminative SVM anomaly detection, 3) the weighted k -NN, and 4) the one-class SVM learned for both of the classes.

The cross-outlier method [Papadimitriou and Faloutsos, 2003] was able to find all of the conditional anomalies in the middle square, but also declared many *fringe* points (points at the outer boundary of the bigger square) as anomalous (see Figure 2, middle row in

[Papadimitriou and Faloutsos, 2003]). Although the authors claim that the fringe points are ‘clearly different from the rest of the points’ [Papadimitriou and Faloutsos, 2003], we prefer methods that only find anomalously labeled instances.

In Figure 23, we also show the top 12 highest scored anomalies from the 4 competing methods. The discriminative SVM anomaly detection (Figure 23, bottom left) could only detect the fringe points from the smaller square, since the anomaly score there corresponds to the most incorrectly classified testing points. Next, the objective of the one-class SVM is to detect the points with minimal support. In Figure 23, bottom right, we see that the one-class SVM ranked with the highest score the fringe points of the smaller square and one of the tiny squares. The weighted k -NN (Figure 23, bottom middle) detects half of the true anomalies, but also falsely detects one of the tiny squares as anomalous. Our method (Figure 23, top right) avoids such a mistake due to the regularization. Although the results of our method do not completely match with the truth, the 3 points detected outside the smaller square are in its vicinity.

6.2.4.4 Conclusions We showed how we use regularization to avoid the detection of isolated and the fringe points. In general, the advantage of the CAD approach over knowledge-based error detection approaches is that the method is evidence-based, and hence requires little or no input from a domain expert.

6.2.5 Evaluation of Expert Assessed Clinically Useful Anomalies

6.2.5.1 Pilot study in 2009 The aim of the study [Hauskrecht et al., 2010] was to test the hypothesis that clinical anomalies lead to good clinical alerts.

Learning anomaly detection models The training set was used to build three types of anomaly detection models: 1) models for detecting unexpected lab-order omissions, 2) models for detecting unexpected medication omissions, and 3) models for detecting unexpected continuation of medications (commissions).

Selection of alerts for the study The alerts for the evaluation study were selected as follows. We first applied all the above anomaly detection models to matching patient instances

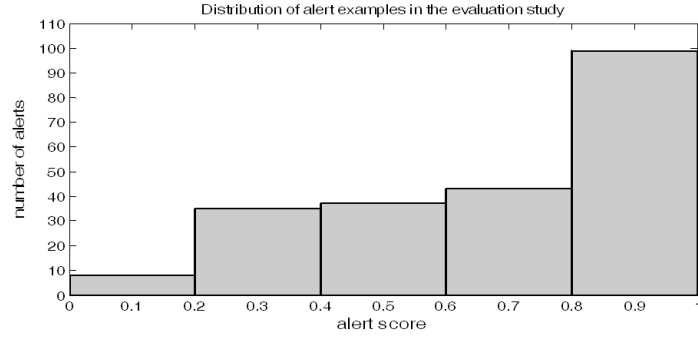


Figure 24: Histogram of alert examples in the study according to their alert score

in the test set. The following criteria were then applied. First, only models with AUC of 0.68 or higher (to limit the number of models to those with a good predictive performance) were considered. This means that many predictive models built did not qualify and were never used. Second, the minimum anomaly score for all alert candidates had to be at least 0.15. Third, for each decision, only the top 125 anomalies and the top 20 alerts obtained from the test data were considered as alert candidates. This led to 3,768 alert candidates, from which we selected 222 alerts for 100 patients, such that 101 alerts were lab-omission alerts, 55 were medication-omission alerts, and were 66 medication-commission alerts. The cases were selected such that their alert scores cover the whole range of alert scores, biased towards the more anomalous cases. Figure 24 shows the distribution of alerts in the study according to the alert score.

Alert reviews. The alerts selected for the study were assessed by physicians with expertise in post-cardiac surgical care. The reviewers 1) were given the patient cases and model-generated alerts for some of the patient management decisions, and 2) were asked to assess the clinical usefulness of these alerts. We recruited 15 physicians to participate in the study, of which 12 were fellows and 3 were faculty from the Departments of Critical Care Medicine and Surgery. The reviewers were divided randomly into five groups, with three reviewers per group, for a total of 15 reviewers. Overall, each clinician made assessments of 44 or 45 alerts, generated for 20 different patients. The total number of alerts reviewed by all

clinicians was 222 and included: 101 lab omission alerts, 55 medication omission alerts, and 66 medication commission alerts. The survey was conducted over the Internet using a secure web-based interface [Post and Harrison, 2008].

Alert assessments. The pairwise kappa agreement scores for the groups of three ranged from 0.32 to 0.56. We use the majority rule to define the gold standard. That is, an alert was considered to be useful if at least two out of three reviewers found it to be useful. Out of the 222 alerts selected for the evaluation study, 121 alerts were agreed upon by the panel (via the majority rules) as a useful alert.

Analysis of clinical usefulness of alerts. We analyze the extent to which the alert score from a model was predictive of it producing clinically important alerts. Figure 25 summarizes the results by binning the alert scores (in intervals of the width of 0.2, as in Figure 24) and presenting the true alert rate per bin. The true alert rates vary from 19% for the low alert scores to 72% for the high alert scores, indicating that higher alert scores are indicative of higher true alert rates. This is also confirmed by a positive slope of the line in Figure 25, which is obtained by fitting the results via linear regression and the results of the ROC analysis. All alerts reviewed were ordered according to their alert scores, from which we generated an ROC curve. The AUC for our alert score was 0.64. This is statistically significantly different from 0.5, which is the value one expects to see for random or non-informative orderings. Again, this supports that higher alert scores induce better true alert rates. Finally, we would like to note that alert rates in Figure 4 are promising and despite alert selection restrictions, they compare favorably to alert rates of existing clinical alert systems [Schedlbauer et al., 2009, Bates et al., 2003].

6.2.5.2 Soft harmonic anomaly detection For this experiment, we use the PCP dataset (Section 6.2.2) and reuse the human expert evaluations from Section 6.2.5.1. We compute the anomaly scores according to (Section 4.6.2)

Scaling for multi-task anomaly detection So far, we have described CAD only for a single task (anomaly in a single label). In this dataset, we have 749 binary tasks that correspond to 749 different possible orders of lab tests or medications. In our experiments, we compute the CAD score for each task independently. Figure 26 shows the CAD scores

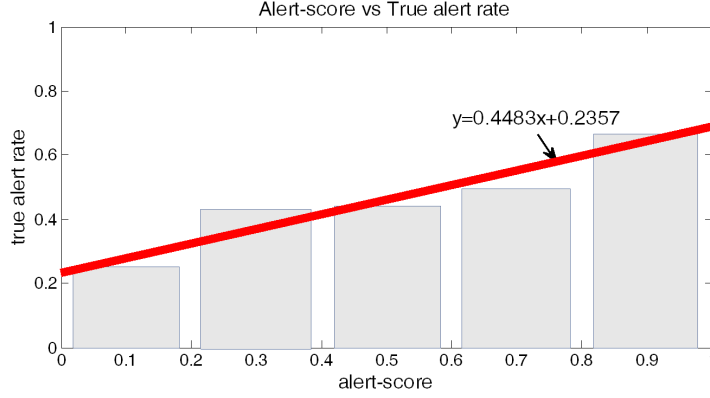


Figure 25: The relationship between the alert score and the true alert rate

for two of them. CAD scores close to 1 indicate that the order should be done, while the scores close to 0 indicate the opposite. The ranges for the anomaly scores can vary among the different tasks, as one can notice in Figure 26. The scores for the top and bottom task range from 0.1 to 0.9 and from 0.25 and 0.61, respectively. The arrow in both cases points to the scores of the evaluated examples, both with negative labels. Despite the lower score for the bottom task, we may believe that it is more anomalous, because it is more extreme within the scores for the same task. However, we want to output an anomaly score, which is comparable among the different tasks so we can set a unified threshold when the system is deployed in practice. Another reason for comparable scores is that we can have, for instance, 2 models each alerting that a certain medication was omitted. Nevertheless, omitting one of the medications can be more severe than the other (eg. antibiotics vs. vitamins). To achieve the score comparability, we propose a simple approach, where we take the minimum and the maximum score obtained for the training set and scale all scores for the same task linearly so that the score after scaling ranges from 0 to 1.

In Figure 27, we fix $\gamma_g = 1$ and vary the number of examples we sample from the training set to construct the similarity graph, and also compare it to the weighted k -NN. The error bars show the variances over 10 runs. Notice that both of the methods are not too sensitive to the graph size. This is due to the multiplicity adjustment for the backbone graph

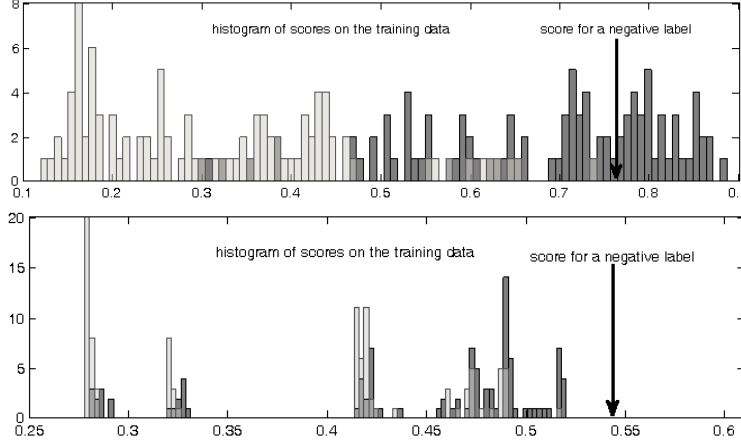


Figure 26: Histogram of anomaly scores for 2 different tasks

(Section 4.6.2). Since we use the same graph both for SoftHAD and the weighted k -NN, we anticipate that we are able to outperform the weighted k -NN due to the label propagation over the data manifold and not only within the immediate neighborhood. In Figure 28, we compare SoftHAD to the CAD using SVM with an RBF kernel for different regularization settings. We sampled 200 examples to construct a graph (or train an SVM) and varied the γ_g regularizer (or cost c for SVM). We outperform the SVM approach over the range of regularizers. The AUC for the one-class SVM with an RBF was consistently below 55%, so we do not show it in the figure. We also compared the two methods with scaling adjustment for this multi-task problem (Figure 28). The scaling of anomaly scores improved the performance of both methods and makes the methods less sensitive to the regularization settings.

6.2.5.3 Conclusions In the evaluations with human experts on the real-world data, we showed we can indeed learn clinically useful alerts. The results reported here support that this is a promising methodology for raising clinically useful alerts. Moreover, we showed that with label propagation on a data similarity graph built from patient records, we can significantly outperform previously proposed SVM-based anomaly detection in detecting conditional anomalies.

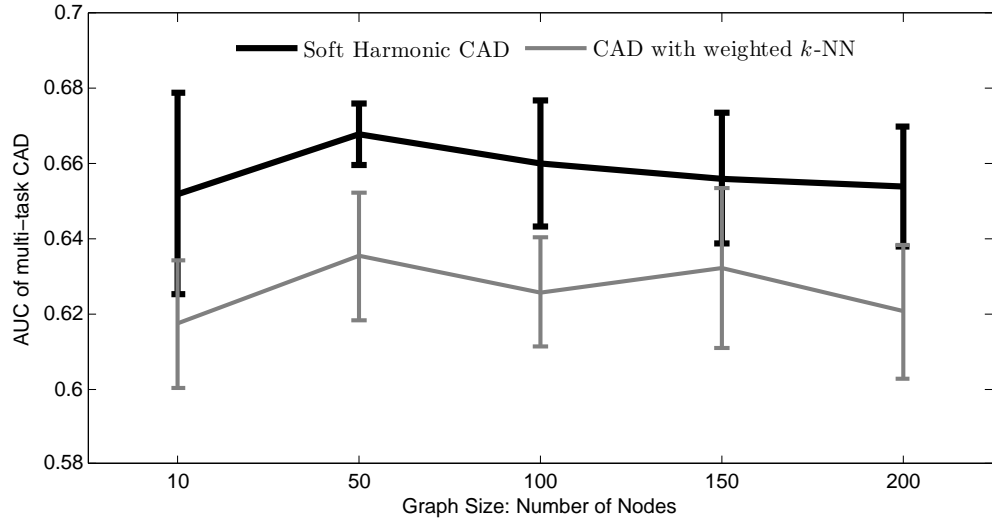


Figure 27: Medical Dataset: Varying graph size

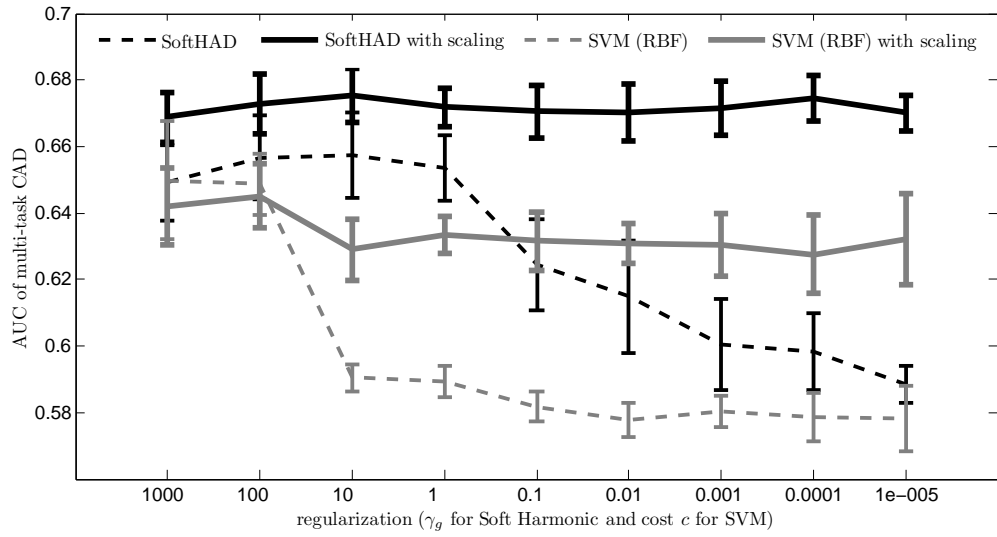


Figure 28: Medical Dataset: Varying regularization

7.0 DISCUSSION

We have presented several algorithms for semi-supervised learning and conditional anomaly detection. The algorithms are based on label propagation on a similarity graph built from examples in a dataset. Label propagation on graphs is polynomial, but still a computationally expensive method. Therefore, we focused on the approximation approaches for the cases with large datasets and when the data arrive in a stream. The main contributions of this dissertation to the field of machine learning are summarized below.

- We presented one of the first works on *online semi-supervised learning*. Despite a very natural scenario, this setting has not been extensively studied in the past. To our best knowledge this is the first work on online semi-supervised learning that comes with theoretical guarantees. Moreover, we built a real-time system that works on noisy real-world data.
- We introduced a label propagation method for conditional anomaly detection and applied it to compute the anomaly score for the class labels. We presented a general framework where the discriminative models need to be regularized to decrease the effect caused by isolated and fringe points in the data.
- We presented a new semi-supervised learning algorithm based on max-margin graph cuts, which in some classes of learning functions can perform better than the manifold regularization approach.
- We introduced a joint learning of the backbone graph and the label propagation and show its relationship to the elastic nets. This is one of the first works, besides [Zhu and Lafferty, 2005], that relates propagated labels and cluster centers.

We also made contributions to the area of health informatics:

- The existing error detection systems deployed in hospitals are built entirely by human experts. Although these systems are time-consuming and costly to build, they typically do not cover all the specialties of medical care. The statistical anomaly detection approach for error detection, proposed and studied in this work, relies solely on data that are extracted from existing patient record repositories and little or no expert input is required. This reduces the cost of the approach and its deployment. Our most important finding is that the alert systems can be learned from the past patient data instead of creating rule-based alert systems that require expensive human time to tune and are currently used in hospitals.
- We proposed a non-parametric method that can discover anomalies in clinical actions. The common use cases are: 1) discovery of an omitted order of a lab test 2) commission of a drug that has interactions with previously taken drugs 3) controlling overspending: a detection of expensive actions that were not necessary, when the resources could have been used better.
- We conducted an extensive study with the human evaluation of the alerts on the real patient records, showing that the higher anomaly scores corresponded to the higher severity of the alerts.

There are, however, some assumptions and limitation of our methods:

- We assume that the data can be modeled with pair-wise similarities between the nodes and that such a model is meaningful.
- The similarity function between the graph nodes needs to be given or learned.
- Our methods are expected to perform well when the manifold assumption holds.
- In the approximation settings, when we create a summary graph (both online and in a large scale setting), we assume that we can model the data well with a reduced number of nodes.

Moreover, electronic health records (EHRs) are a necessary requirement for the successful deployment of the conditional anomaly methods described here. With an increasing number of medical groups adopting EHR systems [[Gans et al., 2005](#)], more people will benefit

from reduced medical errors. We imagine that the inclusion of our method into the existing EHR systems will require no extra time from physicians. Our anomaly detection framework serves more as background monitoring system that raises alerts only when the confidence of an anomaly is high. Since our conditional anomaly methods produce a soft score reflecting the confidence, the threshold for alerting could be adjusted. Nevertheless, the statistical anomalies that our methods produce may not need to always correspond to useful alerts. For instance, an omission of a routine lab test or administration of a vitamin may be a significant statistical anomaly, but might not be worthy of physician’s attention.

We now outline some related open questions and research opportunities.

- *Structured Anomaly Detection*

In this dissertation we applied our conditional anomaly detection method to discover unusual clinical actions. Although, we did it separately for each action, these actions are not independent. For example, a clinician usually prescribes a set of drugs such that:

- drugs with the same effect do not tend to be given at the same time.
- drugs with the opposite effect do not tend to be given at the same time.
- drugs with negative interactions do not tend to be given at the same time.

Therefore, we can form groups of drugs from which at most one is administered at the same time. This additional information could be given a priori or learned from the data.

- *Graph Parametrization:* Despite the research in this area, the graph construction is still not well understood. There are some rules of thumb, such as $\log(n)$ for the number of neighbors, but a problem-specific calibration is usually needed. In particular, the clinical data could benefit from the similarity measures (kernels) that would measure the similarity of the conditions from the electronic health data.
- *Multi-manifold Learning* In our multi-manifold learning approach, we decomposed the graph and kept updating each of the components independently in parallel. There can be some benefit in accuracy if we allow the components to exchange some information.
- *Concept Drift* In this dissertation we were concerned with adapting to the distribution in a short-term period. The problem of concept drift is concerned with long-term changes,

such as when a face of a person changes as he or she grows older or when medical practices change. One possible extension of our methods can be the online graph-based learning with forgetting the history. For example, we can delete the graph nodes which were added a long time ago and do not change the current prediction much if they are removed.

We expect that future research will address these questions. We hope that online semi-supervised learning will become more studied and used to address machine learning problems. We believe that our conditional anomaly detection methods will prevent some of the adverse outcomes, especially in medicine.

This work was supported by the NIH grants R21 LM009102-01A1, R01 1R01LM010019-01A1 and by the Mellon Foundation.

BIBLIOGRAPHY

- [Aggarwal et al., 2003] Aggarwal, C. C., Han, J., Wang, J., and Yu, P. S. (2003). A framework for clustering evolving data streams. In *Proceedings of the 29th international conference on Very large data bases - Volume 29*, VLDB '2003, pages 81–92. VLDB Endowment.
- [Aggarwal and Yu, 2001] Aggarwal, C. C. and Yu, P. S. (2001). Outlier detection for high dimensional data. In *SIGMOD '01: Proceedings of the 2001 ACM SIGMOD international conference on Management of data*, pages 37–46, New York, NY, USA. ACM.
- [Akoglu et al., 2010] Akoglu, L., McGlohon, M., and Faloutsos, C. (2010). Oddball: Spotting anomalies in weighted graphs. In *Advances in Knowledge Discovery and Data Mining, 14th Pacific-Asia Conference, PAKDD 2010, Hyderabad, India, June 21-24, 2010. Proceedings. Part II*, pages 410–421.
- [Aktolga et al., 2010] Aktolga, E., Ros, I., and Assogba, Y. (2010). Detecting outlier sections in us congressional legislation. In *Proceedings of SIGIR*.
- [Asuncion and Newman, 2011] Asuncion, A. and Newman, D. (2011). UCI machine learning repository.
- [Bates et al., 2003] Bates, D. W., Kuperman, G. J., Wang, S., Gandhi, T., Kittler, A., Volk, L., Spurr, C., Khorasani, R., Tanasijevic, M., and Middleton, B. (2003). Ten commandments for effective clinical decision support: making the practice of evidence-based medicine a reality. *J Am Med Inform Assoc*, 10(6):523–530.
- [Belkin et al., 2004] Belkin, M., Matveeva, I., and Niyogi, P. (2004). Regularization and semi-supervised learning on large graphs. In *Proceeding of the 17th Annual Conference on Learning Theory*, pages 624–638.
- [Belkin et al., 2006] Belkin, M., Niyogi, P., and Sindhvani, V. (2006). Manifold regularization: A geometric framework for learning from labeled and unlabeled examples. *Journal of Machine Learning Research*, 7:2399–2434.
- [Bengio et al., 2004] Bengio, Y., Paiement, J., Vincent, P., Delalleau, O., Le Roux, N., and Ouimet, M. (2004). Out-of-sample extensions for LLE, isomap, MDS, eigenmaps, and spectral clustering. In Thrun, S., Saul, L., and Schölkopf, B., editors, *Advances in Neural Information Processing Systems 16*. MIT Press, Cambridge, MA.

- [Bennett and Demiriz, 1999] Bennett, K. and Demiriz, A. (1999). Semi-supervised support vector machines. In *Advances in Neural Information Processing Systems 11*, pages 368–374.
- [Bezdek and Hathaway, 2002] Bezdek, J. C. and Hathaway, R. J. (2002). Some notes on alternating optimization. In *Proceedings of the 2002 AFSS International Conference on Fuzzy Systems. Calcutta: Advances in Soft Computing*, AFSS’02, pages 288–300, London, UK. Springer-Verlag.
- [Bousquet and Elisseeff, 2002] Bousquet, O. and Elisseeff, A. (2002). Stability and generalization. *Journal of Machine Learning Research*, 2:499–526.
- [Bradski, 2000] Bradski, G. (2000). The OpenCV Library. *Dr. Dobb’s Journal of Software Tools*.
- [Breunig et al., 2000] Breunig, M. M., Kriegel, H.-P., Ng, R. T., and Sander, J. (2000). Lof: identifying density-based local outliers. *SIGMOD Rec.*, 29(2):93–104.
- [Brodley and Friedl, 1999] Brodley, C. E. and Friedl, M. A. (1999). Identifying mislabeled training data. *J. Artif. Intell. Res. (JAIR)*, 11:131–167.
- [Burges, 1998] Burges, C. J. C. (1998). A tutorial on support vector machines for pattern recognition. *Data Mining and Knowledge Discovery*, 2(2):121–167.
- [Chandola et al., 2009] Chandola, V., Banerjee, A., and Kumar, V. (2009). Anomaly detection: A survey. *ACM Comput. Surv.*, 41:15:1–15:58.
- [Chang and Lin, 2001] Chang, C.-C. and Lin, C.-J. (2001). *LIBSVM: a library for support vector machines*. Software available at <http://www.csie.ntu.edu.tw/~cjlin/libsvm>.
- [Chapelle et al., 2006] Chapelle, O., Schölkopf, B., and Zien, A., editors (2006). *Semi-Supervised Learning*. MIT Press, Cambridge, MA.
- [Charikar et al., 1997] Charikar, M., Chekuri, C., Feder, T., and Motwani, R. (1997). Incremental clustering and dynamic information retrieval. In *Proceedings of the 29th Annual ACM Symposium on Theory of Computing*, pages 626–635.
- [Chawla et al., 2003] Chawla, N. V., Lazarevic, A., Hall, L. O., and Bowyer, K. W. (2003). Smoteboost: Improving prediction of the minority class in boosting. In *PKDD*, pages 107–119.
- [Chung, 1997] Chung, F. (1997). *Spectral Graph Theory*. American Mathematical Society.
- [Cortes et al., 2008] Cortes, C., Mohri, M., Pechyony, D., and Rastogi, A. (2008). Stability of transductive regression algorithms. In *Proceedings of the 25th International Conference on Machine Learning*, pages 176–183.

- [Cramér, 1999] Cramér, H. (1999). *Mathematical methods of statistics*. Princeton landmarks in mathematics and physics. Princeton University Press.
- [Das, 2009] Das, K. (2009). *Detecting Patterns of Anomalies*. PhD thesis, Carnegie Mellon University.
- [Das et al., 2008] Das, K., Schneider, J., and Neill, D. B. (2008). Anomaly pattern detection in categorical datasets. In *Proceeding of the 14th ACM SIGKDD international conference on Knowledge discovery and data mining*, KDD '08, pages 169–176, New York, NY, USA. ACM.
- [Delalleau et al., 2005] Delalleau, O., Bengio, Y., and Roux, N. L. (2005). Efficient non-parametric function induction in semi-supervised learning. In *AISTAT*, pages 96–103.
- [Drineas and Mahoney, 2005] Drineas, P. and Mahoney, M. W. (2005). On the Nyström method for approximating a Gram matrix for improved kernel-based learning. In *Proceedings of COLT, 2005*.
- [Eskin, 2000] Eskin, E. (2000). Anomaly detection over noisy data using learned probability distributions. In *Proc. 17th International Conf. on Machine Learning*, pages 255–262. Morgan Kaufmann, San Francisco, CA.
- [Fergus et al., 2009] Fergus, R., Weiss, Y., and Torralba, A. (2009). Semi-supervised learning in gigantic image collections. In Bengio, Y., Schuurmans, D., Lafferty, J., Williams, C. K. I., and Culotta, A., editors, *Advances in Neural Information Processing Systems 22*, pages 522–530. NIPS Foundation (<http://books.nips.cc>).
- [Fine and Scheinberg, 2001] Fine, S. and Scheinberg, K. (2001). Efficient SVM training using low-rank kernel representations. *Journal of Machine Learning Research*, 2:243–264.
- [Fowlkes et al., 2004] Fowlkes, C., Belongie, S., Chung, F., and Malik, J. (2004). Spectral grouping using the Nyström method. *IEEE Transactions on PAMI*, 26(2).
- [Gans et al., 2005] Gans, D., Kralewski, J., Hammons, T., and Dowd, B. (2005). Medical groups’ adoption of electronic health records and information systems. *Health Aff (Millwood)*, 24(5):1323–1333.
- [Goldberg et al., 2008] Goldberg, A., Li, M., and Zhu, X. (2008). Online manifold regularization: A new learning setting and empirical study. In *Proceeding of European Conference on Machine Learning and Principles and Practice of Knowledge Discovery in Databases*.
- [Goldberg et al., 2011] Goldberg, A., Zhu, X., Furger, A., and Xu, J.-M. (2011). Oasis: Online active semisupervised learning. In *Proceedings of the Twenty-Fifth AAAI Conference on Artificial Intelligence*.
- [Goldberg et al., 2009] Goldberg, A. B., Zhu, X., Singh, A., Xu, Z., and Nowak, R. (2009). Multi-manifold semi-supervised learning. *Journal of Machine Learning Research*, 5:169–176.

- [Goldberger et al., 2004] Goldberger, J., Roweis, S. T., Hinton, G. E., and Salakhutdinov, R. (2004). Neighbourhood components analysis. In *NIPS*.
- [Gorban and Zinovyev, 2009] Gorban, A. and Zinovyev, A. (2009). Principal graphs and manifolds. In *Handbook of Research on Machine Learning Applications and Trends: Algorithms, Methods and Techniques*, pages 28 – 59. Information Science Reference.
- [Grabner et al., 2008] Grabner, H., Leistner, C., and Bischof, H. (2008). Semi-supervised on-line boosting for robust tracking. In *Proceedings of the 10th European Conference on Computer Vision*, pages 234–247.
- [Gray and Neuhoff, 1998] Gray, R. and Neuhoff, D. (1998). Quantization. *IEEE Transactions on Information Theory*, 44(6):2325–2383.
- [Hanley and Mcneil, 1982] Hanley, J. A. and Mcneil, B. J. (1982). The meaning and use of the area under a receiver operating characteristic (roc) curve. *Radiology*, 143(1):29–36.
- [Hastie et al., 2001] Hastie, T., Tibshirani, R., and Friedman, J. H. (2001). *The Elements of Statistical Learning*. Springer.
- [Hauskrecht et al., 2006] Hauskrecht, M., Pelikan, R., Valko, M., and Lyons-Weiler, J. (2006). *Fundamentals of Data Mining in Genomics and Proteomics*, chapter Feature Selection and Dimensionality Reduction in Genomics and Proteomics. Springer.
- [Hauskrecht et al., 2010] Hauskrecht, M., Valko, M., Batal, I., Clermont, G., Visweswaram, S., and Cooper, G. (2010). Conditional outlier detection for clinical alerting. *Annual American Medical Informatics Association Symposium*.
- [Hauskrecht et al., 2007] Hauskrecht, M., Valko, M., Kveton, B., Visweswaram, S., and Cooper, G. (2007). Evidence-based anomaly detection. In *Annual American Medical Informatics Association Symposium*, pages 319–324.
- [Haykin, 1994] Haykin, S. (1994). *Neural Networks: A Comprehensive Foundation*. Prentice Hall PTR, Upper Saddle River, NJ, USA, 1st edition.
- [He and Carbonell, 2008] He, J. and Carbonell, J. (2008). Nearest-neighbor-based active learning for rare category detection. In Platt, J., Koller, D., Singer, Y., and Roweis, S., editors, *Advances in Neural Information Processing Systems 20*, pages 633–640. MIT Press, Cambridge, MA.
- [He et al., 2007] He, J., Carbonell, J., and Liu, Y. (2007). Graph-based semi-supervised learning as a generative model. In *Proceedings of the 20th international joint conference on Artificial intelligence*, pages 2492–2497, San Francisco, CA, USA. Morgan Kaufmann Publishers Inc.
- [Heard et al., 2010] Heard, N. A., Weston, D. J., Platanioti, K., and Hand, D. J. (2010). Bayesian anomaly detection methods for social networks. *Annals of Applied Statistics*, 4:645–662.

- [Hein et al., 2007] Hein, M., Audibert, J.-Y., and Luxburg, U. v. (2007). Graph laplacians and their convergence on random neighborhood graphs. *J. Mach. Learn. Res.*, 8:1325–1370.
- [Hendrickson and Leland, 1995] Hendrickson, B. and Leland, R. (1995). A multilevel algorithm for partitioning graphs. In *Proceedings of Supercomputing*.
- [Jiang and Zhou, 2004] Jiang, Y. and Zhou, Z.-H. (2004). Editing training data for knn classifiers with neural network ensemble. In *Lecture Notes in Computer Science 3173*, pages 356–361.
- [Karypis and Kumar, 1999] Karypis, G. and Kumar, V. (1999). A fast and high quality multilevel scheme for partitioning irregular graphs. *SIAM Journal on Scientific Computing*, 20:359–392.
- [Kivinen et al., 2002] Kivinen, J., Smola, A. J., and Williamson, R. C. (2002). Online learning with kernels. In Dietterich, T. G., Becker, S., and Ghahramani, Z., editors, *Advances in Neural Information Processing Systems 14*, Cambridge, MA. MIT Press.
- [Kolar et al., 2010] Kolar, M., Song, L., Ahmed, A., and Xing, E. P. (2010). Estimating time-varying networks. *Annals of Applied Statistics*, 4:94–123.
- [Kveton et al., 2010a] Kveton, B., Valko, M., Philipose, M., and Huang, L. (2010a). Online semi-supervised perception: Real-time learning without explicit feedback. In *Proceedings of the 4th IEEE Online Learning for Computer Vision Workshop*.
- [Kveton et al., 2010b] Kveton, B., Valko, M., Rahimi, A., and Huang, L. (2010b). Semi-supervised learning with max-margin graph cuts. In *Proceedings of the 13th International Conference on Artificial Intelligence and Statistics*, pages 421–428.
- [Lazarevic and Kumar, 2005] Lazarevic, A. and Kumar, V. (2005). Feature bagging for outlier detection. In *KDD '05: Proceedings of the eleventh ACM SIGKDD international conference on Knowledge discovery in data mining*, pages 157–166, New York, NY, USA. ACM.
- [Lee and Wasserman, 2010] Lee, A. B. and Wasserman, L. (2010). Spectral connectivity analysis. *Journal of the American Statistical Association*, 0(0):1–15.
- [Luxburg, 2007] Luxburg, U. (2007). A tutorial on spectral clustering. *Statistics and Computing*, 17(4):395–416.
- [Ma and Perkins, 2003] Ma, J. and Perkins, S. (2003). Online novelty detection on temporal sequences. In *KDD '03: Proceedings of the ninth ACM SIGKDD international conference on Knowledge discovery and data mining*, pages 613–618, New York, NY, USA. ACM.
- [Madigan et al., 2002] Madigan, D., Raghavan, I., Dumouchel, W., Nason, M., Posse, C., and Ridgeway, G. (2002). Likelihood-based data squashing: a modeling approach to instance construction. *Data Mining and Knowledge Discovery*, 6(2):173–190.

- [Manevitz and Yousef, 2002] Manevitz, L. M. and Yousef, M. (2002). One-class svms for document classification. *J. Mach. Learn. Res.*, 2:139–154.
- [Markou and Singh, 2003a] Markou, M. and Singh, S. (2003a). Novelty detection: a review, part 1: statistical approaches. *Signal Process.*, 83(12):2481–2497.
- [Markou and Singh, 2003b] Markou, M. and Singh, S. (2003b). Novelty detection: a review, part 2: neural network based approaches. *Signal Process.*, 83(12):2499–2521.
- [McCullagh and Nelder, 1989] McCullagh, P. and Nelder, J. A. (1989). *Generalized Linear Models*. Chapman and Hall, London, 2nd edition.
- [Mitra et al., 2002] Mitra, P., Murthy, C. A., and Pal, S. K. (2002). Density-based multiscale data condensation. *IEEE Transactions on PAMI*, 24(6):1–14.
- [Moonesignhe and Tan, 2006] Moonesignhe, H. D. K. and Tan, P.-N. (2006). Outlier detection using random walks. In *ICTAI '06: Proceedings of the 18th IEEE International Conference on Tools with Artificial Intelligence*, pages 532–539, Washington, DC, USA. IEEE Computer Society.
- [Nene et al., 1996] Nene, S. A., Nayar, S. K., and Murase, H. (1996). Columbia Object Image Library (COIL-100). Technical report, Columbia University.
- [OpenMP, 2008] OpenMP (2008). *OpenMP Application Program Interface – Version 3.0*. OpenMP Architecture Review Board.
- [Papadimitriou and Faloutsos, 2003] Papadimitriou, S. and Faloutsos, C. (2003). Cross-outlier detection. In Hadzilacos, T., Manolopoulos, Y., Roddick, J. F., and Theodoridis, Y., editors, *Advances in Spatial and Temporal Databases, 8th International Symposium, SSTD 2003, Santorini Island, Greece, July 24-27, 2003, Proceedings*, volume 2750, pages 199–213.
- [Pelleg and Moore, 2005] Pelleg, D. and Moore, A. W. (2005). Active learning for anomaly and rare-category detection. In Saul, L. K., Weiss, Y., and Bottou, L., editors, *Advances in Neural Information Processing Systems 17*, pages 1073–1080. MIT Press, Cambridge, MA.
- [Post and Harrison, 2008] Post, A. R. and Harrison, J. H. (2008). Temporal data mining. *Clin Lab Med*, 28(1):83–100, vii.
- [Rubin et al., 2005] Rubin, S., Christodorescu, M., Ganapathy, V., Giffin, J. T., Kruger, L., Wang, H., and Kidd, N. (2005). An auctioning reputation system based on anomaly detection. In *Proceedings of the 12th ACM conference on Computer and communications security, CCS '05*, pages 270–279, New York, NY, USA. ACM.
- [Sanchez et al., 2003] Sanchez, J., Barandela, R., Marques, A. I., Alejo, R., and J., B. (2003). Analysis of new techniques to obtain quality training sets. *Pattern Recognition Letters* 24, pages 1015–1022.

- [Schedlbauer et al., 2009] Schedlbauer, A., Prasad, V., Mulvaney, C., Phansalkar, S., Stanton, W., Bates, D. W., and Avery, A. J. (2009). What evidence supports the use of computerized alerts and prompts to improve clinicians’ prescribing behavior? *J Am Med Inform Assoc*, 16(4):531–538.
- [Scholkopf et al., 1999] Scholkopf, B., Platt, J. C., Shawe-taylor, J., Smola, A. J., and Williamson, R. C. (1999). Estimating the support of a high-dimensional distribution. *Neural Computation*, 13:2001.
- [Smola and Kondor, 2003] Smola, A. and Kondor, R. (2003). Kernels and regularization on graphs. In Schölkopf, B. and Warmuth, M., editors, *Proceedings of the Annual Conference on Computational Learning Theory and Kernel Workshop*, Lecture Notes in Computer Science. Springer.
- [Song et al., 2007] Song, X., Wu, M., and Jermaine, C. (2007). Conditional anomaly detection. *IEEE Transactions on Knowledge and Data Engineering*, 19(5):631–645. Fellow-Sanjay Ranka.
- [Syed and Rubinfeld, 2010] Syed, Z. and Rubinfeld, I. (2010). Unsupervised risk stratification in clinical datasets: Identifying patients at risk of rare outcomes. In Fürnkranz, J. and Joachims, T., editors, *ICML*, pages 1023–1030. Omnipress.
- [Szummer and Jaakkola, 2001] Szummer, M. and Jaakkola, T. (2001). Partially labeled classification with markov random walks. In *Advances in Neural Information Processing Systems*, volume 14.
- [Valizadegan and Tan, 2007] Valizadegan, H. and Tan, P.-N. (2007). Kernel based detection of mislabeled training examples. In *Proceedings of the Seventh SIAM International Conference on Data Mining, April 26-28, 2007, Minneapolis, Minnesota, USA*.
- [Valko et al., 2008] Valko, M., Cooper, G., Seybert, A., Visweswaran, S., Saul, M., and Hauskrecht, M. (2008). Conditional anomaly detection methods for patient-management alert systems. In *Workshop on Machine Learning in Health Care Applications in The 25th International Conference on Machine Learning*.
- [Valko and Hauskrecht, 2008] Valko, M. and Hauskrecht, M. (2008). Distance metric learning for conditional anomaly detection. In *Twenty-First International Florida Artificial Intelligence Research Society Conference*. AAAI Press.
- [Valko and Hauskrecht, 2010] Valko, M. and Hauskrecht, M. (2010). Feature importance analysis for patient management decisions. In *13th International Congress on Medical Informatics MEDINFO 2010*.
- [Valko et al., 2010] Valko, M., Kveton, B., Huang, L., and Ting, D. (2010). Online semi-supervised learning on quantized graphs. In *Proceedings of the 26th Conference on Uncertainty in Artificial Intelligence*.

- [Valko et al., 2011] Valko, M., Valizadegan, H., Kveton, B., Cooper, G. F., and Hauskrecht, M. (2011). Conditional anomaly detection using soft harmonic functions: An application to clinical alerting. In *The 28th International Conference on Machine Learning Workshop on Machine Learning for Global Challenges*.
- [Vapnik, 1995] Vapnik, V. N. (1995). *The nature of statistical learning theory*. Springer-Verlag New York, Inc., New York, NY, USA.
- [Verbaeten and Assche., 2003] Verbaeten, S. and Assche., A. V. (2003). Ensemble methods for noise elimination in classification problems. In *Proceeding of 4th International Workshop on Multiple Classifier Systems*.
- [Wahba, 1999] Wahba, G. (1999). *Support Vector Machines, Reproducing Kernel Hilbert Spaces, and Randomized GACV*, pages 69–88. MIT Press, Cambridge, MA.
- [Williams and Seeger, 2001] Williams, C. and Seeger, M. (2001). Using the Nyström method to speed up kernel machines. In *Neural Information Processing Systems, 2001*.
- [Yan et al., 2009] Yan, D., Huang, L., and Jordan, M. (2009). Fast approximate spectral clustering. In *Proceedings of the 15th ACM SIGKDD Conference on Knowledge Discovery and Data Mining*.
- [Zhou et al., 2004] Zhou, D., Bousquet, O., Lal, T. N., Weston, J., and Scholkopf, B. (2004). Learning with local and global consistency. *Advances in Neural Information Processing Systems*, 16:321–328.
- [Zhu, 2008] Zhu, X. (2008). Semi-supervised learning literature survey. Technical Report 1530, University of Wisconsin-Madison.
- [Zhu et al., 2003] Zhu, X., Ghahramani, Z., and Lafferty, J. (2003). Semi-supervised learning using gaussian fields and harmonic functions. In *Proceedings of the 20th International Conference on Machine Learning*, pages 912–919.
- [Zhu and Lafferty, 2005] Zhu, X. and Lafferty, J. (2005). Harmonic mixtures: combining mixture models and graph-based methods for inductive and scalable semi-supervised learning. In *Proceedings of the 22nd international conference on Machine learning, ICML '05*, pages 1052–1059, New York, NY, USA. ACM.